

1 Modelling the influence of biotic plant stress on atmospheric aerosol 2 particle processes throughout a growing season

3 Ditte Taipale^{1,2,3,4}, Veli-Matti Kerminen¹, Mikael Ehn¹, Markku Kulmala¹, Ülo Niinemets²

4 ¹Institute for Atmospheric and Earth System Research / Physics, Faculty of Science, University of Helsinki, P.O. Box 64,
5 00014 Helsinki, Finland

6 ²Institute of Agricultural and Environmental Sciences, Estonian University of Life Sciences, Kreutzwaldi 1, Tartu 51006,
7 Estonia

8 ³Institute for Atmospheric and Earth System Research / Forest Sciences, Faculty of Agriculture and Forestry, University of
9 Helsinki, PO Box 27, 00014 Helsinki, Finland

10 ⁴Hyytiälä Forestry Field Station, Hyytiäläntie 124, 35500 Korkeakoski, Finland

11 Correspondence to: Ditte Taipale (ditte.taipale@helsinki.fi)

12
13 **Abstract.** Most trees emit volatile organic compounds (VOCs) continuously throughout their life, but the rate of emission,
14 and spectrum of emitted VOCs, become substantially altered when the trees experience stress. Still, models to predict the
15 emissions of VOCs do not account for perturbations caused by biotic plant stress. Considering that such stresses have generally
16 been forecast to increase in both frequency and severity in future climate, the neglect of plant stress-induced emissions in
17 models might be one of the key obstacles for realistic climate change predictions, since changes in VOC concentrations are
18 known to greatly influence atmospheric aerosol processes. Thus, we constructed a model to study the impact of biotic plant
19 stresses on new particle formation and growth throughout a full growing season. We simulated the influence on aerosol
20 processes caused by herbivory by European gypsy moth (*Lymantria dispar*) and autumnal moth (*Epirrita autumnata*) feeding
21 on pedunculate oak (*Quercus robur*) and mountain birch (*Betula pubescens* var. *pumila*), respectively, and also fungal
22 infections of pedunculate oak and balsam poplar (*Populus balsamifera* var. *suaveolens*) by oak powdery mildew (*Erysiphe*
23 *alphitoides*) and poplar rust (*Melampsora larici-populina*), respectively. Our modelling results indicate that all the investigated
24 plant stresses are capable of substantially perturbing both the number and size of aerosol particles in atmospherically relevant
25 conditions, with increases in the amount of newly formed particles by up to about one order of magnitude and additional daily
26 growth of up to almost 50 nm. We also showed that it can be more important to account for biotic plant stresses in models for
27 local and regional predictions of new particle formation and growth during the time of infestation/infection than significant
28 variations in e.g. leaf area index, and temperature and light conditions, which are currently the main parameters controlling
29 predictions of VOC emissions. Our study, thus, demonstrates that biotic plant stress can be highly atmospherically relevant.
30 To validate our findings, field measurements are urgently needed to quantify the role of stress emissions in atmospheric aerosol
31 processes and for making integration of biotic plant stress emission responses into numerical models for prediction of
32 atmospheric chemistry and physics, including climate change projection models, possible.

33 1 Introduction

34 Formation and subsequent growth of atmospheric aerosol particles is globally a major source of cloud condensation nuclei
35 (CCN) (Spracklen et al., 2008; Merikanto et al., 2009; Dunne et al., 2016). CCN impact various cloud processes, such as cloud
36 formation, albedo and lifetime (Twomey, 1977; Albrecht, 1989; Makkonen et al., 2009; Kerminen et al., 2005), and
37 atmospheric aerosol particles are thereby able to influence our climate indirectly, in addition to interacting directly with
38 incoming solar radiation. Though atmospheric aerosol particles provide the single largest cooling effect on our climate, they

39 are also connected with the greatest uncertainty in climate change projections (IPCC, 2013). Part of this uncertainty is caused
40 by limited knowledge about the aerosol precursor molecules.

41 Oxidation products of certain volatile organic compounds (VOCs) participate in both the formation of new particles
42 (Donahue et al., 2013; Schobesberger et al., 2013; Kulmala et al., 2014; Riccobono et al., 2014; Kirkby et al., 2016; Tröstl et
43 al., 2016) and growth of existing particles via gas-to-particle condensation (Riipinen et al., 2012; Ehn et al., 2014; Bianchi et
44 al., 2019). Globally, and especially in forested regions, the majority of these organic compounds originate from terrestrial
45 vegetation (Kanakidou et al., 2005; Jimenez et al., 2009). Thus, increases in the emissions of certain biogenic VOCs can lead
46 to enhanced formation of atmospheric aerosol particles and subsequently to a rise in CCN concentration (Kerminen et al.,
47 2012; Paasonen et al., 2013).

48 Many plants emit VOCs constitutively, i.e. that they emit VOCs regardless of the experience of stress. Biotic plant
49 stress (i.e. stress caused to a plant by living species such as e.g. herbivores and pathogens) is known to substantially alter both
50 the rates of emission and spectrum of VOCs emitted constitutively (Holopainen and Gershenson, 2010; Niinemets, 2010;
51 Niinemets et al., 2013; Faiola and Taipale, 2020). For example, constitutively emitted isoprene, which is thought to suppress
52 the formation of new atmospheric aerosol particles (Kiendler-Scharr et al., 2009, 2012; Lee et al., 2016; McFiggans et al.,
53 2019; Heinritzi et al., 2020), is usually reduced in response to such stress (e.g. Brillì et al., 2009; Copolovici et al., 2014, 2017;
54 Jiang et al., 2016), while the emissions of other VOCs are greatly increased. Emissions of VOCs which are increased, or started
55 to be emitted, in response to plant stress, are referred to as induced plant volatile emissions. A large fraction of stress-induced
56 compounds (e.g. monoterpenes, sesquiterpenes, 4,8-dimethyl-1,3,7-nonatriene (DMNT) and methyl salicylate) has a high
57 potential to produce and grow atmospheric aerosol particles (e.g. Mentel et al., 2013; Joutsensaari et al., 2015; Yli-Pirilä et al.,
58 2016; Ylisirniö et al., 2020), while other induced compounds (e.g. methanol and lipoxygenase oxidation products (LOX),
59 which mostly include C₆ aldehydes, alcohols and esters) are anticipated to suppress aerosol processes (e.g. Mentel et al., 2013).

60 While much attention has been given to representing constitutive emissions of VOCs in numerical models, VOC
61 emissions caused by stress, and in particular biotic stress, have been mostly excluded (Grote et al., 2013; Faiola and Taipale,
62 2020), despite the fact that biotic plant stress is largely ubiquitous. This is mainly due to a lack of measurements, combined
63 with the fact that variations in emission responses are highly stressor-specific (e.g. Holopainen and Gershenson, 2010;
64 Niinemets, 2010; Faiola and Taipale, 2020). Thus, no consistent mechanism for the emissions of VOCs from plants under
65 stress exists. Though the most extensively used biogenic emissions model, MEGAN (Guenther et al., 2012), considers a stress
66 emission category, the treatment is not quantitative. The emission factor for stress VOCs is, for example, the same for all plant
67 functional types and is supposed to represent a large range of different types of stresses. Recently, Grote et al. (2019) proposed
68 a new modelling framework for estimating emissions of VOCs induced by both biotic and abiotic plant stresses, while Douma
69 et al. (2019) developed a model to predict both the emissions and concentrations of stress-induced VOCs, which was
70 parameterized to simulate a gypsy moth infested black poplar canopy. Both are promising tools, but in their current states, they
71 exclude important storage emissions which are usually released upon wounding (e.g. Blande et al., 2009; Faiola et al., 2018;
72 Kari et al., 2019), and they do not fully (Grote et al., 2019) - or at all (Douma et al., 2019) - consider how the constitutive
73 emissions of isoprene are modulated. This is as such understandable considering that emissions of isoprene might be either
74 reduced (e.g. Brillì et al., 2009; Copolovici et al., 2017) or increased (e.g. Schaub et al., 2010; Ye et al., 2019) in response to
75 biotic plant stress, but nevertheless problematic since isoprene is globally the VOC that is emitted in largest quantities
76 (Guenther et al., 2012) and it is thought to suppress the formation of aerosol particles (see above). Whilst Grote et al. (2019)
77 assumed a linear response to the degree of damage, which has been shown not always to be true, especially at severe stress
78 levels (e.g. Niinemets et al., 2013; Jiang et al., 2016; Yli-Pirilä et al. 2016; Copolovici et al., 2017; Faiola and Taipale, 2020),
79 it is not obvious how the model results by Douma et al. (2019) depend on the degree of damage, as they operate with “number
80 of larvae” rather than a stand level of defoliation. Additionally, Grote et al. (2019) did not account for an explicit dependency
81 of the emissions on temperature, which is usually considered as one of the most important environmental parameters for

82 emissions of VOCs (e.g. Grote et al., 2013). Common for both studies is that they only simulate rather short time scales (i.e. a
83 few days).

84 Since measurements have clearly illustrated that biotic plant stress is able to significantly influence the amount and
85 size of formed atmospheric aerosol particles over short periods at least (Mentel et al., 2013; Joutsensaari et al., 2015; Yli-Pirilä
86 et al., 2016; Faiola et al., 2019, 2018) via perturbations in VOC emissions, there is an urgent need to quantify the atmospheric
87 importance of biotic plant stress. This need is amplified by the fact that insect outbreaks and fungal diseases generally are
88 expected to increase in both frequency and severity in the future (Cannon, 1998; Bale et al., 2002; Harrington et al., 2007;
89 Pautasso et al., 2012; Boyd et al., 2013). Unfortunately, such quantitative estimates are currently very scarce, connected with
90 a large degree of uncertainty, and not necessarily reaching the same conclusions. For example, Berg et al. (2013) used bark
91 beetle-induced monoterpene emission responses and several years of bark beetle-induced tree mortality data from western
92 North America as input to a global model in order to investigate the impact of bark beetle attacks on regional secondary organic
93 aerosol (SOA) formation. The authors found that the concentration of SOA might increase regionally by up to 40 % or 300 %
94 in case of bark beetle attacks on lodgepole pine and spruce trees, respectively (Berg et al., 2013). At the same time, Berg et al.
95 (2013) concluded that the enhancement in the concentrations of SOA is in most cases small in comparison to the impact of
96 wildfires on total organic aerosol in western North America. Bergström et al. (2014), on the other hand, used a regional
97 chemical transport model to simulate the impact of *de novo* emissions, induced by aphid infestation, on SOA formation, and
98 estimated that these induced emissions currently account for 20-70 % of total biogenic SOA in northern and central European
99 forests. Meanwhile, Joutsensaari et al. (2015) calculated a local increase of up to 480 % in aerosol mass and 45 % in CCN
100 concentration, when it was assumed that 10 % of the boreal forest area experienced stress which increased constitutive
101 monoterpenes emission rates by an order of magnitude. Using satellite observations, Joutsensaari et al. (2015) also found a 2-
102 fold increase in aerosol optical depth over Canadian pine forests during a bark beetle outbreak. Thus, the degree of necessity
103 of considering biotic plant stress emissions for predictions of new particle formation in the atmosphere is still uncertain, and
104 therefore there is a great need for field observations of different scales to constrain and quantify the role of stress emissions in
105 SOA formation, but also for innovative model approaches which improve the quantitative representation of the emissions. To
106 our knowledge, no one has previously considered the dynamics of insect herbivory when simulating the emitted VOCs and
107 produced and grown aerosols from stressed plants. Additionally, there has so far been no attempts to measure nor model the
108 impact of pathogenic infections on atmospheric aerosol processes.

109 We constructed a conceptual model to investigate the atmospheric impacts of biotic plant stresses. We used this model
110 to simulate formation and growth of atmospheric aerosol particles throughout a growing season in pure oak, poplar and birch
111 forest stands in stress-free conditions and under herbivory or fungal stress. By considering the dynamics of insect herbivory
112 and pathogenic infections in combination with seasonal changes in environmental parameters, our aim was to contribute to a
113 discussion about whether biotic plant stress perturbs atmospheric aerosol processes sufficiently to warrant their inclusion in
114 larger scale models.

115

116 **2 Materials and methods**

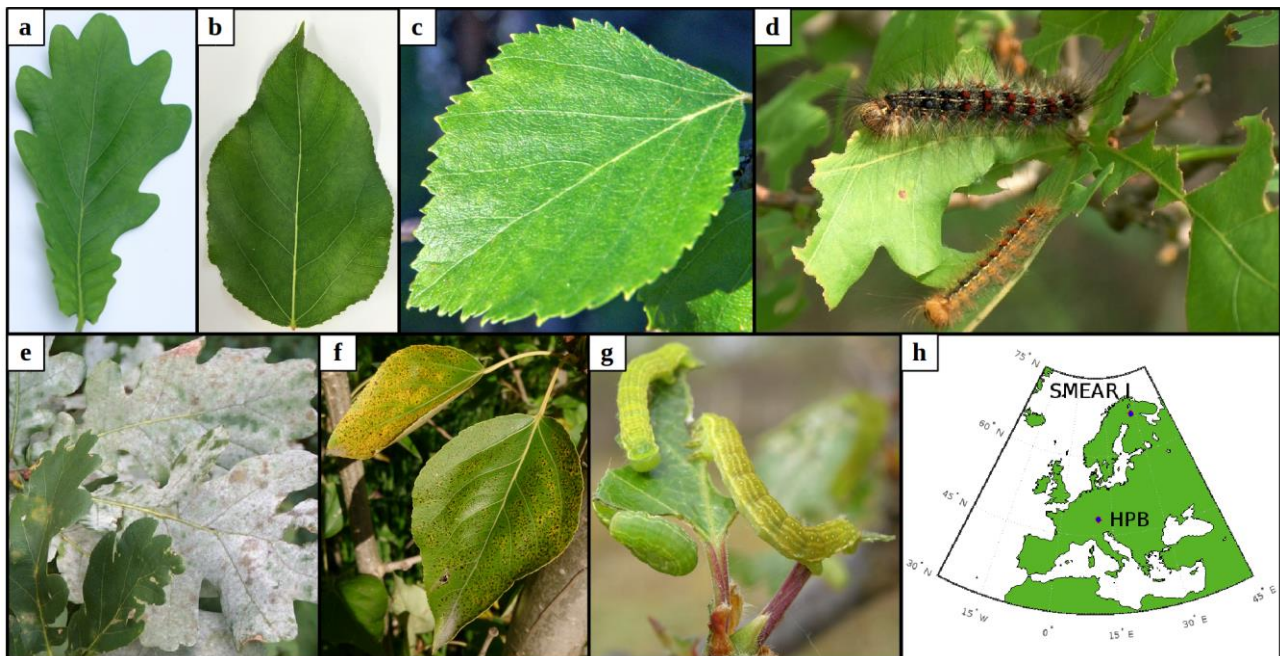
117 We constructed a 0D box model that includes modules for emissions of VOCs from stress-free and biotically stressed tree
118 species (Sec. 2.4), boundary layer meteorology (Sec. 2.5), atmospheric chemistry (Sec. 2.6) and aerosol dynamics (Sec. 2.7).
119 The calculated canopy VOC emissions from biotically stressed trees depend on the dynamics of the biotic stressors of interest
120 (Sec. 2.1 and 2.2) and changes in the leaf area index (Sec. 2.3).

121

122 2.1 Simulations of larval infestation dynamics

123 Whereas mountain birch (*Betula pubescens* var. *pumila*; former *spp. czerepanovii*, Fig. 1c) is the main host for autumnal moths
124 (*Epirrita autumnata*, Fig. 1g, Klemola et al., 2004; Ammunét et al., 2011), European gypsy moth (*Lymantria dispar*, Fig. 1d)
125 is one of the major defoliating insects feeding on pedunculate oak (*Quercus robur*, Fig. 1a,
126 <https://www.cabi.org/isc/datasheet/31807#tohostsOrSpeciesAffected>, last accessed 11th of June, 2021). The larval eggs of
127 both moths hatch in spring synchronously with bud burst (Kaitaniemi et al., 1997; Kaitaniemi and Ruohomäki, 1999; Spear,
128 2005; McManus et al., 1989). Both sexes have five larval stages (instar), though female gypsy moths have six. These stages
129 are separated by periods of molting where the larvae do not feed. A complete defoliation of vast areas can occur within 4-6
130 weeks by autumnal moth (Kaitaniemi and Ruohomäki, 1999) and within 6-8 weeks by gypsy moth (McManus et al., 1989).
131 Several thousands of square kilometres of birch forests have previously been reported to become defoliated due to just a single
132 outbreak of autumnal moth in Fennoscandinavia (Tenow 1975; Nikula 1993), while gypsy moth, in North America alone, is
133 estimated to have defoliated >95 million acres of forest during years 1920 to 2020 (Coleman et al., 2020). Adults do not feed
134 on leaves (Tammaru et al., 1996; Waring and Townsend, 2009). For simulations of autumnal moth infested mountain birch,
135 our model incorporates atmospheric and ecological conditions observed at the Station for Measuring Ecosystem-Atmosphere
136 Relations (SMEAR I, Fig. 1h), Värriö, Eastern Finnish Lapland (e.g. Hari et al., 1994), due to the high data quality and
137 availability, and since autumnal moth infested mountain birch is common at the site (Hunter et al., 2014). In our simulations,
138 bud burst occurs on 6th of June, the subsequent full leaf state is attained on 10th of June (dates are based on long-term
139 observations from the station), and senescence onsets on 20th of August (Gill et al., 2015). We assumed that the larvae feed for
140 five weeks, starting on 6th of June and they pupate on 11th of July (Kaitaniemi and Ruohomäki, 1999). The larvae dynamics
141 (i.e. relative leaf consumption and time spent in each larval stage) that is incorporated in our model is based on Lempa et al.
142 (2004). For simulations of European gypsy moth infested pedunculate oak, our model incorporates mainly atmospheric
143 conditions observed at the Meteorological Observatory Hohenpeißenberg (e.g. Birmili et al., 2003), rural southern Germany
144 (Fig. 1h), since this station has been classified as a representative measurement location for central Europe (Naja et al., 2003),
145 where oak is a very common species. In our simulations, bud burst occurs on 15th of May, the subsequent full leaf state is
146 attained 20 days later on 4th of June, and senescence onsets on 20th of September (Gill et al., 2015). Durations of the various
147 developmental states of the larvae are based on Zúbrik et al. (2007), which is also in agreement with Stoyenoff et al. (1994).
148 Though the length of the larval state of female larvae feeding on pedunculate oak is typically a few days longer than the total
149 duration of the male larval state (e.g. Zúbrik et al., 2007), we did not differentiate between the two genders, but utilised the
150 length of the female larval state due to simplification and since the female is the main consumer (Miller et al., 1991). We
151 assumed that the larvae feed for 41 days (Zúbrik et al., 2007), starting on 15th of May and they pupate on 25th of June. The
152 relative leaf consumption within the different larval stages is based on Kula et al. (2013). The ratio in relative leaf consumption
153 between 4th and 5th instar is also within the range that is reported by Stoyenoff et al. (1994) (where no other ratios were
154 provided). We neglected periods of molting, as those are typically in the order of less than one day (Ayres and MacLean,
155 1987). We assumed that either 30 % or 80 % of the total leaf area in the forest stand was consumed by the end of the feeding
156 period (Fig. 2a,b).

157



158
159
160
161
162
163
164
165
166

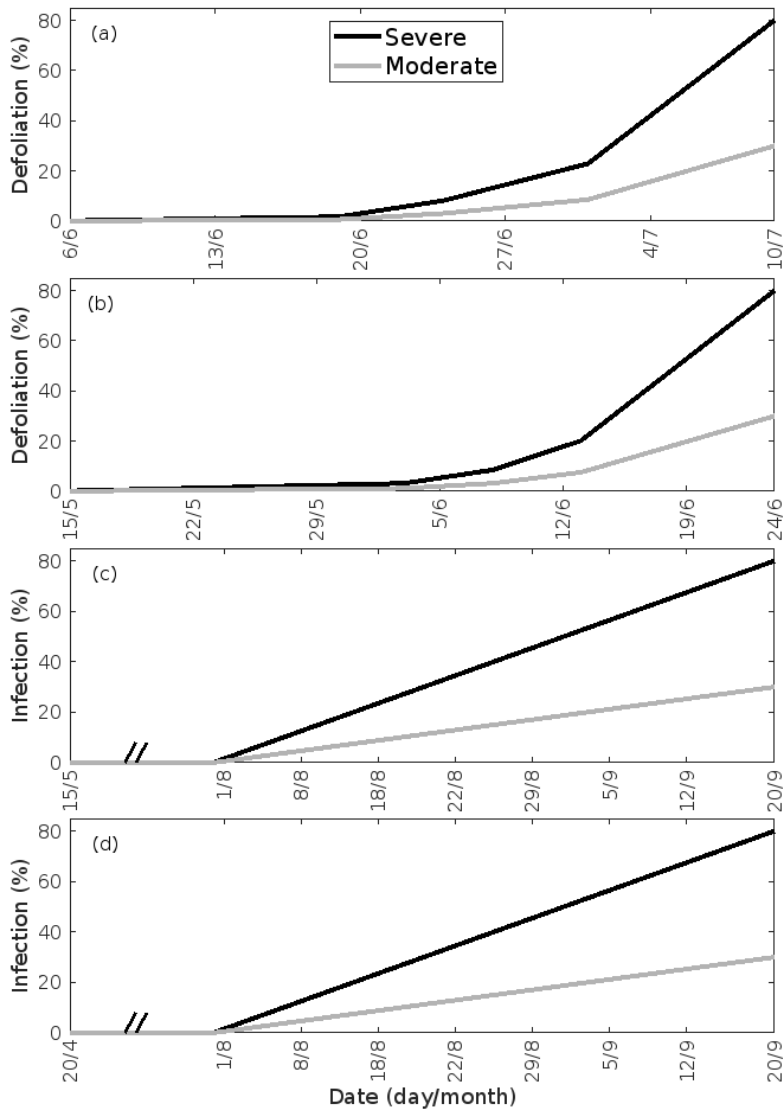
Figure 1. The plant species and biotic stresses we considered together with locations. Non-infected leaves; pedunculate oak (*Quercus robur*) (a), balsam poplar (*Populus balsamifera* var. *suaveolens*) (b) and mountain birch (*Betula pubescens* var. *pumila*; former spp. *czerepanovii*) (c). Fungal infected or moth infested leaves; pedunculate oak infested by European gypsy moth (*Lymantria dispar*) (d) or infected by oak powdery mildew (*Erysiphe alphitoides*) (e), poplar infected by rust fungus (*Melampsora larici-populina*) (f) and mountain birch infested by autumnal moth (*Epirrita autumnata*) (g). h, location of the two sites that serve as boundary conditions in our simulations. Photo courtesy: a+c: Juho Aalto, b: Yifan Jiang, d+e: Haruta Ovidiu, University of Oradea, Bugwood.org, f: Ülo Niinemets, g: Tero Klemola.

167 2.2 Simulations of fungal infection dynamics

168 Oak powdery mildew (*Erysiphe alphitoides*) is one of the main foliar diseases of pedunculate oak (*Quercus robur*) in Europe
169 (Desprez-Loustau et al., 2011). Among the *Melampsora* species, *Melampsora larici-populina* is the most widespread poplar
170 rust (Vialle et al., 2011). *M. larici-populina* has five morphologically and functionally different spore stages during its life
171 cycle, where the two first stages are retrieved on larch and the last three on poplar (Vialle et al., 2011). The pathogenic fungal
172 infections do not decrease the leaf area of their victim, but as they cover the leaf, they absorb nutrients from the cells of the
173 leaf (Glawe, 2008) and change the physiology of the leaf (e.g. Major et al., 2010; Voegele and Mendgen, 2003; El-Ghany et
174 al., 2009). The severity and spread of fungal infections depend largely on weather and growth conditions (e.g. Åhman, 1998;
175 Johansson and Alström, 2000; Covarelli et al., 2013), where especially high rainfall in the beginning of the summer greatly
176 enhances both the severity, but also the onset of infection (Covarelli et al., 2013; Pinon et al., 2006). The onset of attack by
177 oak powdery mildew is limited by its morphological development, hence the infection usually starts to appear between the end
178 of June and August (in France; Marçais et al., 2009; Marçais and Desprez-Loustau, 2014; Bert et al., 2016). *M. larici-populina*
179 has been observed to attack young poplar trees as early as June (in Italy, Covarelli et al., 2013), though generally the disease
180 emerges between July and September (in France and Italy, Gérard et al., 2006; Covarelli et al., 2013). In our simulations, we
181 assumed that both fungi started to infect their host on 1st of August. In the case of *M. larici-populina* we only simulated the
182 attack on poplar as the host (and not larch). *Populus balsamifera* var. *suaveolens* was chosen as the poplar species due to the
183 availability of suitable published VOC emissions measurements. Based on Bert et al. (2016), we assumed that the severity of
184 infection increases linearly with time, starting on 1st of August and ending on 20th of September. We assumed that either 30 %
185 or 80 % of the total leaf area in the forest stands was covered by fungi by the end of the growing season (Fig. 2c,d). For these
186 simulations, our model incorporates the same atmospheric conditions as for simulations of gypsy moth infested oak. Poplar

187 bud burst occurs on 20th of April in our model (Tripathi et al., 2016) and we assumed the same timing of senescence as for
 188 simulations of oak (Gill et al., 2015; Tripathi et al., 2016).

189



190

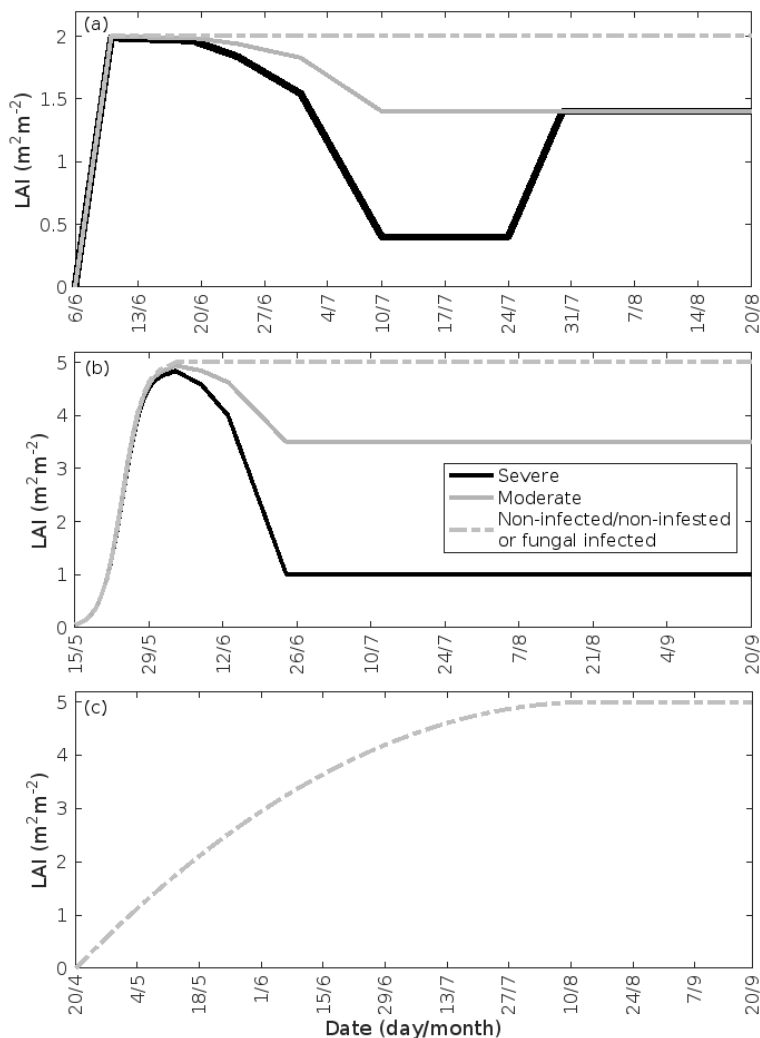
191 **Figure 2.** Infection dynamics. (a) birch infested with autumnal moth larvae, (b) oak infested with European gypsy moth larvae,
 192 (c) oak infected by oak powdery mildew and (d) poplar infected by rust fungus. The infection dynamics of oak powdery
 193 mildew and rust fungus is assumed to be similar, but the duration of growth of the two tree species is different. The dynamics
 194 are specific to the locations of Lapland (a) and central Europe (b-d). 30 % (moderate infection scenario) or 80 % (severe
 195 infection scenario) of the total leaf area in the forest stands is assumed to be consumed by the end of the feeding period or
 196 infected by fungi by the onset of senescence. Note the different time axes.

197

198 2.3 Treatment of the leaf area index

199 Low soil temperatures usually prevent growth of a second leaf flush in birch trees (Aphalo et al., 2006). Thus, we assumed
 200 that the leaf area index (LAI) of a non-infested mountain birch stand in Lapland increases linearly from 0 – 2.0 m² m⁻²
 201 (Dahlberg et al., 2004) in the time period 6th-10th of June (bud burst to full leaf), and stays constant until the onset of senescence
 202 (Fig. 3a). The LAI of an infested stand decreases proportionally with the level of defoliation (Fig. 3a). Refoliation only occurs
 203 in totally, or near-totally, defoliated mountain birch trees (Kaitaniemi et al., 1997). Hence, we assumed that the LAI of a
 204 heavily defoliated stand resumes to 70 % of the original LAI within three weeks of defoliation (personal communication with
 205 adj. Prof. Dr. Pekka Kaitaniemi, University of Helsinki, Fig. 3a). Poplar trees produce leaves throughout the season, and we

206 therefore assumed that the LAI of poplar stands increases quadratically from 20th of April (bud burst) until 15th of August (Fig.
 207 3c, Tripathi et al., 2016). Oak, on the other hand, usually only produces one significant leaf flush, hence we assumed that the
 208 LAI of oak stands increases with a sigmoid shape from 15th of May (bud burst) until 4th of June (full leaf state attained) (Fig.
 209 3b, Oláh et al., 2012). In our simulations, the maximum LAI of poplar and oak is 5.0 m² m⁻². The LAI of a gypsy moth infested
 210 oak stand decreases proportionally with the level of defoliation (Fig. 3b). The fungal infections do not decrease the leaf area
 211 of their host, nor do they prevent the tree from producing multiple flushes of leaves (Marçais and Desprez-Loustau, 2014).
 212 The LAI might, however, in reality be less in an infected stand than in a non-infected stand, though this depends highly on the
 213 specific genotypes and their individual fungal resistance (Verlinden et al., 2013; Shifflett et al., 2016), but naturally also on
 214 the timing of infection. Since most summer leaves already appear before the onset of infection, we did not assume a decrease
 215 in LAI. Severe powdery mildew infection (>50 %) has been shown to greatly reduce the infected leaf lifespan (Hajji et al.,
 216 2009). The median time before shedding of deformed oak leaves has been estimated to be 10-31 days (Hajji et al., 2009). In
 217 our scenario of a heavily infected stand (80 % of the stand leaf area is infected by the end of the season), an infection level of
 218 50 % is reached on 1st of September. Since senescence is assumed to onset on 20th of September, we excluded an earlier
 219 shedding of leaves. Hence, in our simulations of fungal infections, we assumed that the LAI is the same as in a non-infected
 220 stand (Fig. 3b,c).
 221



222
 223 **Figure 3.** Leaf area index throughout the growing season in infected and non-infected forest stands. **(a)** mountain birch, **(b)**
 224 oak and **(c)** poplar. 30 % (moderate infection scenario) or 80 % (severe infection scenario) of the total leaf area in the forest
 225 stands is assumed to be consumed by the end of the feeding period in simulations of herbivory, while fungal infections do not
 226 decrease the leaf area. Note the different time axes.

228 **2.4 Plant emissions of volatile organic compounds**

229 The plant emissions (F_i) of individual VOCs (i) from various pure stands were computed as:

$$230 F_i = \varepsilon_i \times \text{LAI} \times \gamma_L \times \gamma_T \quad (1)$$

231 where ε_i is the emission rate of i at standard conditions (25 °C, 1000 $\mu\text{mol m}^{-2} \text{s}^{-1}$), LAI is the one-sided leaf area index and
 232 treated as mentioned in Sec. 2.3, and γ_L and γ_T are the activity factors that account for changes in light and temperature from
 233 standard conditions. This expression is adopted from Guenther et al. (2012), Eq. 1-2, when we assume that the soil moisture
 234 and ambient CO₂ concentration in our stands are optimal. Generally, we excluded the effect of leaf age on the emissions of
 235 VOCs, since we do not know the effect of leaf age on stress-induced emissions. However, we also tested whether the impact
 236 of leaf maturity would be able to change the conclusions of our study when making certain assumptions about the leaf age
 237 effect. The treatment of the leaf age effects and the results of these tests are presented in Appendix B and discussed in Sec.
 238 3.2.

239 Similarly to e.g. Simpson et al. (1999; 2012) and Bergström et al. (2014), we utilised a simple non-canopy approach,
 240 where ambient and leaf temperature are assumed to equal, and where the use of branch-level emission factors accounts for the
 241 canopy shading effect (Guenther et al., 1994). We utilised emission rates, reported as a function of the degree of damage, from
 242 Copolovici et al. (2017; 2014), Jiang et al. (2016), and Yli-Pirilä et al. (2016). The emission rates reported by Copolovici et al.
 243 (2017; 2014) and Jiang et al. (2016) were all retrieved by leaf-level measurements, hence we decreased the reported emission
 244 rates by a factor of 0.57, since branch-level emission factors for light sensitive emissions are typically a factor of 1.75 smaller
 245 than the corresponding leaf-level values (Simpson et al., 1999; 2012). We did not decrease the emission rates reported by Yli-
 246 Pirilä et al. (2016), since these were based on measurements of the whole plant. Instead, the emission rates from mountain
 247 birch seedlings (Yli-Pirilä et al., 2016) were upscaled in order to represent the emissions from mature trees, assuming a leaf
 248 mass area of 75 g m⁻² for leaves growing on mature mountain birch trees (Riipi et al., 2005). Since emission response
 249 measurements are usually stopped, at a maximum, a few days after the herbivore activity has ceased, we assumed that the
 250 effect of stress on the emissions of VOC stops the day that the larvae pupate (e.g. Yli-Pirilä et al., 2016), in order to not
 251 overestimate the impact of the stress. The light and temperature dependent emission activity factors are computed using Eq. 2
 252 in Guenther (1997), since none of the considered broadleaved species poses storages and birch has specifically been shown to
 253 only emit *de novo* (Ghirardo et al., 2010). Similarly to Guenther et al. (2012), we assumed that stress-induced emissions are
 254 controlled by light and temperature in a similar way as constitutive emissions, thus the used emission rates from the literature
 255 were standardised according to Eq. 1. Copolovici et al. (2014) and Jiang et al. (2016) have also shown that the emissions of
 256 isoprene from oak powdery mildew and rust infected oaks and poplars have the same response to light as control plants.
 257 Copolovici et al. (2014) additionally demonstrated that the emissions of monoterpenes from oak powdery mildew infected oak
 258 depend strongly on light, even though the majority of emitted monoterpenes were not e.g. ocimene and linalool, which are
 259 known to be light dependent (Niinemets et al., 2002; Arimura et al., 2008). LOX (lipoxygenase pathway volatile) compounds,
 260 on the other hand, are released shortly after damage of leaf tissue, independent of the light conditions (Arimura et al., 2008).
 261 LOX compounds do not contribute to the formation and growth processes of atmospheric aerosol particles, but they were
 262 included in the model in order to illustrate the changes in the atmospheric concentrations of LOX as a function of stress severity
 263 and stress type, and for evaluating the reliability of our modelling results, since LOX, in reality, affect the atmospheric
 264 concentration of OH, which was constrained in the model. The equations, which we used in the model for linking the emission
 265 factors to the severity of stress, are provided in Table 1 together with the parameters needed for the equations. The emission
 266 factors at a few different degrees of stress are written out in Table A1 in Appendix A.

268 **Table 1.** Equations to calculate the emission factors ($\varepsilon_{i,\mathcal{A}}$, in unit nmol m^{-2} one-sided LAI s^{-1}), as a function of the degree of
 269 stress (\mathcal{A}), together with the parameters needed for the equations. The equations are valid for infection levels ranging from 0
 270 % to 80 % unless otherwise stated. The emission factors for oak and poplar are presented without the downscaling by a factor
 271 of 0.57 (see bulk text in Sec. 2.4). LMA_f is the fraction of the leaf mass area of leaves growing on mature mountain birch /
 272 growing on mountain birch seedlings, which is included so that the emission factors for mountain birches are also
 273 representative of mature trees. ISO = isoprene, MT = monoterpenes, MeSa = methyl salicylate, LOX = lipoxygenase pathway
 274 volatile compounds, DMNT = 4,8-dimethyl-1,3,7-nonatriene, MeOH = methanol, SQT = sesquiterpenes, α -Eud = α -Eudesmol.

Infestation of pedunculate oak (<i>Quercus robur</i>) by European gypsy moth (<i>Lymantria dispar</i>) based on Copolovici et al. (2017).						
VOC	$\varepsilon_{i,\mathcal{A}}$ ($\text{nmol m}^{-2} \text{s}^{-1}$)	$\varepsilon_{i,0}$ ($\text{nmol m}^{-2} \text{s}^{-1}$)	A ($\text{nmol m}^{-2} \text{s}^{-1}$)	B	C ($\text{nmol m}^{-2} \text{s}^{-1}$)	
ISO	$\varepsilon_{i,0} + \frac{\mathcal{A} \times A}{B + \mathcal{A}}, 0 \leq \mathcal{A} \leq 60$ $\varepsilon_{i,60} \times 0.5, 60 < \mathcal{A} \leq 80$	30.26	-47.40	34.48		
MT	$\varepsilon_{i,0} + \frac{\mathcal{A} \times A}{B + \mathcal{A}}$	$4.0 \cdot 10^{-2}$	9.22	33.42		
MeSa	$\mathcal{A} \times A$		$3.5 \cdot 10^{-3}$			
LOX	$A \times \mathcal{A}^2 + C \times \mathcal{A}$		$1.1 \cdot 10^{-3}$		$4.7 \cdot 10^{-2}$	
DMNT	$A \times \mathcal{A}^2 + C \times \mathcal{A}$		$1.0 \cdot 10^{-5}$		$1.3 \cdot 10^{-3}$	
Infection of pedunculate oak (<i>Quercus robur</i>) by oak powdery mildew (<i>Erysiphe alphitoides</i>) based on Copolovici et al. (2014)						
VOC	$\varepsilon_{i,\mathcal{A}}$ ($\text{nmol m}^{-2} \text{s}^{-1}$)	$\varepsilon_{i,0}$ ($\text{nmol m}^{-2} \text{s}^{-1}$)	A ($\text{nmol m}^{-2} \text{s}^{-1}$)	B ($\text{nmol m}^{-2} \text{s}^{-1}$)	C ($\text{nmol m}^{-2} \text{s}^{-1}$)	
ISO	$\varepsilon_{i,0} + A \times \mathcal{A} + B \times \mathcal{A}^2 + C \times \mathcal{A}^3$	10.6	-0.244	$3.69 \cdot 10^{-3}$	$-2.05 \cdot 10^{-5}$	
MT	$\varepsilon_{i,0} + A \times \mathcal{A} + B \times \mathcal{A}^2 + C \times \mathcal{A}^3$	$4.0 \cdot 10^{-2}$	$8.7 \cdot 10^{-3}$	$-7.1 \cdot 10^{-5}$	$3.7 \cdot 10^{-7}$	
MeSa	0, $\mathcal{A} = 0$ $A \times \frac{\varepsilon_{MT,\mathcal{A}}}{\varepsilon_{MT,60}}, 0 < \mathcal{A} \leq 80$		0.437			
LOX	$A + B \times \mathcal{A}$		$2.13 \cdot 10^{-3}$	$6.24 \cdot 10^{-3}$		
Infection of balsam poplar (<i>Populus balsamifera</i> var. <i>suaveolens</i>) by poplar rust (<i>Melampsora larici-populina</i>) based on Jiang et al. (2016)						
VOC	$\varepsilon_{i,\mathcal{A}}$ ($\text{nmol m}^{-2} \text{s}^{-1}$)	$\varepsilon_{i,0}$ ($\text{nmol m}^{-2} \text{s}^{-1}$)	A ($\text{nmol m}^{-2} \text{s}^{-1}$)	B ($\text{nmol m}^{-2} \text{s}^{-1}$)	C	E ($\text{nmol m}^{-2} \text{s}^{-1}$)
ISO	$A + \frac{B}{C + \mathcal{A}}$		12.3	366.8	4.98	
MT	0.0625, $\mathcal{A} = 0$		0.112	$1.84 \cdot 10^{-3}$		$1.5 \cdot 10^{-4}$

	$A + B \times \text{Æ} + E \times \text{Æ}^2, 0 < \text{Æ} \leq 80$					
MeSa	$A \times \text{Æ} + B \times \text{Æ}^2 + E \times \text{Æ}^3$		$6.32 \cdot 10^{-3}$	$-8.6 \cdot 10^{-5}$		$5.75 \cdot 10^{-7}$
LOX	$0.4814, \text{Æ} = 0$ $(A + B \times \text{Æ} + E \times \text{Æ}^2) \times C, 0 < \text{Æ} \leq 80$		2.51	$-2.51 \cdot 10^{-2}$	$0.76, 0 < \text{Æ} < 30$ $0.85, 30 \leq \text{Æ} < 60$ $0.93, 60 \leq \text{Æ} \leq 80$	$3.25 \cdot 10^{-3}$
DMNT	$\varepsilon_{DMNT,60} \times \frac{\varepsilon_{MeSa,\text{Æ}}}{\varepsilon_{MeSa,60}}, 0 \leq \text{Æ} < 60$ $\varepsilon_{MeSa,\text{Æ}} \times C, 60 \leq \text{Æ} \leq 80$				0.36	
MeOH	$\varepsilon_{i,0} + A \times \text{Æ} + B \times \text{Æ}^2$	16.9	-0.338	$1.36 \cdot 10^{-2}$		
SQT	$\varepsilon_{SQT,60} \times \frac{\varepsilon_{MeSa,\text{Æ}}}{\varepsilon_{MeSa,60}}, 0 \leq \text{Æ} < 60$ $\varepsilon_{MeSa,\text{Æ}} \times C, 60 \leq \text{Æ} \leq 80$				2.414	
α -Eud	$\varepsilon_{\alpha-Eud,60} \times \frac{\varepsilon_{MeSa,\text{Æ}}}{\varepsilon_{MeSa,60}}, 0 \leq \text{Æ} < 60$ $\varepsilon_{MeSa,\text{Æ}} \times C, 60 \leq \text{Æ} \leq 80$				0.397	
Infestation of mountain birch (<i>Betula pubescens</i> var. <i>pumila</i>) by autumnal moth (<i>Epirrita autumnata</i>) based on Yli-Pirilä et al. (2016)						
VOC	$\varepsilon_{i,\text{Æ}}$ (nmol m ⁻² s ⁻¹)	A	B	C	E (nmol m ⁻² s ⁻¹)	LMA _f
MT	$\left(A + \frac{\text{Æ} \times B}{\sqrt{1 + \frac{B^2 \times \text{Æ}^2}{C^2}}} \right) \times E \times \text{LMA}_f$	$7.65 \cdot 10^{-2}$	$9.33 \cdot 10^{-3}$	0.2146	0.769	2.23
LOX	$(A \times \text{Æ} + B) \times E \times \text{LMA}_f$	$6.325 \cdot 10^{-3}$	$4.868 \cdot 10^{-2}$		0.8	2.23
DMNT	$\left(A + \frac{\text{Æ} \times B}{\sqrt{1 + \frac{B^2 \times \text{Æ}^2}{C^2}}} \right) \times E \times \text{LMA}_f$	$7.11 \cdot 10^{-4}$	$3.39 \cdot 10^{-4}$	$8.63 \cdot 10^{-3}$	0.769	2.23
SQT	$\frac{\varepsilon_{MT,\text{Æ}}}{3}$					

275

276 2.5 Meteorological conditions

277 The daily maximum radiation during the entire growing season was fixed to 1000 $\mu\text{mol m}^{-2} \text{s}^{-1}$ (Table 2), which corresponds
278 to the average maximum photosynthetic photon flux density (PPFD) observed at the SMEAR I station during the growing
279 seasons of 2015-2017 (Aalto et al., 2019). The daily pattern of PPFD then follows the solar zenith angle. For simulations of
280 mountain birch, we utilised the maximum and minimum mean temperatures on every day in the growing season during 2015-
281 2017 observed at 9 m at the SMEAR I station (Aalto et al., 2019). The daily maximum and minimum temperatures ranged
282 from 9.8 to 19.6 °C, and from 2.0 to 11.3 °C, respectively, in the time period of interest (6th of June - 20th of August, Fig. 4a).

283 For simulations of oak and poplar, we utilised the maximum and minimum temperatures for southern Germany averaged over
 284 the past three decades (data obtained via [https://www.currentresults.com/Weather/Germany/average-annual-](https://www.currentresults.com/Weather/Germany/average-annual-temperatures.php)
 285 [temperatures.php](https://www.currentresults.com/Weather/Germany/average-annual-temperatures.php)). This was done due to availability and restriction of data obtained at the Hohenpeißenberg Meteorological
 286 Observatory and since our aim was not as such to simulate the atmospheric impact at Hohenpeißenberg, but instead at any
 287 relevant location, i.e. where oaks and poplars, including the biotic stresses of interests, are common. The monthly averaged
 288 daily maximum and minimum temperatures ranged from 15 to 26 °C, and from 6 to 16 °C, respectively, in the time period of
 289 interest (April - September, Fig. 4b). For simplicity, the daily temperature pattern followed that of the solar zenith angle with
 290 a forward shift of 1 h. The default daytime mixing length was kept constant to a value of 700 m (simulations of mountain
 291 birch) and 2000 m (simulations of oak and poplar) above ground level (Seidel et al., 2012) (Table 2).

292
 293 **Table 2.** Model inputs. Representative summer time conditions in rural central Europe (here indicated by HPB: the
 294 Hohenpeißenberg Meteorological Observatory) and Lapland (here indicated by the SMEAR I station), used as default model
 295 input. The conditions are chosen such that they are realistic and representative, but they do not inhibit the formation of new
 296 particles. The concentrations of OH and sulfuric acid are provided as daily maxima in the table, but their concentrations
 297 decrease as a function of the decrease in solar light in the simulations. The concentration of ozone and the condensation sink
 298 (CS) are both kept constant throughout the simulations. BHL is the planetary boundary layer height. The photosynthetic photon
 299 flux density (PPFD) is provided as the daily maximum in the table, but the daily pattern of PPFD follows the solar zenith angle
 300 in the model.

	HPB	SMEAR I
[O ₃] (ppb)	45	30
[OH] _{max} (molec cm ⁻³)	6·10 ⁶	8·10 ⁵
[H ₂ SO ₄] _{max} (molec cm ⁻³)	1·10 ⁷	2.5·10 ⁶
CS (s ⁻¹)	2.5·10 ⁻³	7·10 ⁻⁴
BLH (m)	2000	700
PPFD _{max} (μmol m ⁻² s ⁻¹)	1000	

301

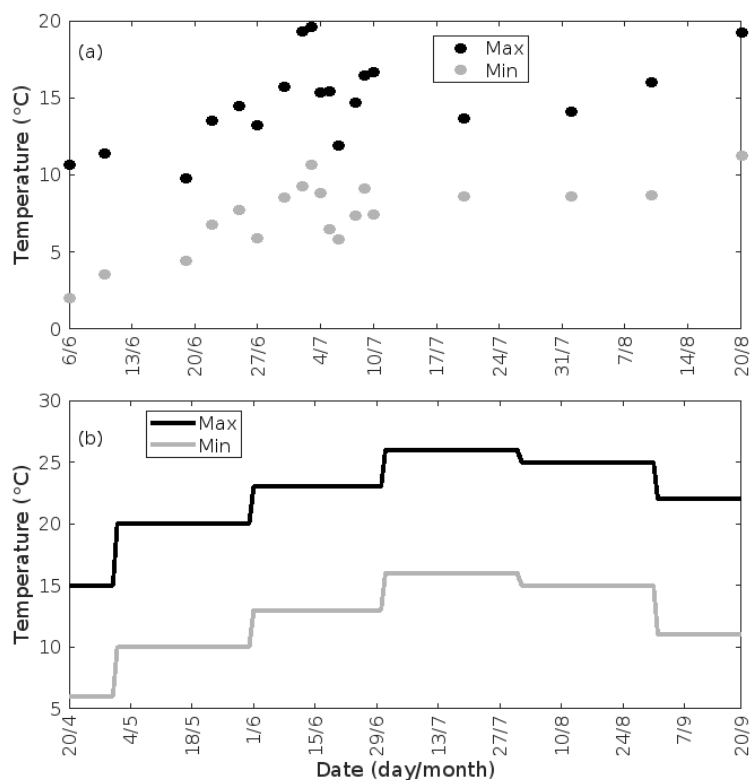


Figure 4. Daily maximum and minimum temperatures throughout the growing season at **(a)** SMEAR I, Lapland, and **(b)** Southern Germany, used as default model input. Note the different time axes.

2.6 Atmospheric gas phase chemistry

Similarly to previous atmospheric modelling studies of herbivory (Bergström et al., 2014; Douma et al., 2019), we constrained the concentrations of atmospheric oxidants within the model, though in reality, the concentration of atmospheric oxidants can decrease or increase depending on changes in the concentrations of individual specific VOCs (Table 3). This was done, partly because it is difficult to accurately predict the concentration of oxidants (e.g. Di Carlo et al., 2004; Sinha et al., 2010; Mogensen et al., 2011, 2015; Nölscher et al., 2012, 2016; Zannoni et al., 2016; Praplan et al., 2019; Lelieveld et al., 2008; Taraborrelli et al., 2012), and partly because accounting for varying oxidant concentrations is not necessary for the objectives of our study (Sec. 3.2, Fig. 11a-b,f-g,k-l,p-q). Thus, in our simulations, the default daily maximum concentration of OH is therefore fixed to $6 \cdot 10^6$ molec cm^{-3} (Petäjä et al., 2009) and $8 \cdot 10^5$ molec cm^{-3} (calculated using observed summertime UVB radiation from the SMEAR I station and the proxy presented by Petäjä et al. (2009)) for simulations of Hohenpeißenberg and Lapland, respectively (Table 2). The daily pattern of the OH concentration then follows the solar zenith angle. The concentration of ozone is kept constant to a value of 45 ppb (Naja et al., 2003) and 30 ppb (Ruuskanen et al., 2003) for simulations of oak and poplar (Hohenpeißenberg conditions) and mountain birch (SMEAR I conditions), respectively (Table 2). NO_3 was not considered, since emission and atmospheric processes were only simulated during day time, when the concentration of NO_3 is insignificant.

The only source of sulfuric acid (H_2SO_4), in our model, is the reaction between OH and SO_2 , while the only sink is the condensation sink. The concentration of SO_2 is chosen such that the default daytime maximum concentration of H_2SO_4 is $1 \cdot 10^7$ molec cm^{-3} in Hohenpeißenberg (Petäjä et al., 2009; Birmili et al., 2003) and $2.5 \cdot 10^6$ molec cm^{-3} in Lapland (Kyrö et al., 2014) (Table 2). The size distribution of the pre-existing particle population is kept fixed during the simulations, so the number concentration of pre-existing particles is defined by the condensation sink (CS), which is kept constant to a value of $2.5 \cdot 10^{-3} \text{ s}^{-1}$ (in rural southern Germany) and $7 \cdot 10^{-4} \text{ s}^{-1}$ (in Lapland; Dal Maso et al., 2007; Vana et al., 2016) (Table 2).

327 We included reactions for the atmospheric oxidation of SO₂ and the emitted VOCs (Appendix C). Certain VOCs, and
 328 especially VOCs with endocyclic double bonds, can form HOM (highly oxygenated organic molecules) upon oxidation by, in
 329 particular O₃, but also OH and NO₃ (e.g. Ehn et al., 2012, 2014; Jokinen et al., 2015; Berndt et al., 2016; Bianchi et al., 2019;
 330 Zhao et al., 2020). HOM have been found to be a major component of secondary organic aerosol (e.g. Ehn et al., 2014; Mutzel
 331 et al., 2015). HOM yields are specific to individual molecules and isomers and most yields have not been investigated for the
 332 exact compounds, which are emitted from the tree species considered in this study. Thus, the yields applied for the production
 333 of HOM in the model (Appendix C) are connected with a large degree of uncertainty. The influence of changing HOM yields
 334 on our results was therefore also investigated (Sec. 3.2, Fig. 11e,j,o,t). Formation of oxygenated organics from oxidation of
 335 sesquiterpenes and methyl salicylate are also included (Appendix C). The sum of all organic compounds, which contribute to
 336 aerosol processes, is referred to as “OxOrg”.

337

338 **Table 3.** Common changes in the atmospheric concentrations of volatile organic compounds (VOC) and OH during biotic
 339 plant stress. LOX are lipoxygenase pathway volatile compounds.

	Change in VOC concentration	Change in OH concentration	Reference
Stress↑	[LOX]↑ [methyl salicylate]↑ [methanol]↑ [monoterpenes]↑	[OH]↓	Mentel et al. (2013) Calvert et al. (2000) Atkinson et al. (1992) Hakola et al. (1994)
	[sesquiterpenes]↑	[OH]↑	Atkinson and Arey (2003) Winterhalter et al. (2009)
	[isoprene]↓	[OH]?, but most probably [OH]↑	Lelieveld et al. (2008) Taraborrelli et al. (2012) Wells et al. (2020)

340

341 2.7 Calculation of the formation and growth of secondary organic aerosol particles

342 The clustering and activation of new particles are expressed by a formation rate of neutral 2 nm sized clusters, J_2 (cm⁻³ s⁻¹),
 343 which is computed by Eq. 20, using coefficients (α_{1-3}) from Table 3, both found in Paasonen et al. (2010):

$$344 J_2 = \alpha_1 \times [\text{H}_2\text{SO}_4]^2 + \alpha_2 \times [\text{H}_2\text{SO}_4][\text{OxOrg}] + \alpha_3 \times [\text{OxOrg}]^2 \quad (2)$$

345 It is here assumed that new particles are formed via heteromolecular homogeneous nucleation between sulfuric acid and
 346 oxidised organic compounds (OxOrg) as well as via homogeneous nucleation of sulfuric acid and OxOrg alone. For
 347 simplification, we only operated with one growing aerosol mode and therefore included a unit-less correction term (KK),
 348 which determines how large a fraction of the activated clusters reaches the growing mode (Kerminen and Kulmala, 2002):

$$349 \text{KK} = \exp(\eta \times [1/D_p - 1/D_{clus}]) \quad (3)$$

350 where D_p and D_{clus} are the diameters of the growing mode and clusters, respectively, and $D_{clus} = 2$ nm as stated above. Further,
 351 η (nm) is (Eq. 11-12 and Table 1 in Kerminen and Kulmala, 2002):

$$352 \eta = 1830 \text{ nm}^2 \cdot \text{s} \cdot \text{h}^{-1} \times \text{CS}/\text{GR} \quad (4)$$

353 where CS (s⁻¹) is the condensation sink. When used together with Eq. 3, the value of CS is that of sulfuric acid. The
 354 condensational particle diameter growth rate (GR, nm h⁻¹) of newly formed 2-3 nm particles is calculated according to
 355 Nieminen et al. (2010):

$$356 \text{GR}_{2-3 \text{ nm}} = 0.5 \text{ nm} \cdot \text{h}^{-1} \times \text{CC} \times 10^{-7} \text{ cm}^3 \quad (5)$$

357 where CC is the concentration of condensable vapours which we assumed to be the sum of sulfuric acid and OxOrg. In addition,
 358 we assumed that the molar mass of OxOrg are 3.5 times larger than that of sulfuric acid (Ehn et al., 2014), hence:

$$359 \quad CC = [H_2SO_4] + [OxOrg] \times 3.5^{1/3} \quad (6)$$

360 It is a complex matter to model nanoparticle growth, especially in forested environments, since thousands of individual
 361 molecules with different vapour pressures contribute to the growth, but particle growth rates have been observed to be strongly
 362 size-dependent in the field (Hirsikko et al., 2005; Yli-Juuti et al., 2011; Häkkinen et al., 2013). Hence, we accounted for this
 363 size-dependency by enhancing the growth rates of particles larger than 3 nm, as according to Hirsikko et al. (2005) and Yli-
 364 Juuti et al. (2011):

$$365 \quad GR_{3-7 \text{ nm}} = 2 \times GR_{2-3 \text{ nm}} \quad (7)$$

$$366 \quad GR_{>7 \text{ nm}} = 2.3 \times GR_{2-3 \text{ nm}} \quad (8)$$

367 The increase in the diameter of the growing mode (D_p) is defined by the growth rate:

$$368 \quad \Delta D_p / \Delta t = GR / 3600 \text{ s} \cdot \text{h}^{-1} \quad (9)$$

369 while the increase in the number of new particles (N_p , cm^{-3}) is determined by the formation of new particles which reaches
 370 the growing mode and the coagulation of particles in the growing mode by:

$$371 \quad \Delta N_p / \Delta t = J_2 \times KK - \text{CoagS} \times N_p \quad (10)$$

372 where the coagulation sink (CoagS , s^{-1}) is calculated according to (Lehtinen et al., 2007):

$$373 \quad \text{CoagS} = \text{CS} \times (0.71 \text{ nm} / D_p)^{1.6} \quad (11)$$

374

375 **3 Results and discussion**

376 **3.1 Simulations of biotically stressed and non-infected forest stands throughout a growing season**

377 Simulation results of one full growing season from various non-infected, and moderately and severely infected forest stands
 378 are presented in Figs. 5-9. In the figures, emissions, concentrations, the isoprene-to-monoterpenes carbon concentration ratio
 379 ($R = [\text{isoprene C}] / [\text{monoterpenes C}] = 0.5 \cdot [\text{isoprene}] / [\text{monoterpenes}]$), the formation and growth rates, and number of newly
 380 formed particles are expressed as median values during 10:00-16:00 local time, while the particle diameter of the growing
 381 mode is provided as the daily maximum. We underline that our modelling study is of a conceptual character and that the
 382 modelling results therefore also should be treated accordingly. Modelling results are compared in detail to observations in the
 383 sections below in order to put our findings into perspective.

384

385 **3.1.1 Canopy emissions of VOCs**

386 The emissions of VOCs (Figs. 5a,c,e,g, 7a,b, 8a,b, 9a-c) change throughout the season due to variations in temperature, light,
 387 LAI and infection severity. The impact of leaf maturity development on emission predictions are presented in Appendix B and
 388 its atmospheric relevance discussed in Sec. 3.2. Canopy emissions of VOCs are highly different from non-infected and infected
 389 forest stands, due to plant stress responses, but also due to a decrease in LAI in case of larval infestations (Figs. 5a,c,e, g, 9a-
 390 c). Constitutive isoprene emitters (i.e. oak and poplar) decrease their emissions of isoprene significantly during the episodes
 391 of biotic stress, and a stronger reduction is observed as a function of an increase in stress severity (Figs. 5a, 7a, 8a). All
 392 investigated stresses cause the plants to increase their emissions of monoterpenes greatly (Figs. 5c, 7b, 8b, 9a). The induction
 393 in the emissions of monoterpenes increases as a function of stress severity per unit leaf area, but the LAI simultaneously
 394 decreases in case of larval infestations, which result in smaller canopy scale emissions from severely defoliated stands
 395 compared to moderately stressed stands (Figs. 5c, 9a). Also the emissions of compounds, and groups of compounds, such as
 396 methyl salicylate, LOX, methanol, DMNT, sesquiterpenes and oxygenated sesquiterpenes are significantly increased as a result
 397 of biotic plant stress (Figs. 5e,g, 7a,b, 8a,b, 9b,c). These compounds, together with monoterpenes, are in most cases not emitted
 398 constitutively at all or only in very small abundances from the considered tree species. Though the emissions of all induced

399 VOCs increase as a function of the degree of damage, the responses to the level of stress severity are not necessarily the same
400 for all VOCs and all individual stresses. This difference can, for example, be seen in the emissions of monoterpenes (Fig. 5c)
401 and LOX compounds (Fig. 5e) from gypsy moth infested oak forests, which do not peak at the same time in the season.

402

403 3.1.2 Ambient concentrations of VOCs and OxOrg

404 Since the concentrations of OH and O₃ are constrained within the simulations, the VOC emission patterns are reflected in the
405 concentration patterns (Figs. 5b,d,f,h, 7c-e, 8c-e, 9e-g). All VOCs, except LOX and methanol, contribute to the formation of
406 OxOrg (Figs. 6a, 7c, 8c, 9d), but the contributions from oxidation of the individual VOCs, or groups of VOCs, vary between
407 the various stress cases and infection severity levels due to differences in emission rates and OxOrg forming yields (Appendix
408 C). For example, in herbivory infested stands, OxOrg originating from monoterpenes make up by far the largest fraction of
409 total OxOrg. This is mainly due to the fact that the induced emissions of monoterpenes are significantly higher than the
410 emissions of other VOCs which contribute to OxOrg formation (Figs. 5c,g, 9a,c). In case of oak powdery mildew infected oak,
411 HOM from monoterpenes and oxygenated organics from methyl salicylate reactions contribute about evenly to the total OxOrg.
412 The reason for this is that the canopy emissions of these VOCs are roughly similar (Fig. 7a,b), the OxOrg yield of methyl
413 salicylate is significantly higher than that of monoterpenes, but oxidation of methyl salicylate is correspondingly slower
414 (Appendix C). The main contributor to the total OxOrg in poplar rust infected poplar stands is sesquiterpenes. Contributions
415 from methyl salicylate, DMNT and α -Eudesmol to total OxOrg are individually rather small, but together, they are close to
416 matching the contribution from monoterpenes. When emissions of sesquiterpenes are omitted from simulations of a severely
417 rust infected poplar stand, the concentration of OxOrg decreases with ~46 %, while, in comparison, the concentration of OxOrg
418 decreases with ~30 % if the emissions of monoterpenes are instead excluded.

419 In the simulations, the daily median (10:00-16:00) ambient concentration of OxOrg is at maximum $\sim 4.2 \times 10^7 \text{ cm}^{-3}$ in
420 a gypsy moth infested oak stand (Fig. 6a), $\sim 1.1 \times 10^7 \text{ cm}^{-3}$ in an oak powdery mildew infected oak stand (Fig. 7c), $\sim 4.2 \times 10^7$
421 cm^{-3} in a rust infected poplar stand (Fig. 8c), and $\sim 3.3 \times 10^7 \text{ cm}^{-3}$ in an autumnal moth infested mountain birch stand (Fig. 9d).
422 The ambient concentration of OxOrg is much higher in gypsy moth infested oak stands, than in a non-infested oak stand,
423 during the period of stress (Fig. 6a). When the period of feeding has been concluded, the concentration of OxOrg is higher in
424 non-infested oak stands than in stands that have been exposed to stress due to a higher LAI. However, the concentration of
425 OxOrg is then only ~15-20 % of the OxOrg concentration during the period of stress and it is almost exclusively composed of
426 HOM originating from isoprene. The concentration of OxOrg increases as a function of fungal infection severity, and in our
427 simulations the concentration of OxOrg is higher in fungally infected stands by a factor of up to ~6.9 (oak powdery mildew
428 infected oak stands, Fig. 7c) and ~3.3 (poplar rust infected poplar stands, Fig. 8c). Since the investigated poplar species is a
429 great constitutive isoprene emitter, relatively high concentrations of OxOrg are predicted for the non-infested poplar stand
430 (Fig. 8c). In mountain birch stands, the concentration of OxOrg is up to 2-2.5 times higher in autumnal moth infested stands
431 during the feeding period than in a non-infested birch stand (Fig. 9d). The difference in OxOrg concentration between
432 moderately and severely infested birch stands is small, due to the combined effects of stress response (which is a function of
433 the degree of damage) and LAI reduction (Fig. 9d), but towards the conclusion of the feeding period, the concentration of
434 OxOrg is significantly higher in the less defoliated stand.

435

436 3.1.3 Formation of new particles

437 New particles are assumed to be formed from OxOrg and sulfuric acid (Sec. 2.7, Eq. 2). Since the concentration of sulfuric
438 acid is constrained within the simulations, the concentration pattern of OxOrg is reflected in the seasonal pattern of the
439 formation rates (Figs. 6c-e, 7f, 8f, 9h,i). Thus, in case of gypsy moth infested oak, the formation rates are much higher (increase

440 by up to a factor of ~ 5 (J_2), ~ 7 (J_3), and ~ 11 (J_{10}) in stressed stands than in non-infested stands during the period when the
441 plants are exposed to stress (Figs. 6c-e). The predicted J_2 in gypsy moth infested oak stands is comparable to e.g. observations
442 from Melpitz, Germany ($\sim 9.4 \text{ cm}^3 \text{ s}^{-1}$, Paasonen et al., 2010) and San Pietro Capofiume, Italy ($\sim 13 \text{ cm}^3 \text{ s}^{-1}$, Paasonen et al.,
443 2010). Both Melpitz and San Pietro Capofiume are rural sites influenced by anthropogenic pollution (Paasonen et al., 2010).
444 The modelled J_2 in a non-infested oak stand is comparable to observations from Hohenpeissenberg ($\sim 2.3 \text{ cm}^3 \text{ s}^{-1}$, Paasonen et
445 al., 2010) and similar or even higher than typical formation rates measured in the boreal Scots pine forest in Hyytiälä, Finland
446 ($\sim 1\text{-}2 \text{ cm}^3 \text{ s}^{-1}$, Paasonen et al., 2010; Kulmala et al., 2012, 2013; Vana et al., 2016) and in the hemiboreal forest in Järveljä,
447 Estonia ($\sim 1.09 \pm 1.06 \text{ cm}^3 \text{ s}^{-1}$, Vana et al., 2016). By analysing data from Hyytiälä and Järveljä, Vana et al. (2016) showed that
448 the values of J_3 were in general about 60-80 % of those of J_2 . Our simulations of a non-infested oak stand follow this threshold,
449 thus, the predicted J_3 in a non-infested oak stand is somewhat higher than observations from Hyytiälä ($\sim 0.6 \text{ cm}^3 \text{ s}^{-1}$, Kulmala
450 et al., 2012, 2013; Nieminen et al., 2014; Vana et al., 2016) and Järveljä ($\sim 0.8 \text{ cm}^3 \text{ s}^{-1}$, Vana et al., 2016). J_3 in gypsy moth
451 infested oak stands is high, but similar values have occasionally been observed in Hyytiälä (up to about $10 \text{ cm}^3 \text{ s}^{-1}$, Nieminen
452 et al., 2014). Formation rates of 5 nm particles ($J_5=1.0 \pm 1.1 \text{ cm}^3 \text{ s}^{-1}$, Yu et al., 2014) measured in an oak forest in Missouri,
453 USA, are much less than J_{10} in our simulated infested stands, and so are e.g. also formation rates of 10 nm particles ($J_{10}=1.2$
454 $\text{cm}^3 \text{ s}^{-1}$, Yli-Juuti et al., 2009) measured in a mixed forest in K-pusztá, rural Hungary. Thus, the predicted formation rates in a
455 non-infested oak stand are comparable, and in the case of gypsy moth infested oak stands, often much higher than observations
456 from forests with intense new particle formation events.

457 The formation rates of new particles are always higher in oak powdery mildew infected oak stands than in a non-
458 infected oak stand (Fig. 7f), though the fungus is not able to perturb the formation rates as strongly (increase by up to a factor
459 of ~ 2.3 (J_2), ~ 3.0 (J_3), and ~ 5.3 (J_{10})) as herbivory by gypsy moth larvae.

460 Simulations of poplar stands suggest that particles will be formed at high rates in the range $\sim 3.6\text{-}11.4 \text{ cm}^3 \text{ s}^{-1}$ (J_2) and
461 $\sim 2.7\text{-}10.6 \text{ cm}^3 \text{ s}^{-1}$ (J_3) during the late summer when the full leaf state has been attained, and our simulations suggest that new
462 particles will be formed the fastest in severely rust infected stands (increase by up to a factor of ~ 3.2 (J_2), and ~ 3.9 (J_3)).

463 In our simulations, herbivory by autumnal moth increases the formation rates of new particles in mountain birch
464 stands by up to a factor of ~ 2.5 (J_2) and ~ 2.6 (J_3). The formation rates of 2 and 3 nm particles are predicted to vary between
465 $0.38 \text{ cm}^3 \text{ s}^{-1}$ and $2.5 \text{ cm}^3 \text{ s}^{-1}$ (J_2), and $0.31 \text{ cm}^3 \text{ s}^{-1}$ and $2.5 \text{ cm}^3 \text{ s}^{-1}$ (J_3) in stressed stands, and between $0.32 \text{ cm}^3 \text{ s}^{-1}$ and 1.1
466 $\text{cm}^3 \text{ s}^{-1}$ (J_2), and $0.26 \text{ cm}^3 \text{ s}^{-1}$ and $0.99 \text{ cm}^3 \text{ s}^{-1}$ (J_3) in non-infested stands. The higher end of these values is comparable to
467 rates observed in Hohenpeissenberg and Hyytiälä (see above). Kyrö et al. (2014) reported that the monthly averaged formation
468 rate of 3 nm particles during 2005 - 2011, at the SMEAR I station in Värriö, varied throughout the year by $0.04\text{-}0.45 \text{ cm}^3 \text{ s}^{-1}$,
469 and by $0.16\text{-}0.23 \text{ cm}^3 \text{ s}^{-1}$ during the summer months. Analysis of years 2013 and 2014, also in Värriö, led to a median formation
470 rate of $0.14 \pm 0.05 \text{ cm}^3 \text{ s}^{-1}$ (J_3) (Vana et al., 2016). Thus, the predicted formation rates in, especially, non-infested mountain
471 birch stands in Lapland are generally within range, but often somewhat higher than observations from the same location. It
472 should, though, be mentioned that these literature values cannot be used to validate our simulation results, since Scots pines,
473 and not mountain birches, dominate the SMEAR I site (Kyrö et al., 2014), and the LAI of mountain birches at the station is
474 significantly less than $2 \text{ m}^2 \text{ m}^{-2}$ (Ylivinkka et al., 2020). The modelled formation rates are not compared to observations from
475 the mountain birch dominated areas in Lapland, since such observations do not, to our knowledge, exist.

476 A very recent investigation of long-term field observations (25 years) from the SMEAR I station (Ylivinkka et al.,
477 2020), where autumnal moth larvae are prominent defoliators of mountain birches, did, however, not find any evidence that
478 herbivory by autumnal moth would enhance the formation, nor growth, of atmospheric aerosol particles during the summer of
479 infestation. Instead there was some evidence of elevated total particle concentrations for a few years after summers with larval
480 infestation, which was speculated to be caused by delayed defense responses of mountain birches. It is, however, possible that
481 the total foliage mass of mountain birches in the area is too small, or that the level of infestation was too low during the
482 investigated time period, in order to cause detectable changes in aerosol variables (Ylivinkka et al., 2020).

483 The amount of newly formed particles is predicted to be up to about one order of magnitude higher in a gypsy moth
484 infested oak stand than in a non-infested oak stand, with a 10:00-16:00 median of up to $\sim 1.4 \times 10^5 \text{ cm}^{-3}$ in an infested stand
485 (Fig. 6f). Such a high production of new particles is comparable to observations from e.g. Melpitz (Größ et al., 2018). The
486 number of produced particles in a non-infested oak stand ($\sim 1.1 \times 10^4 \text{ cm}^{-3}$; Fig. 6f) is comparable to e.g. the number of new
487 particles produced during a typical new particle formation event in Hyytiälä ($\sim 1\text{-}2 \times 10^4 \text{ cm}^{-3}$; Dal Maso et al., 2008; Nieminen
488 et al., 2014), but significantly higher than observations from a Missouri oak forest, where sub-5 nm particles were measured
489 to be up to $\sim 2 \times 10^4 \text{ cm}^{-3}$, and 5-25 nm particles to $\sim 3000 \text{ cm}^{-3}$, during typical new particle formation events (Yu et al., 2014).
490 After the period of stress, the number of particles in the growing mode is predicted to range between $\sim 7 \times 10^3 \text{ cm}^{-3}$ and $\sim 17 \times 10^3$
491 cm^{-3} in a non-infested stand, $\sim 6 \times 10^3 \text{ cm}^{-3}$ and $\sim 12 \times 10^3 \text{ cm}^{-3}$ in a 30 % defoliated stand and between $\sim 3 \times 10^3 \text{ cm}^{-3}$ and $\sim 5 \times 10^3$
492 cm^{-3} in a 80 % defoliated oak stand (Fig. 6f). Oak powdery mildew is predicted to enhance the number of particles in the
493 growing mode by up to a factor of ~ 4 compared to the corresponding non-infected stand, resulting in a maximum of $\sim 1.7 \times 10^4$
494 cm^{-3} in an infected stand, under the used border conditions (Fig 7g). Under the same environmental conditions, a severely
495 poplar rust infected poplar stand is predicted to produce up to about five times as many new particles as a non-infected poplar
496 stand, leading to a maximum of about $1.1 \times 10^5 \text{ cm}^{-3}$ in a severely infected stand (Fig 8h). Finally, it is predicted that herbivory
497 by autumnal moth enhances the amount of produced particles by up to a factor of ~ 2.7 , with a maximum number of particles
498 in the growing mode of $\sim 3 \times 10^4 \text{ cm}^{-3}$ in an infested birch stand (Fig. 9j). The predicted amount of particles in a non-infested
499 mountain birch stand is in the same order as observations from Finnish Lapland (Komppula et al., 2006).

500

501 3.1.4 New particle growth

502 New particles are assumed to grow by sulfuric acid and OxOrg (Sec. 2.7, Eq. 5-8), hence the seasonal patterns of formation
503 rates and OxOrg concentration are reflected in the pattern of the growth rates (Figs. 6g, 7h, 8g, 9k), and therefore also in the
504 season pattern of the number (Figs. 6f, 7g, 8h, 9j) and size (Figs. 6h, 7g, 8g, 9l) of the growing particle mode. We predict that
505 the 10:00-16:00 median growth rate in a gypsy moth infested oak stand is at maximum $\sim 5.9 \text{ nm h}^{-1}$ under the assumed boundary
506 conditions, whereas the corresponding growth rate in a non-infested oak stand is around 1.6 nm h^{-1} , when the full leaf state has
507 been attained (Fig. 6g). For comparison, the growth rate of new particles has been reported to range from 0.5 to 12 nm h^{-1} in
508 Hyytiälä (Dal Maso et al., 2007), with median values of 2.1 nm h^{-1} (Vana et al., 2016), 2.5 nm h^{-1} (Dal Maso et al., 2007), and
509 3.3 nm h^{-1} (Paasonen et al., 2010), depending on which years the data covered. Dal Maso et al. (2007) reported that the growth
510 rate of new small particles in Aspöreten, a rural site in Sweden dominated by deciduous and conifer forests and some farmlands,
511 ranged between 1 and 11 nm h^{-1} , with a median value of 3.4 nm h^{-1} . The growth rate was found to range from 2.1 to 22.9 nm h^{-1} ,
512 with a median value of 7.25 nm h^{-1} during spring in a mixed deciduous forest area close to Heidelberg in Germany, under
513 influence of anthropogenic pollution (Fiedler et al., 2005). Growth rates from an oak forest in Missouri, USA, were in the
514 range $1.6\text{-}11.2 \text{ nm h}^{-1}$ (Yu et al., 2014). Median values for the growth rate have been reported to be 4.2 nm h^{-1} in Melpitz
515 (Paasonen et al., 2010), 4.6 nm h^{-1} in Järveljä (Vana et al., 2016), 4.8 nm h^{-1} in Hohenpeißenberg (Paasonen et al., 2010) and
516 9.5 nm h^{-1} in San Pietro Capofiume (Paasonen et al., 2010). Thus, we can conclude that our predicted growth rates are
517 comparable to atmospheric observations from several different rural sites. Growth rates obtained from areas influenced by
518 anthropogenic pollution are generally higher than our simulated rates, but this is expected, since our model is constrained by
519 conditions representative for rural sites.

520 Growth rates are predicted to be lower in an oak powdery mildew infected oak forest, than in a gypsy moth infested
521 oak forest. The rates are predicted to, at maximum, be $\sim 2.0 \text{ nm h}^{-1}$ (80 % of leaf area covered by mildew), $\sim 1.6 \text{ nm h}^{-1}$ (30 %
522 of leaf area covered by mildew) and $\sim 1.2 \text{ nm h}^{-1}$ (non-infected, in the same environmental conditions as the infected trees)
523 (Fig. 7h). Thus, the growth rates are similar to the lower end of the observed range.

524 The growth of small particles in non-infected and rust infected poplar stands are predicted to range between ~ 2.1 nm
525 h^{-1} and ~ 5.7 nm h^{-1} , during the late summer when the full leaf state has been attained, with the fastest growth in a heavily rust
526 infected forest stand (Fig. 8g). This range in growth rates is thus similar to simulation results of herbivory infested oak (see
527 above; Fig. 6g).

528 The predicted growth rates are smallest in simulations of non-infested mountain birch stands in Lapland. The 10:00-
529 16:00 median growth rate is at maximum predicted to be ~ 1.4 nm h^{-1} in an infested stand and varies between ~ 0.6 nm h^{-1} and
530 ~ 2.0 nm h^{-1} in a non-infested stand (Fig. 9k). These values are in line with observations from Värriö (median: 1.6 ± 0.9 nm h^{-1} ,
531 Vana et al., 2016; monthly summer mean: 3.7-4.4 nm h^{-1} , Kyrö et al., 2014; range: 1-10 nm h^{-1} , median: 2.4 nm h^{-1} , Dal Maso
532 et al., 2007) and from Pallas, Finnish Lapland (median: 2.0 nm h^{-1} , daily range: 0.5-11 nm h^{-1} , Dal Maso et al., 2007; monthly
533 range: 1.9-4.6 nm h^{-1} , Asmi et al., 2011).

534 According to our predictions, new particles will grow up to about 46 nm larger in an oak gypsy moth infested oak
535 stand compared to a non-infested oak stand within one day (Fig. 6h). Simulation results for the other species/stressors show
536 that new particles will grow up to about 8 nm more in an oak powdery mildew infected stand (Fig. 7g), ~ 28 nm more in a
537 poplar rust infected poplar stand (Fig. 8g), and ~ 26 nm larger in an autumnal moth infested mountain birch stand (Fig. 9l),
538 within one day, compared to their corresponding non-infested stands. In our simulations, the newly formed particles in non-
539 infected oak stands are always mainly formed and grown by sulfuric acid (Figs. 6h, 7g), but in modelling of non-infested
540 poplar, more than half of the formation and growth is due to HOM originating from isoprene (Fig. 8g), while HOM formed
541 from monoterpenes account for a large fraction of the predicted formation and growth in non-infested birch stands (Fig. 9l).

543 3.1.5 R: the isoprene-to-monoterpenes carbon concentration ratio

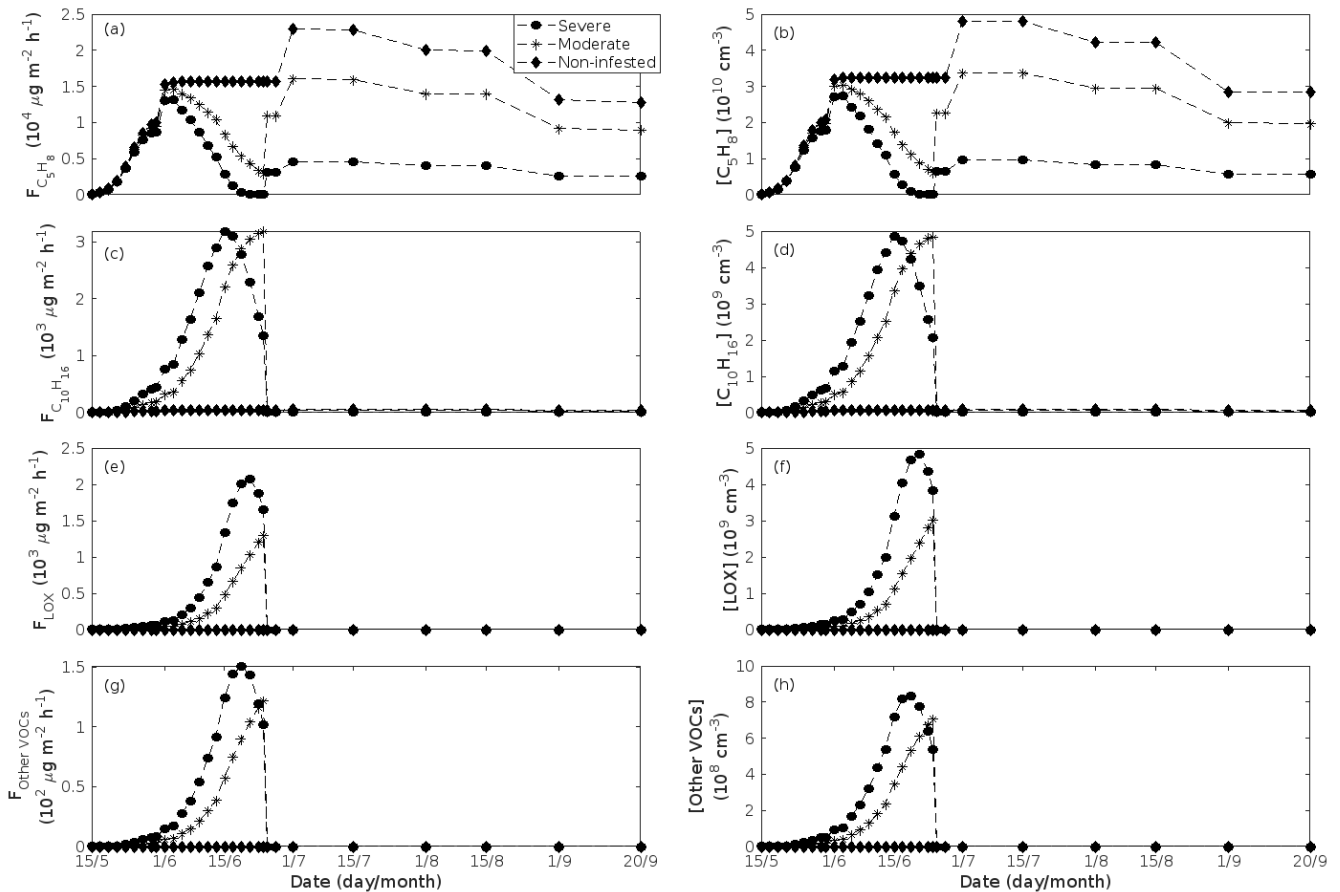
544 Previous chamber studies (Kiehl-Scharr et al., 2009, 2012; McFiggans et al., 2019; Heinritzi et al., 2020) have suggested
545 that isoprene suppresses the formation of new particles from monoterpenes when the isoprene-to-monoterpene carbon
546 concentration ratio (R) becomes too high. New particle formation has rarely been observed in the field when $R > 1$ (e.g.
547 Kanawade et al., 2011; Pöschl et al., 2010; Pöhlker et al., 2012; Lee et al., 2016). For example, Yu et al. (2014) observed
548 formation of sub-5 nm particles during 64 % of the measured days in an oak forest, though R was 15.3 ± 7.2 during the
549 campaign period. However, since the formation of new particles occurs on a regional scale, the authors suggested that the
550 detected particles could have been formed at lower R and advected to their measurement site. Contrarily, it has earlier been
551 proposed that oxidation products of isoprene (e.g. IEPOX) promote the growth of existing new particles ($D_p > 3$ nm, e.g. Surratt
552 et al., 2010; Lin et al., 2013), while Heinritzi et al. (2020) observed the growth of particles above 3.2 nm to be unaffected by
553 the concentration of isoprene. It is thus likely that the zone of R values, inside which the probability for new particle formation
554 to occur changes, is influenced by other environmental factors and is therefore location and/or season dependent.

555 New particle formation has also been observed in the upper troposphere in tropical regions (Andreae et al., 2018;
556 Williamson et al., 2019) where isoprene dominates the emission spectrum greatly. The hypothesis is that isoprene is vertically
557 transported via strong convection and new particles are formed from isoprene oxidation products, which is possible due to
558 lower temperature conditions in the upper troposphere.

559 The concentration ratio of isoprene-to-monoterpene carbon is very high in non-infested oak and poplar stands and in
560 oak stands which are no longer exposed to herbivory (Figs. 6b, 7d, 8d), and it is therefore questionable whether particles will
561 be formed at all in the atmospheric boundary layer from these stands when they are not experiencing stress. Biotic stress greatly
562 reduces R in all three cases. R is most significantly decreased to a minimum 10:00-16:00 median value of 0.004 in simulations
563 of gypsy moth infested oak stands (Fig. 6b), but the period with low R values is rather short. For example, $R < 1$ during only
564 11 and 4 days, respectively, while $R < 22.5$ (probably the highest ratio at which new particles formation has been observed in
565 the field, Yu et al., 2014) during 32 and 21 days, respectively, in our simulations of a severely and moderately European gypsy

566 moth infested oak stand (Fig. 12e). R is predicted to be close to 1, though never below 1, in simulations of both oak powdery
 567 mildew infected oak stands and rust infected poplar stands. The duration where R is e.g. less than 22.5 is 39 days in a severely
 568 mildew infected oak stand, 31 days in a moderately mildew infected oak stand, and 27 days in a severely rust infected poplar
 569 stand (Fig. 12e). For comparison, R is never predicted to be less than 22.5 in a moderately infected poplar stand (Fig. 8d).
 570 Even if new particles are not formed from oak powdery mildew or poplar rust infected stands in the boundary layer, then both
 571 the potential to form new particles in the upper troposphere (Figs. 7f,g, 8f,h) and the potential to grow already existing particles,
 572 which are formed in nearby stands and horizontally transported to the infected stands (Figs. 7g,h, 8g), are still predicted to be
 573 greater than in our simulations of the correspondingly non-infested stands. R is not relevant in the case of mountain birch,
 574 since this tree species does not emit isoprene constitutively, nor in response to herbivory stress by autumnal moth larvae (Yli-
 575 Pirilä et al., 2016; Rieksta et al., 2020).

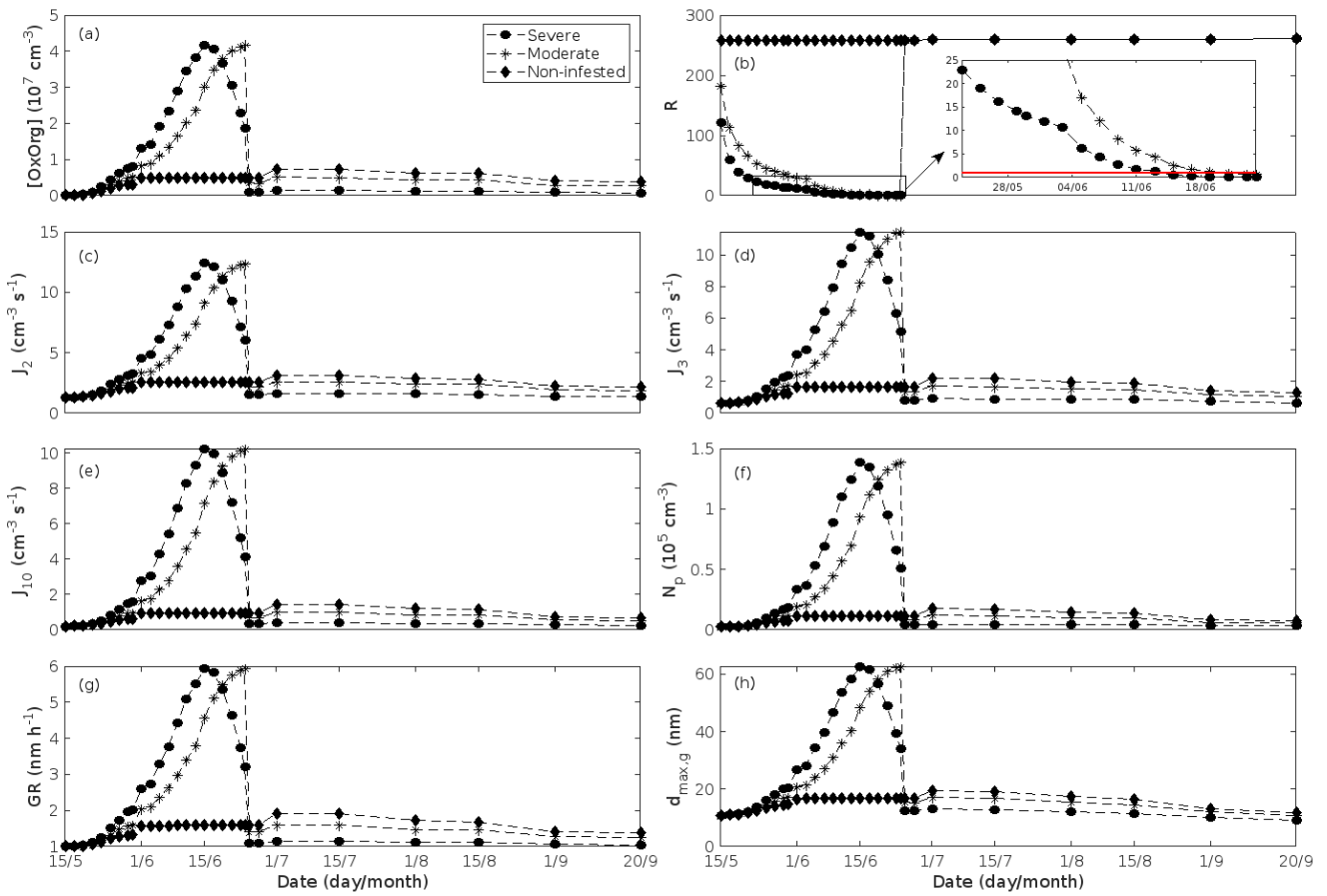
576



577

578 **Figure 5.** A pure oak stand infested with European gypsy moth larvae in comparison to a non-infested pure oak stand. Canopy
 579 emissions of (a) isoprene, (c) monoterpenes, (e) lipoxygenase pathway volatiles (LOX), and (g) the sum of other VOCs which
 580 contribute to OxOrg formation (here i.e. methyl salicylate and dimethyl-nonatriene). Atmospheric concentrations of (b)
 581 isoprene, (d) monoterpenes, (f) lipoxygenase pathway volatiles, and (h) the sum of other VOCs which contribute to OxOrg
 582 formation. “Moderately” and “severely” refer to 30 % and 80 %, respectively, of the leaf area that has been consumed by the
 583 end of the feeding period.

584



585

586

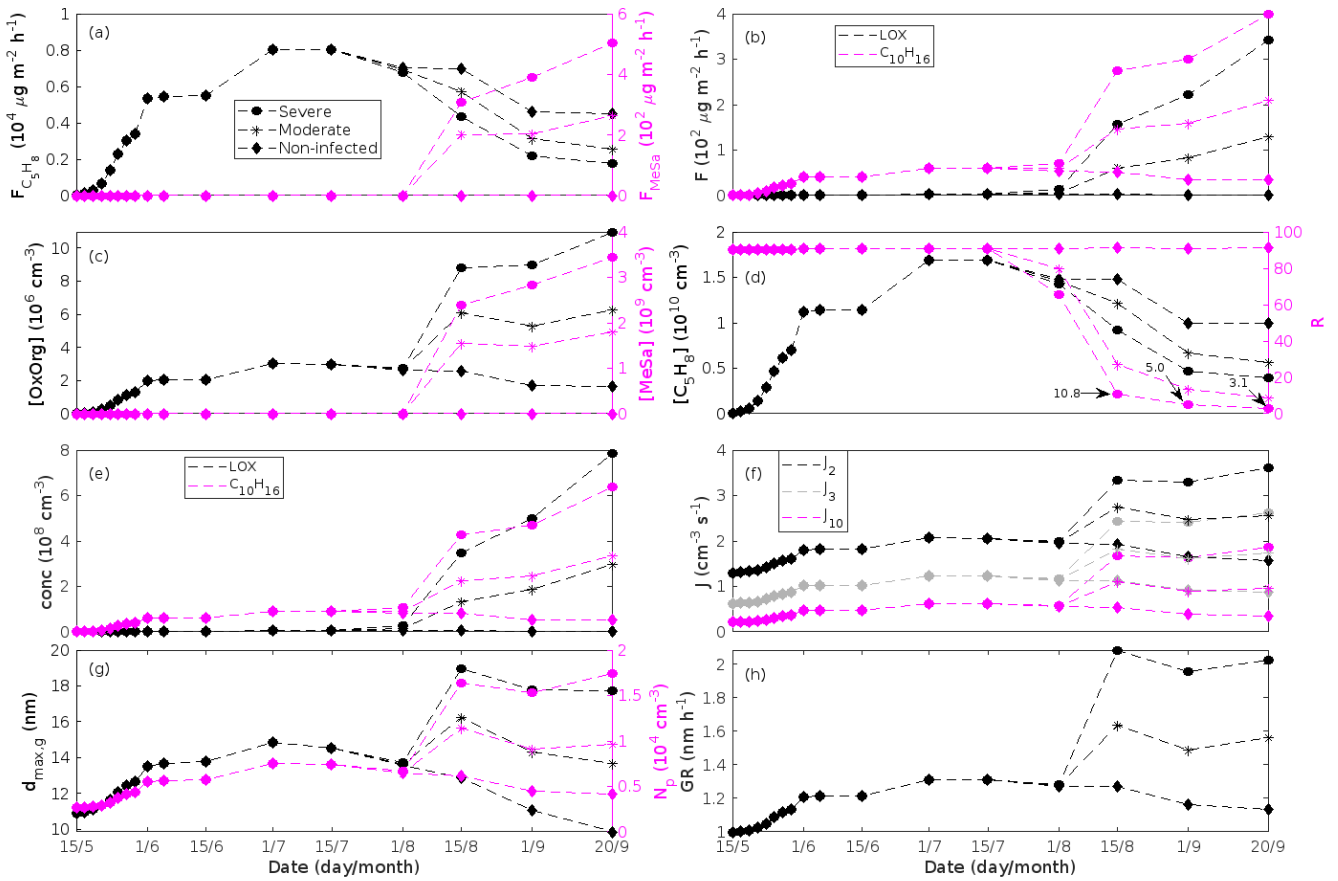
587

588

589

590

Figure 6. A pure oak stand infested with European gypsy moth larvae in comparison to a non-infested pure oak stand. (a) atmospheric concentrations of OxOrg. (b) the ratios of isoprene-to-monoterpenes carbon concentrations, where the red line indicates $R = 1$. Formation rates of (c) 2, (d) 3 and (e) 10 nm particles. (f) number concentrations of formed particles, (g) growth rates of newly formed particles, and (h) the daily maxima diameter of the growing particle mode. “Moderately” and “severely” refer to 30 % and 80 %, respectively, of the leaf area that has been consumed by the end of the feeding period.



592

593

594

595

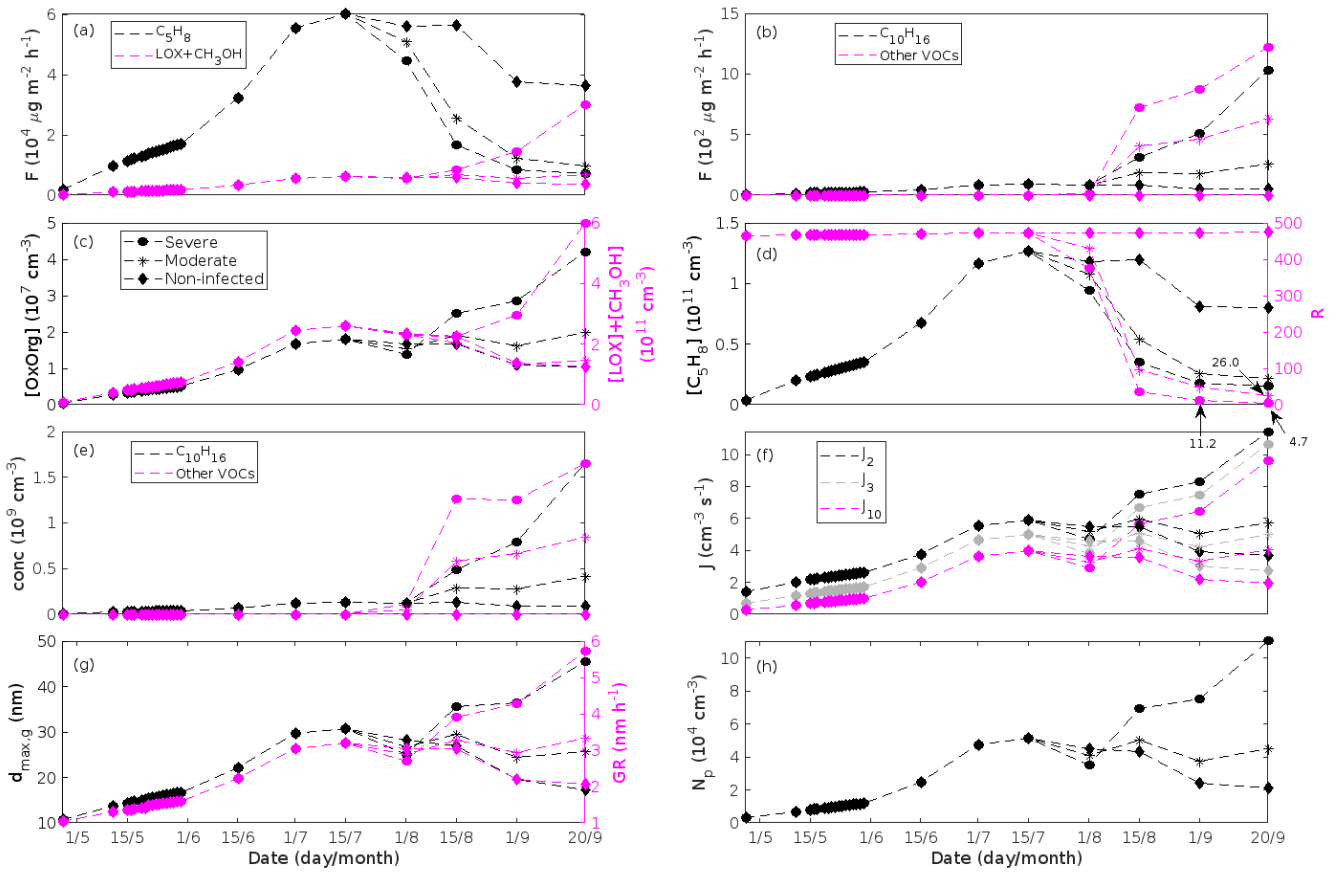
596

597

598

599

Figure 7. A pure oak stand infected by oak powdery mildew in comparison to a non-infected pure oak stand. Canopy emissions of (a, left axis) isoprene, (a, right axis) methyl salicylate, (b) lipoxygenase pathway volatiles and monoterpenes. Atmospheric concentrations of (c, left axis) OxOrg, (c, right axis) methyl salicylate, (d, left axis) isoprene, and (e) lipoxygenase pathway volatiles and monoterpenes. (d, right axis) the ratios of isoprene-to-monoterpene carbon concentrations. (f) formation rates of 2, 3 and 10 nm particles. (g, left axis) daily maxima diameter of the growing particle mode, and (g, right axis) number concentrations of formed particles. (h) growth rates of newly formed particles. “Moderately” and “severely” refer to 30 % and 80 %, respectively, of the leaf area that has been infected by fungi by the onset of senescence.



601

602

603

604

605

606

607

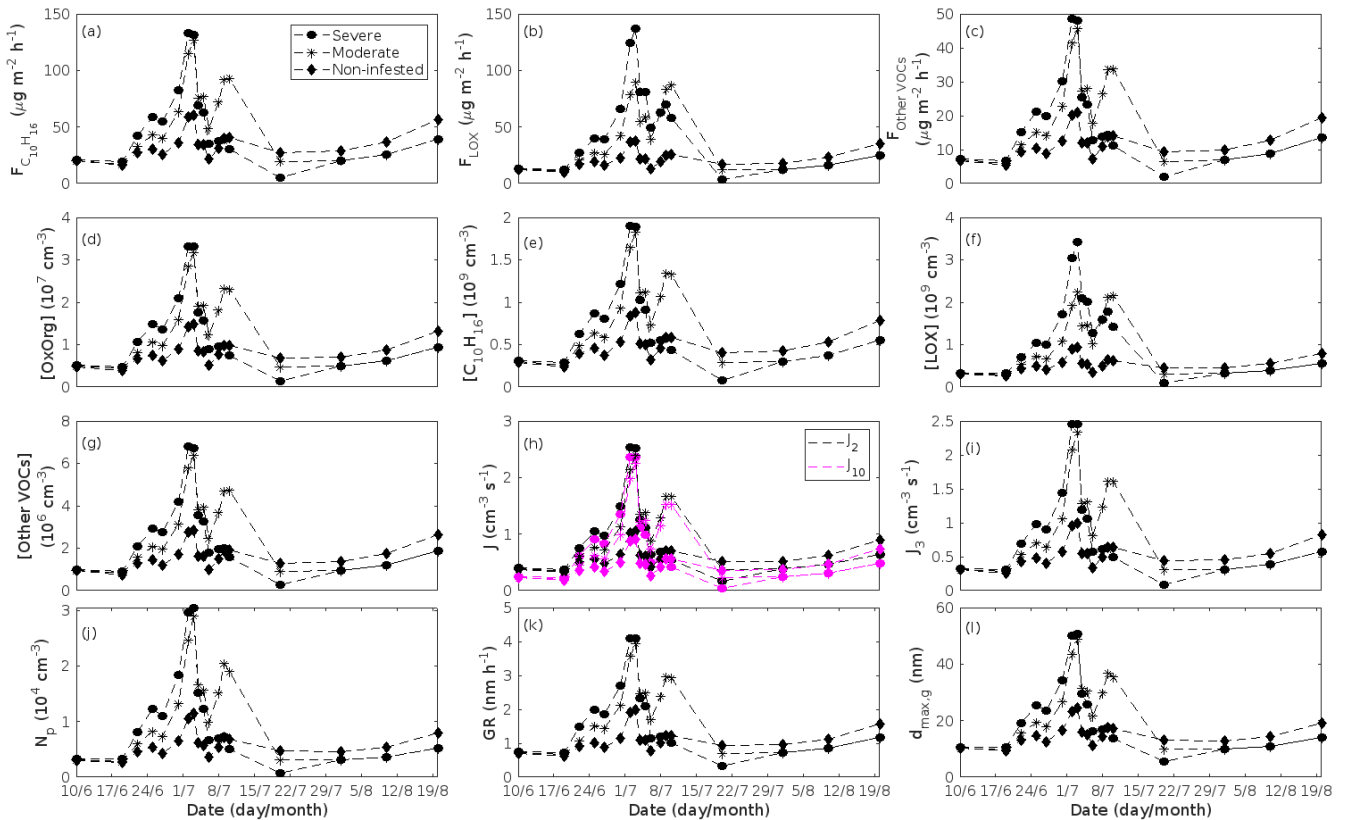
608

609

610

611

Figure 8. A pure poplar stand infected by rust fungi in comparison to a non-infected pure poplar stand. Canopy emissions of (a) isoprene and the sum of lipoxygenase pathway volatiles and methanol, (b) monoterpenes and the sum of other VOCs which contribute to OxOrg formation (here i.e. methyl salicylate, dimethyl-nonatriene, α -Eudesmol and sesquiterpenes). Atmospheric concentrations of (c, left axis) OxOrg, (c, right axis) the sum of lipoxygenase pathway volatiles and methanol, (d, left axis) isoprene, and (e) monoterpenes and the sum of other VOCs which contribute to OxOrg formation. (d, right axis) the ratios of isoprene-to-monoterpene carbon concentrations. (f) formation rates of 2, 3 and 10 nm particles. (g, left axis) daily maxima diameter of the growing particle mode, and (g, right axis) growth rates of newly formed particles. (h) number concentrations of formed particles. “Moderately” and “severely” refer to 30 % and 80 %, respectively, of the leaf area that has been infected by fungi by the onset of senescence.



612

613 **Figure 9.** A pure mountain birch stand infested with autumnal moth larvae in comparison to a non-infested pure mountain
 614 birch stand. Canopy emissions of (a) monoterpenes, (b) lipoxygenase pathway volatiles, and (c) the sum of other VOCs which
 615 contribute to OxOrg formation (here i.e. dimethyl-nonatriene and sesquiterpenes). Atmospheric concentrations of (d) OxOrg,
 616 (e) monoterpenes, (f) lipoxygenase pathway volatiles, and (g) the sum of other VOCs which contribute to OxOrg formation.
 617 Formation rates of (h) 2, 10 and (i) 3 nm particles. (j) number concentrations of formed particles. (k) growth rates of newly
 618 formed particles. (l) daily maxima diameter of the growing particle mode. “Moderately” and “severely” refer to 30 % and 80
 619 %, respectively, of the leaf area that has been consumed by the end of the feeding period.

620

621 3.2 Estimating the reliability of our results

622 Since aerosol processes are very sensitive to changes in environmental conditions - conditions which can vary greatly, both
 623 interannually, but also from day to day, we investigated the influence of a wide range of realistic and relevant environmental
 624 conditions (Table D1 in Appendix D) on our model predictions (Figs. 10-11, D1-2 in Appendix D). Nine different sensitivity
 625 tests (ST1-9) were conducted for all plant species and infections, where only one parameter was changed at a time (Table D1).
 626 For these simulations, the default values listed in Table 2 were used, while the default maximum daily temperature at
 627 Hohenpeissenberg and SMEAR I were assigned to 25 °C and 20 °C, respectively, and the default LAI for oak/poplar and birch
 628 was assumed to be 5 m² m⁻² and 2 m² m⁻², respectively. All aerosol parameters (formation and growth rates, diameter, number
 629 of particles) show a similar response to changes in the considered environmental parameters, thus only the impact on the
 630 number of newly formed particles (Figs. 10-11) and the rate at which new small particles grow (Figs. D1-2) is displayed.

631 As is also observed in nature, certain conditions suppress or prevent the formation of new particles, such as for
 632 example a high condensation sink (Fig. 11d,i,n,s; e.g. Hyvönen et al., 2005; Nieminen et al., 2015; Vana et al., 2016) and low
 633 sulfuric acid concentration (Fig. 11c,h,m,r; e.g. Boy et al., 2005; Nieminen et al., 2014), making the atmospheric relevance of
 634 the forest stands minor. Since we have assumed realistic conditions, but at the same time conditions which do not prevent the
 635 formation of new particles, in our simulations, the number of predicted days with occurring new particle formation is the
 636 theoretical maximum for clean environments, which our aerosol theory is based on (Sec. 2.7). Though the absolute number of

637 predicted new particles depend highly on the assumed environmental conditions (Figs. 10-11), the relative difference between
638 non-infected and stressed stands of the same tree species is not impacted: e.g. the number of new particles is always
639 significantly higher in gypsy moth infested, and oak powdery mildew infected, oak stands, than in non-infected oak stands,
640 when the environmental conditions are assumed to be the same in all stands (Figs. 10a-h, 11a-j). Likewise, more particles are
641 always formed in moderately, than severely, moth infested oak and birch stands, since the decrease in LAI is stronger than the
642 increase in the stress-induced emission response per unit leaf area (Figs. 10a-d,m-p, 11a-e,p-t). This is emphasised in very
643 severely infested mountain birch stands (e.g. 80 % defoliation), where the number of produced particles is always less than in
644 its corresponding non-infested stand (Figs. 10m-p, 11p-t).

645 Sensitivity tests were also carried out in order to assess whether the simplifications made in the model are valid: (1)
646 As mentioned earlier (Sec. 2.4), we did not incorporate a full canopy environment in the model - an approach which has also
647 been taken by other investigators (e.g. Simpson et al., 1999, 2012; Bergström et al., 2014). In ST2 (Table D1, Figs. 10b,f,j, n,
648 D1b,f,j,n) changes in light conditions exclusively impact the predicted emissions of VOCs. From Figs. 10b,f,j,n, D1b,f,j,n it is
649 clear that even assuming extremely different light environments would not change our conclusions about the atmospheric
650 importance of biotic plant stresses, since our results show that stressed forest with a maximum light availability down to 200
651 $\mu\text{mol m}^{-2} \text{s}^{-1}$ would still produce more new particles than its correspondingly non-infested stand at theoretically clear sky
652 conditions (Fig. 10b,f,j,n). A highly autumnal moth stressed mountain birch stand (80 % defoliation) would possibly produce
653 slightly more particles than a non-infested stand, if a full canopy environment would be considered. For example, the number
654 of produced particles is slightly higher in a birch stand experiencing a stress level of 80 % under 1000 $\mu\text{mol m}^{-2} \text{s}^{-1}$ than a non-
655 infested stand under 400 $\mu\text{mol m}^{-2} \text{s}^{-1}$ (Fig. 10n). However, the LAI of mountain birch stands is usually rather low (Heiskanen,
656 2006), making the difference in light environment between a non-infested and a highly defoliated stand small. Since mildew
657 and rust do not decrease the leaf area of their host, a different treatment of the light environment would not influence the
658 relative atmospheric importance of fungally infected oak and poplar vs their correspondingly non-infested stands (Fig. 10f,j).

659 (2) In ST3 (Table D1, Figs. 10c,g,k,o, D1c,g,k,o) and in our seasonal simulations (Figs. 5-9), the change of
660 temperature only impacts the emission rates of VOCs. In reality, the vapour pressures of oxidised compounds increase non-
661 linearly with an increase in temperature (e.g. Bilde et al., 2015), and less HOM, and other oxidised organic compounds, will
662 therefore condense at higher temperatures, whereby the formation and subsequent growth of particles will decrease
663 (Stolzenburg et al., 2018; Simon et al., 2020). Gas phase chemistry, including the formation of HOM, is also in reality
664 temperature dependent (e.g. Quéléver et al., 2019). These effects have not been included in the model. Since the range of daily
665 maximum temperatures throughout the growing season is assumed to be rather narrow (Fig. 4), this effect does not greatly
666 impact our results (Sec. 3.1), but it means that the number of particles produced at high temperatures (Fig. 10c,g,k,o), and the
667 growth rate at which they are produced (Fig. D1c,g,k,o), are overestimated for both non-infested and stressed forests.

668 (3) The concentrations of ozone and OH were unaltered between simulations of non-infested forests and forests under
669 varying degrees of infection (Sec. 2.6), though in reality, the atmospheric oxidation capacity is controlled by changes in the
670 concentration of atmospheric trace gases, including VOCs. The total emission of VOCs from oak and poplar stands is greatly
671 dominated by isoprene, but the emission of isoprene decreases as a function of biotic stress severity (Figs. 5a, 7a, 8a). In
672 contrast, the emission of LOX, methyl salicylate, methanol, monoterpenes and sesquiterpenes increases as the level of stress
673 increases (Figs. 5c,e,g, 7a,b, 8a,b). The oxidation of isoprene, LOX, methyl salicylate and methanol is primarily driven by
674 reactions with OH, and also monoterpenes react with OH, which all leads to reductions in the concentration of OH (Table 3),
675 though e.g. ozonolysis of monoterpenes also produce OH, which thus counters part of the reduction. When considering the
676 reaction rates and emission rates of the considered VOCs in simulations of oak and poplar stands, the concentration of OH is
677 mainly controlled by changes in the emission of isoprene. Thus, we expect that the concentration of OH will increase as the
678 degree of stress increases, but even a strong shift in the concentration of OH, will not change the conclusion about the relative
679 atmospheric importance of stressed vs stress-free oak and poplar forests (Figs. 11b,g,l,q, D2b,g,l,q). The absolute number of
680 predicted new particles in herbivory stressed oak stands will, however, be predicted to be smaller at higher levels of OH (Fig.

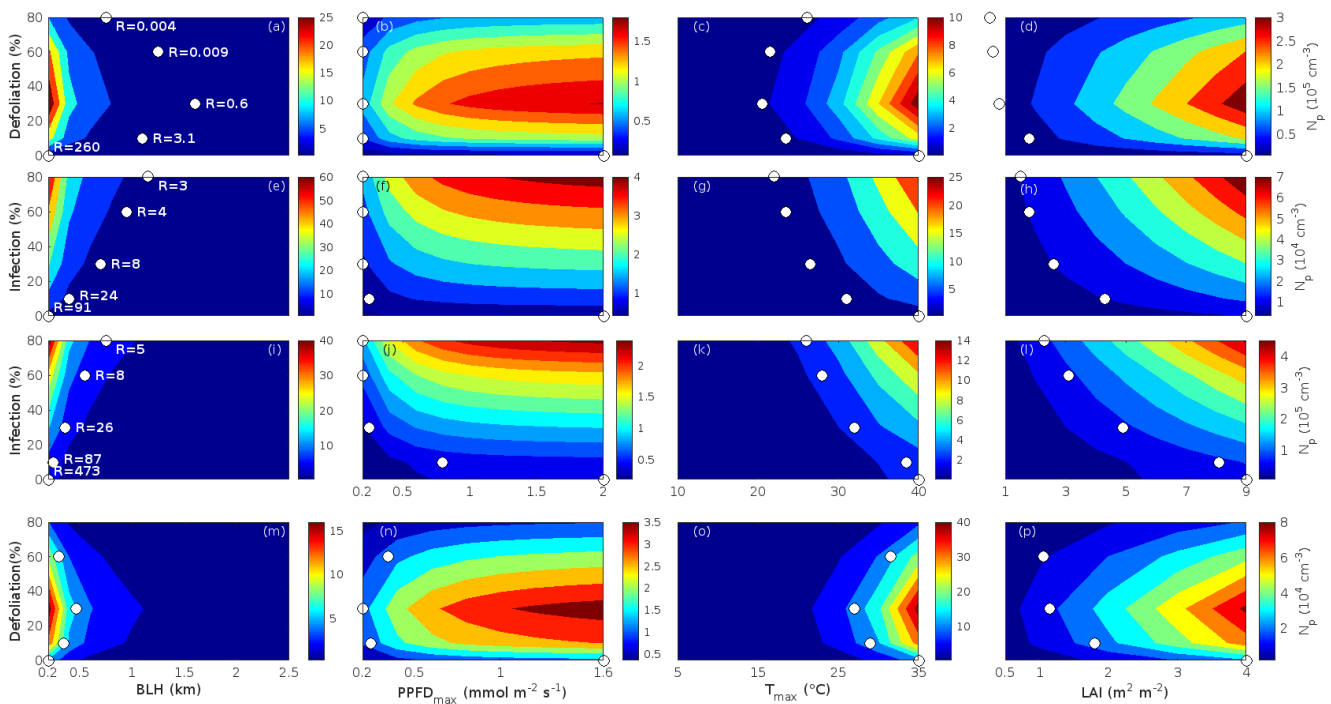
681 11b), because the oxidation of monoterpenes is then more strongly controlled by OH, which leads to a smaller production of
682 HOM, as monoterpenes typically form HOM at a considerably lower yield from reactions with OH than ozone (Appendix C).
683 A similar shift in the oxidation of monoterpenes is happening in case of oak powdery mildew infected oak, but the effect is
684 counted by an increase in the formation of oxidised organic compounds from oxidation of methyl salicylate at high levels of
685 OH, leading totally to higher predicted particle number concentrations (Fig. 11g). Considering the emissions from biotically
686 stressed and non-infested mountain birch, we estimate that the concentration of OH should stay largely the same, or potentially
687 decrease slightly at higher levels of infestation, which will enhance the oxidation of monoterpenes by ozone, which will lead
688 to a larger production of HOM and thereby a slightly higher predicted number of new particles (Fig. 11q). In the atmosphere,
689 the production of sulfuric acid is limited by the availability of OH, and it is therefore possible that the effects of changes in the
690 concentration of OH (Fig. 11b,q) and sulfuric acid (Fig. 11c,r), in herbivory stressed stands, on the absolute number of
691 predicted new particles, will cancel out or even lead to a stronger particle production than predicted. In case of oak powdery
692 mildew infected oak, the two effects will enhance each other and result in an even higher number of predicted particles. In
693 clean, low NO_x environments, which we aimed to simulate, the concentration of ozone is largely unaffected by the ambient
694 concentration of isoprene (e.g. Jenkin et al., 2015). However, isoprene forms ozone progressively with an increased availability
695 of NO_x (e.g. Jenkin and Clemitshaw, 2000). Higher ozone levels support enhanced formation of HOM, and thus aerosol
696 processes, but the production of HOM is also known to decrease as a function of increased NO_x concentration (e.g. Ehn et al.,
697 2014), whereby the formation and growth of new particles becomes suppressed (e.g. Yan et al., 2020; Pullinen et al., 2020).

698 (4) As mentioned earlier (Sec. 2.6), many HOM yields have not been investigated for the exact compounds which are
699 emitted from the tree species, which are the focus of this study. From Fig. 11e,j,o,t it is obvious, that even if all the OxOrg
700 yields used for simulations of only biotically stressed forests were to be decreased significantly - in case of moderately
701 herbivory infested oak (30 % of leaf area defoliated) by down to about 95 % - biotically stressed oak, poplar and mountain
702 birch forests would still, in most cases, produce more particles than non-infested forests of the same tree species. The yields,
703 at which HOM are formed, have been treated as fixed values (Appendix C) in the seasonal simulations (Sec. 3.1), but the yields
704 actually depend on several factors, such as e.g. the concentration of NO_x (point 3 above; Ehn et al., 2014), temperature (point
705 3 above; Quéléver et al., 2019; Simon et al., 2020) and the ambient blend of VOCs (Sec. 3.1.5; McFiggans et al., 2019). Exactly
706 how the formation and growth of new particles depend on the VOC blend is still uncertain, but it has recently been
707 demonstrated that a linear addition of the yields from the individual yields of components in the VOC mixture will result in an
708 overestimation of both the number and size of particles (McFiggans et al., 2019). As we have followed a similar procedure,
709 this effect might cause our predicted aerosol processes (Sec. 3.1) to be overestimated, but since the ratio of isoprene-to-
710 monoterpenes carbon concentration is much higher in non-infested oak and poplar stands than in the correspondingly stressed
711 stands (Figs. 6b, 7d, 8d), the overestimation is expected to be more pronounced in the non-infested stands (McFiggans et al.,
712 2019). The difference in the atmospheric importance of non-infested and biotically stressed oak and poplar stands thereby
713 widens (Fig. 11e,j,o).

714 It is well known that the potential for foliage to emit VOCs depends on the age of the foliage: emerging and growing
715 foliage usually emits isoprene at reduced rates (e.g. Guenther et al., 1991, 2012; Goldstein et al., 1998; Petron et al., 2001) and
716 monoterpenes at enhanced rates (e.g. Guenther et al., 1991, 2012; Aalto et al., 2014; Taipale et al., 2020) compared to that of
717 its corresponding mature foliage. Old leaves do usually additionally emit isoprene at decreased rates (Monson et al., 1994;
718 Schnitzler et al., 1997; Sun et al., 2012). These effects were not considered in our simulations (Sec. 3.1), since the effect of
719 leaf age on biotic plant stress emissions is unexplored. Considering a similar treatment of the impact of leaf maturity on the
720 emissions of VOCs as Gunther et al. (2012) (see Appendix B) would only influence the predicted number and size of particles
721 in herbivory stressed and non-infested oak forests insignificantly (Fig. B2). However, it would decrease the ratio of isoprene-
722 to-monoterpenes carbon so significantly in gypsy moth infested oak stands, that the possible suppression of aerosol processes
723 by isoprene would disappear during most, or even the entire, duration of stress (Fig. B2b). Applying a similar leaf age effect
724 as described in Gunther et al. (2012) on simulations of fungally infected oak and poplar forests would not decrease the ratio of

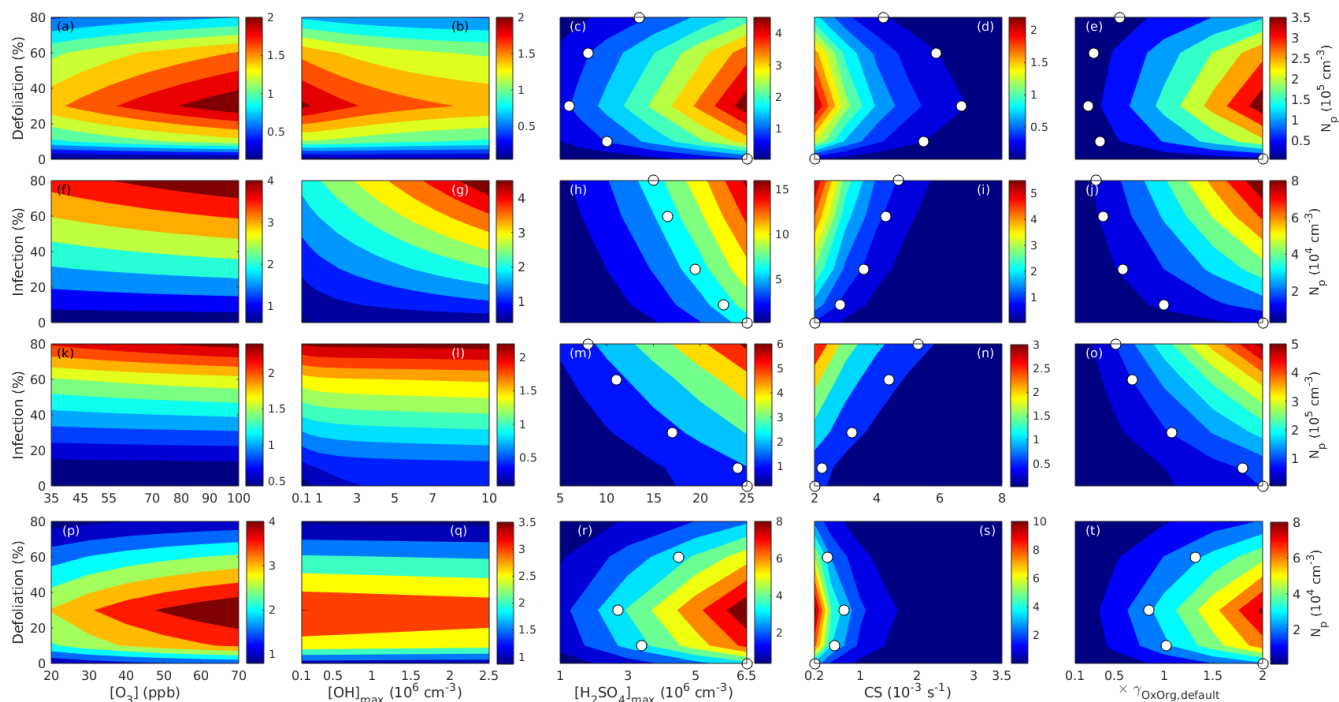
725 isoprene-to-monoterpenes carbon sufficiently in order to avoid the possible suppression effect of isoprene, since Guenther et al. (2012) only assume a reduction of 10 % on the emissions of isoprene from old leaves. We investigated that the emission of isoprene from mildew infected oak would need to decrease by ~68-96 % (severity of stress ranging from 80 to 9 %), in comparison to simulations where the leaf age effect is not considered, in order to reach $R \leq 1$, whereas the emission of isoprene from non-infected oak would need to decrease by ~99 % (Fig. B3a). In comparison, the emission of isoprene from a non-infected poplar stand would need to decline by 99.8 %, and from a rust infected poplar stand by at least 79 %, in order to attain $R \leq 1$ (Fig. B4a). In order to reach $R \leq 22.5$, the upper limit at which new particle formation has been observed in the atmosphere (Yu et al., 2014), the emission of isoprene from a non-infected poplar stand would need to decrease by ~95 %, whereas heavily rust infected poplar forest would already be below this limit without considering an age dependent reduction of the emission potential (Fig B4a). Simulations were not done for mountain birch forest stands, since no emissions are suppressed upon herbivory stress of mountain birch (Yli-Pirilä et al., 2016) and since Yli-Pirilä et al. (2016) did not provide age information on the leaves they measured.

737



738

739 **Figure 10.** Impact of changed boundary conditions on the number concentrations of newly formed particles in non-infected and biotically stressed forest stands. The number concentration of newly formed particles is expressed as a function of changes in the boundary layer height (**a, e, i, m**), light (**b, f, j, n**), temperature (**c, g, k, o**) and leaf area index (**d, h, l, p**) for non-infected and infected oak (**a-d**, gypsy moth, **e-h**, powdery mildew), poplar (**i-l**) and birch (**m-p**) stands. Light (**b, f, j, n**) and temperature (**c, g, k, o**) are given as the daily maxima, but in the simulations the parameters follow a daily cycle. The displayed LAI (**d, h, l, p**) is that of a non-infected stand, hence e.g. at LAI = 7 m² m⁻², the simulation for a larval infestation level of 80 % has been conducted with LAI = 1.4 m² m⁻², which is 20 % of the non-infected stand LAI value. Optimal conditions (i.e. leading to highest number concentrations) for non-infected stands are indicated with white markers at an infection level of 0 %. White markers located at various infection levels mark the conditions at which an identical or slightly higher number concentration, as produced by a non-infected forest stand at optimal conditions, is reached. No markers are used for 80 % defoliated mountain birch (**m-p**), since the corresponding number concentrations are always lower than in a non-infested birch stand at optimal conditions. Be aware that white markers in **d** and **p** are not located at the LAI of a non-infected stand, but instead at the values used for the simulations. R values (**a, e, i**) indicate the ratio of isoprene carbon / monoterpene carbon at the locations of the write markers. Be aware that the x-axes are different for simulations in Hohenpeißenberg (**a-l**) and SMEAR I conditions (**m-p**) except in the case of changing boundary layer height (**a, e, i, m**).



755

756 **Figure 11.** Impact of changed boundary conditions on the number concentrations of newly formed particles in non-infected
 757 and biotically stressed forest stands. The number concentration of newly formed particles is expressed as a function of changes
 758 in the concentration of ozone (a, f, k, p), OH (b, g, l, q) and sulfuric acid (c, h, m, r), the condensation sink (d, i, n, s) and
 759 OxOrg yields (e, j, o, t) for non-infected and infected oak (a-e, gypsy moth, f-j, powdery mildew), poplar (k-o) and birch (p-
 760 t) stands. The concentrations of OH (b, g, l, q) and sulfuric acid (c, h, m, r) are given as the daily maxima, but in the simulations
 761 the parameters follow a daily cycle. White markers are used in a similar way as in Fig. 10. Be aware that the x-axes are different
 762 for simulations in Hohenpeißenberg (a-o) and SMEAR I conditions (p-t) except in the case of changing Oxorg yields (e, j, o,
 763 t).

764

765 3.3 Implications and remaining issues to be explored

766 Our simulation results (Figs. 5-9) illustrate that biotic plant stresses are capable of substantially perturbing both the number
 767 and size of atmospheric aerosol particles throughout a significant fraction of the year (summarised in Fig. 12). Considering
 768 that we calculated *daily* new particle growth, our results point to the direction that induced plant emissions will subsequently
 769 lead to more efficient CCN production in the atmosphere (Fig. 12), which will moreover affect cloud properties, such as cloud
 770 albedo and lifetime (Twomey, 1977; Albrecht, 1989; Grypsperdt et al., 2014; Rosenfeld et al., 2014). The amplitude of the
 771 enhancement, however, depends strongly on the specific stressor and tree species which are attacked.

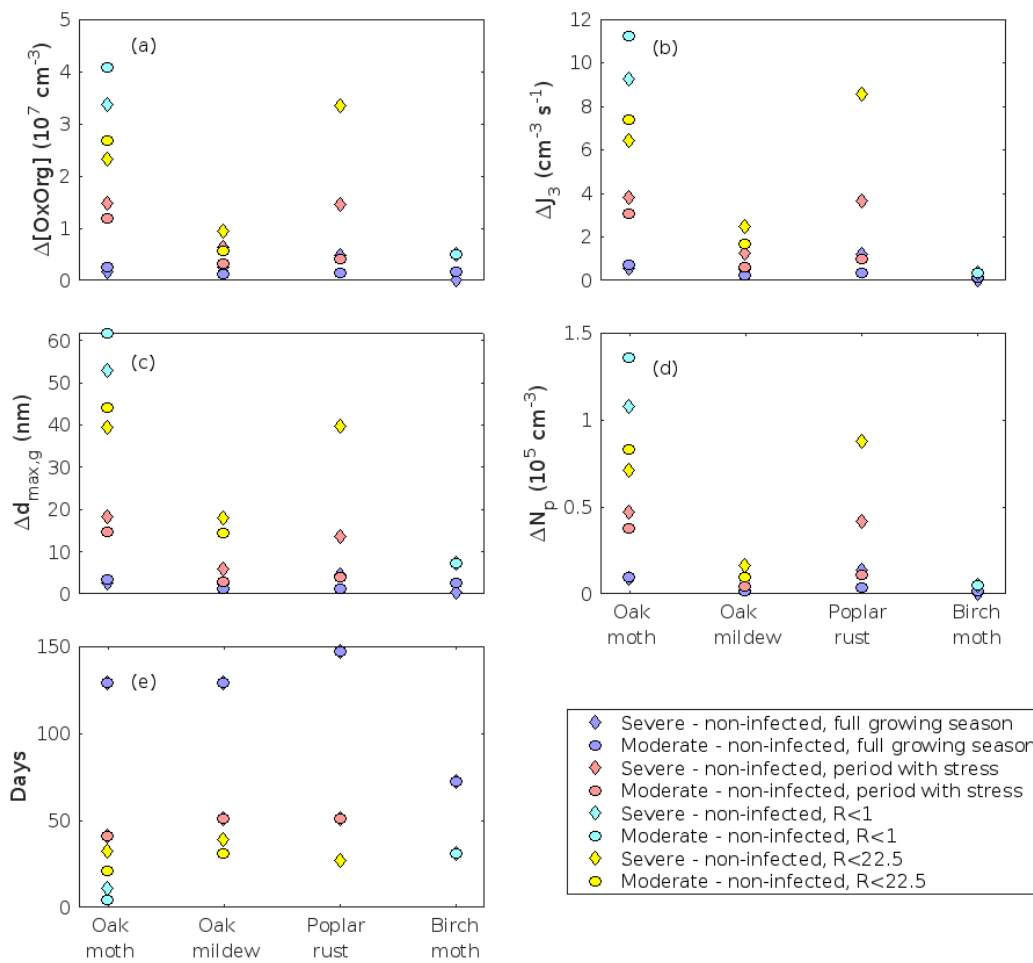
772 Naturally, both the duration of stress (Fig. 12e) and the predicted number (Fig. 12d) and size (Fig. 12c) of new
 773 particles depend highly on our assumptions about e.g. when the fungi start to attack their host, how fast the fungi spread,
 774 whether the larval eggs hatch simultaneously with budburst, how fast larval development occurs, and when senescence onsets
 775 - all which depend strongly on environmental conditions. It is furthermore probable that emissions are also induced from
 776 fungally infected leaves during senescence, which was not simulated here. The duration of stress can, thus, be significantly
 777 longer than what is summarised in Fig. 12e, whereby also the post-defoliation period, in case of herbivory infestations, will be
 778 shorter, and the atmospheric importance of the stresses stronger.

779 We have also shown that it can be more important to account for biotic plant stresses in models for local and regional
 780 predictions of new particle formation and growth during the time of infestation/infection than significant variations in those
 781 environmental parameters which predictions of VOC emissions are currently controlled by, e.g. light conditions (Fig.

782 10b,f,j,n), temperature (Fig. 10c,g,k,o) and LAI (Fig. 10d,h,l,p). Considering changes in the emissions of VOCs caused by
783 stress also seems to be more crucial than accounting for large changes in the concentrations of O₃ (Fig. 11a,f,k,p) and OH (Fig.
784 11b,g,l,q).

785 Considering the frequency and scale of the investigated biotic stresses is important in order to properly evaluate the
786 impact of the stresses on the atmosphere and climate: Fungi are largely ubiquitous and e.g. yearly account for ~10 % of all
787 recorded damage symptoms on trees growing in European forests (ICP Forests, 2020). To put that number in perspective, ~87
788 % of all investigated broadleaved trees (>50000) are yearly reported to have damage symptoms in European forests (ICP
789 Forests, 2020). Considering the duration of stress, and the predicted increase in the number and size of atmospheric aerosol
790 particles in response to fungal infections, together with the fact that especially oak powdery mildew is one of the most common
791 plant diseases, with e.g. ~9 % of pedunculate and sessile oak reported to be infected by powdery mildew in Europe yearly (ICP
792 Forests, 2020), our findings call for initiatives to account for fungal stress emission responses in numerical models in a robust
793 manner. Though larvae are present every summer, the population density of both gypsy and autumnal moths is cyclic, with 8-
794 10 years or 4-5 years between gypsy moth outbreaks, depending on the forest type (mesic vs xeric sites; Johnson et al., 2006),
795 and 9-11 years between autumnal moth outbreaks (Haukioja et al., 1988; Ruohomäki et al., 2000; Ylivinkka et al., 2020).
796 Gypsy moth, in North America alone, is estimated to have defoliated >38 million ha of forest during years 1920 to 2020
797 (Coleman et al., 2020), and yearly, gypsy moth larvae are usually reported to defoliate between ~0.2-0.8 million ha of forested
798 land in the US, but with values as high as ~5 million ha/year (Karel and Man, 2017). In comparison, the total area of forested
799 land in the US is ~333 million ha (www.fs.usda.gov). In European forests, the mean level of defoliation of pedunculate and
800 sessile oak is yearly reported to be ~27 %, while most of the trees are 10-25 % (~39 % of trees) or 25-40 % defoliated (~28 %
801 of trees, ICP Forests, 2020). In comparison, only ~19 % of deciduous temperate oak trees in European forests are yearly
802 reported to not be defoliated at all or that less than 10 % of the trees' foliage have been defoliated by herbivores (ICP Forests,
803 2020). Since European gypsy moth is one of the major defoliating insects feeding on pedunculate oak
804 (<https://www.cabi.org/isc/datasheet/31807#tohostsOrSpeciesAffected>, last accessed 11th of June, 2021), it must be reasonable
805 to assume that a significant fraction of the reported defoliation is caused by feeding by gypsy moth larvae, and thus it is likely
806 that accounting for stress emissions in response to feeding by gypsy moth larval is important for realistic predictions of new
807 particle formation and growth. It is also likely that the reported defoliation which is not caused by gypsy moth larvae, but other
808 herbivores, also impacts SOA formation, though to which direction and with which amplitude is currently unknown. When
809 the larval density of autumnal moth in Fennoscandia is low, the level of defoliation usually remains less than 15 % (Bylund
810 1995), but during outbreak years, large areas (in the order of several thousands of square kilometres) can become either
811 completely or severely defoliated (e.g., Ruohomäki et al., 2000; Tenow 1975; Nikula 1993). Thus, considering the scale of
812 autumnal moth infestation combined with our findings about both the order of the increase in atmospheric new particle
813 formation and growth caused by autumnal moth infestations, and also the absolute number and size of newly formed particles,
814 it could seem that the importance of accounting for autumnal moth infestation in models to predict SOA formation is minor.
815 It should, however, be emphasised that in our simulations we did not account for delayed defense responses, which mountain
816 birches are known to possess (e.g., Kaitaniemi et al., 1998; Ruuhola et al., 2007), and which possibly cause elevated total
817 particle concentrations for few years after larval infestation (Ylivinkka et al., 2020). Also, we did not take multiple co-occurring
818 stresses into account, which are often the rule in nature and which generally enhances the already induced emission response
819 due to biotic plant stress (e.g. Blande et al., 2007; Vapaavuori et al., 2009; Holopainen and Gershenson, 2010; Kivimäenpää
820 et al., 2016; Ghimire et al., 2017). For example, Li et al. (2019) recently showed that warming significantly amplifies the
821 emission response due to autumnal moth feeding. Thus, there is a great need for new field observations in order to validate
822 modelling studies such as ours, and in general to quantify the role of stress emissions in SOA formation. Especially because
823 enclosure studies, which currently are close to the only published measurements studies which have investigated the ability of
824 biotic plant stress to influence aerosol processes, often do not accurately represent what is observed on canopy to landscape

825 scales. In addition to this, robust representations of stress emissions, and the drivers of the emissions, are needed before it is
 826 possible to integrate stress emissions into large scale models without introducing errors in the models.
 827



828
 829 **Figure 12.** Differences in atmospheric response from various non-infected and biotically stressed plant species. (a)
 830 atmospheric concentrations of OxOrg, (b) formation rates of 3 nm particles, (c) daily maximum diameter of the growing
 831 particle mode, (d) number concentration of formed particles, and (e) amount of days considered. a-d are provided as the
 832 differences between the averaged parameter in a stressed and stress-free forest stand of the same plant species type. Differences
 833 and averages are considered based on the complete growing season, the period with stress, when the ratio of isoprene-to-
 834 monoterpenes carbon concentration is less than 1 or less than 22.5. Be aware that R is always zero in simulations of birch. In
 835 cases where R does not reach less than 1 or less than 22.5 in the atmosphere surrounding a non-infected forest stand, but it
 836 does in the case of the corresponding stressed stand, it is assumed that the atmospheric parameter in the non-infected stand is
 837 zero and hence the difference is given as the value of the stressed stand. The concentration differences of OxOrg, formation
 838 rates and number concentrations are calculated based on an average, for the period of interest, of the median values during
 839 10:00-16:00 local time. “Severe” and “moderate” refer to that 80 % or 30 % of the total leaf area has been consumed or infected
 840 by the end of the feeding/infection period, respectively. Southern Germany has been used as border conditions for simulations
 841 of oak and poplar, while SMEAR I, Finnish Lapland, has been used for modelling of birch.

843 **4 Conclusions**

844 We constructed a conceptual model to simulate new particle formation and growth in various broadleaved forest stands, in
845 clean low NO_x environments, under biotically stressed and stress-free conditions, throughout a full growing season.
846 Unsurprisingly, we found that the predicted atmospheric importance of biotic plant stress highly depends on the specific
847 individual stressor and tree species which are attacked. Thus, the amount of newly formed particles was predicted to be up to
848 about one order of magnitude higher in a gypsy moth infested oak stand than in a non-infested oak stand. In comparison, the
849 number of new particles was simulated to be up to about a factor of 3, 4 and 5 higher in autumnal moth, oak powdery mildew
850 and poplar rust infected mountain birch, pedunculate oak and balsam poplar stands, respectively. We furthermore predicted
851 that the new particles will grow up to about 46, 28, 26 and 8 nm larger in an oak gypsy moth, poplar rust, autumnal moth and
852 oak powdery mildew infected stand, respectively, compared to their corresponding non-infested stands within one day. To our
853 knowledge, this study is the first to investigate the atmospheric impact of biotic plant stresses throughout a full growing season.

854 Our modelling results generally indicate that all the investigated plant stresses are capable of substantially perturbing
855 both the number and size of atmospheric aerosol particles, and it is thus likely that the induced emissions will subsequently
856 lead to more efficient CCN production in the atmosphere. We also showed that it can be more important to account for biotic
857 plant stresses in models for local and regional predictions of new particle formation and growth during the time of
858 infestation/infection than significant variations in e.g. LAI, and temperature and light conditions, which are currently the main
859 parameters controlling predictions of VOC emissions. Considering our findings together with the fact that insect outbreaks
860 and fungal diseases are generally expected to increase in both frequency and severity in the future, our study underlines the
861 need for new field measurements to quantify the role of stress emissions in atmospheric aerosol processes and for making
862 integration of biotic plant stress emission responses into numerical models possible.

863
864 *Data availability.* The model code is available upon reasonable request by contacting ditte.taipale[at]helsinki.fi. SMEAR I
865 mountain birch leafing data can be obtained by contacting vesa.haataja[at]helsinki.fi. All other data used to constrain the model
866 is publicly available following the provided references.

867
868 *Author contributions.* Idea and concept by ÜN. ÜN standardised the published emission rates. VM, MK and ME developed
869 the theory for the aerosol module. DT developed the model code, conducted the simulations, and wrote the manuscript, with
870 inputs from all authors. All authors discussed the results, and commented and edited the manuscript.

871
872 *Competing interests.* The authors declare that they have no conflict of interest.

873
874 *Acknowledgements.* This work was supported by the European Regional Development Fund (Centre of Excellence
875 EcolChange), the European Research Council (advanced grant 322603, SIP-VOL+), the Academy of Finland Center of
876 Excellence project (no. 307331), and the Academy of Finland Flagship funding (grant no. 337549). DT was also supported by
877 the Academy of Finland (no. 307957). DT thanks Pekka Kaitaniemi for valuable discussions related to autumnal moth
878 simulation set-up and Juho Aalto, Yifan Jiang and Tero Klemola for use of photos.

879

880 **References**

881 Aalto, J., Kolari, P., Hari, P., Kerminen, V.-M., Schiestl-Aalto, P., Aaltonen, H., Levula, J., Siivola, E., Kulmala, M., and
882 Bäck, J.: New foliage growth is a significant, unaccounted source for volatiles in boreal evergreen forests, *Biogeosciences*, 11,
883 1331–1344, <https://doi.org/10.5194/bg-11-1331-2014>, 2014.

885 Aalto, P., Aalto, T., and Keronen, P. SMEAR I Värriö forest meteorology, air quality and soil, Institute for Atmospheric and
886 Earth System Research, urn:nbn:fi:att:2a9c28bd-ca13-4a17-8b76-922bafa067a7, 2019.

887

888 Åhman, I: Rust scorings in a plantation of *Salix viminalis* clones during ten consecutive years, *Eur. J. For. Path.*, 28, 251-258,
889 <https://doi.org/10.1111/j.1439-0329.1998.tb01180.x>, 1998.

890

891 Albrecht, B. A.: Aerosols, cloud microphysics, and fractional cloudiness, *Science*, 245, 1227-1230, DOI:
892 10.1126/science.245.4923.1227, 1989.

893

894 Ammunét, T., Klemola, T., and Saikkonen, K.: Impact of host plant quality on geometrid moth expansion on environmental
895 and local population scales, *Ecogeg.*, 34, 848-855, doi: 10.1111/j.1600-0587.2011.06685.x, 2011.

896

897 Andreae, M. O., Afchine, A., Albrecht, R., Holanda, B. A., Artaxo, P., Barbosa, H. M. J., Borrmann, S., Cecchini, M. A.,
898 Costa, A., Dollner, M., Fütterer, D., Järvinen, E., Jurkat, T., Klimach, T., Konemann, T., Knote, C., Krämer, M., Krisna, T.,
899 Machado, L. A. T., Mertes, S., Minikin, A., Pöhlker, C., Pöhlker, M. L., Pöschl, U., Rosenfeld, D., Sauer, D., Schlager, H.,
900 Schnaiter, M., Schneider, J., Schulz, C., Spanu, A., Sperling, V. B., Voigt, C., Walser, A., Wang, J., Weinzierl, B., Wendisch,
901 M., and Ziereis, H.: Aerosol characteristics and particle production in the upper troposphere over the Amazon Basin, *Atmos.*
902 *Chem. Phys.*, 18, 921–961, <https://doi.org/10.5194/acp-18-921-2018>, 2018.

903

904 Aphalo, P. J., Lahti, M., Lehto, T., Repo, T., Rummukainen, A., Mannerkoski, H., and Finér, L.: Responses of silver birch
905 saplings to low soil temperature, *Silva Fenn.*, 40, 429-444, <https://doi.org/10.14214/sf.328>, 2006.

906

907 Arimura, G.-I., Köpke, S., Kunert, M., Volpe, V., David, A., Brand, P., Dabrowska, P., Maffei, M. E., and Boland, W.: Effects
908 of feeding *Spodoptera littoralis* on lima bean leaves. IV. Diurnal and nocturnal damage differentially initiate plant volatile
909 emission, *Plant Physiol.*, 146, 965-973, <https://doi.org/10.1104/pp.107.111088>, 2008.

910

911 Asmi, E., Kivekäs, N., Kerminen, V.-M., Komppula, M., Hyvärinen, A.-P., Hatakka, J., Viisanen, Y., and Lihavainen, H.:
912 Secondary new particle formation in Northern Finland Pallas site between the years 2000 and 2010, *Atmos. Chem. Phys.*, 11,
913 12959–12972, <https://doi.org/10.5194/acp-11-12959-2011>, 2011.

914

915 Atkinson, R., and Arey, J.: Atmospheric degradation of volatile organic compounds, *Chem. Rev.*, 103, 4605-4638,
916 <https://doi.org/10.1021/cr0206420>, 2003.

917

918 Atkinson, R., Aschmann, S. M., Arey, J., and Shorees, B.: Formation of OH radicals in the gas phase reactions of O₃ with a
919 series of terpenes, *J. Geophys. Res. A*, 97, 6065-6073, <https://doi.org/10.1029/92JD00062>, 1992.

920

921 Ayres, M. P., and MacLean, Jr. S. F.: Molt as a component of insect development: *Galerucella sagittariae* (Chrysomelidae)
922 and *Epirrita autumnata* (Geometridae), *Oikos* 48, 273-279, doi:10.2307/3565514, 1987.

923

924 Bale, J. S., Masters, G. J., Hodkinson, I. D., Awmack, C., Bezemer, T. M., Brown, V. K., Butterfield, J., Buse, A., Coulson, J.
925 C., Farrar, J., Good, J. E. G., Harrington, R., Hartley, S., Jones, T. H., Lindroth, R. L., Press, M. C., Symrnioudis, I., Watt, A.
926 D., and Whittaker, J. B.: Herbivory in global climate change research: direct effects of rising temperature on insect herbivores,
927 *Glob. Change Biol.*, 8, 1-16, <https://doi.org/10.1046/j.1365-2486.2002.00451.x>, 2002.

929 Berg, A. R., Heald, C. L., Huff Hartz, K. E., Hallar, A. G., Meddens, A. J. H., Hicke, J. A., Lamarque, J.-F., and Tilmes, S.:
930 The impact of bark beetle infestations on monoterpene emissions and secondary organic aerosol formation in western North
931 America, *Atmos. Chem. Phys.*, 13, 3149–3161, <https://doi.org/10.5194/acp-13-3149-2013>, 2013.

932

933 Bergström, R., Hallquist, M., Simpson, D., Wildt, J., and Mentel, T. F.: Biotic stress: a significant contributor to organic
934 aerosol in Europe?, *Atmos. Chem. Phys.*, 14, 13643–13660, <https://doi.org/10.5194/acp-14-13643-2014>, 2014.

935

936 Berndt, T., Richters, S., Jokinen, T., Hyttinen, N., Kurtén, T., Otkjær, R. V., Kjaergaard, H. G., Stratmann, F., Herrmann, H.,
937 Sipilä, M., Kulmala, M., and Ehn, M.: Hydroxyl radical-induced formation of highly oxidized organic compounds, *Nat.*
938 *Commun.*, 7 13677, <https://doi.org/10.1038/ncomms13677>, 2016.

939

940 Berresheim, H., Elste, T., Plass-Dülmer, C., Eisele, F. L., and Tanner, D. J.: Chemical ionization mass spectrometer for long-
941 term measurements of atmospheric OH and H₂SO₄, *Int. J. Mass. Spectrom.*, 202, 91-109, [https://doi.org/10.1016/S1387-](https://doi.org/10.1016/S1387-3806(00)00233-5)
942 [3806\(00\)00233-5](https://doi.org/10.1016/S1387-3806(00)00233-5), 2000.

943

944 Bert, D., Lasnier, J.-B., Capdevielle, X., Dugravot, A., and Desprez-Loustau, M.-L.: Powdery mildew decreases the radial
945 growth of oak trees with cumulative and delayed effects over years, *PLoS ONE*, 11, e0155344, doi:10.1371/journal.
946 [pone.0155344](https://doi.org/10.1371/journal.pone.0155344), 2016.

947

948 Bianchi, F., Kurtén, T., Riva, M., Mohr, C., Rissanen, M. P., Roldin, P., Berndt, T., Crouse, J. D., Wennberg, P. O., Mentel,
949 T. F., Wildt, J., Junninen, H., Jokinen, T., Kulmala, M., Worsnop, D. R., Thornton, J. A., Donahue, N., Kjaergaard, H. G., and
950 Ehn, M.: Highly oxygenated organic molecules (HOM) from gas-phase autoxidation involving peroxy radicals: A key
951 contributor to atmospheric aerosol, *Chem. Rev.*, 119, 3472–3509, <https://doi.org/10.1021/acs.chemrev.8b00395>, 2019.

952

953 Bilde, M., Barsanti, K., Booth, M. D., Cappa, C. D., Donahue, N. M., McFiggans, G., Krieger, U. K., Marcolli, C., Topping,
954 D., Ziemann, P., Barley, M., Clegg, S., Dennis-Smith, B., Emanuelsson, E. U., Hallquist, M., Hallquist, Å. M., Khlystov,
955 A., Kulmala, M., Mogensen, D., Percival, C. P., Pope, F., Reid, J. R., Ribeiro da Silva, M. A. V., Rosenoern, T., Salo, K.,
956 Soonsin, V. P., Yli-Juuti, T., Prisle, N. L., Pagels, J., Rarey, J., Zardini, A. A., and Riipinen, I.: Saturation vapor pressures and
957 transition enthalpies of low-volatility organic molecules of atmospheric relevance: from dicarboxylic acids to complex
958 mixtures, *Chem. Rev.*, 115, 3679-4570, <https://doi.org/10.1021/cr5005502>, 2015.

959

960 Birmili, W., Berresheim, H., Plass-Dülmer, C., Elste, T., Gilge, S., Wiedensohler, A., and Uhrner, U.: The Hohenpeissenberg
961 aerosol formation experiment (HAFEX): a long-term study including size-resolved aerosol, H₂SO₄, OH, and monoterpenes
962 measurements, *Atmos. Chem. Phys.*, 3, 361–376, <https://doi.org/10.5194/acp-3-361-2003>, 2003.

963

964 Blande, J. D., Tiiva, P., Oksanen, E., and Holopainen, J. K.: Emission of herbivore-induced volatile terpenoids from two hybrid
965 aspen (*Populus tremula* × *tremuloides*) clones under ambient and elevated ozone concentrations in the field, *Glob. Chang. Biol.*,
966 13, 2538-2550, [10.1111/j.1365-2486.2007.01453.x](https://doi.org/10.1111/j.1365-2486.2007.01453.x), 2007.

967

968 Blande, J. D., Turunen, K., and Holopainen, J. K.: Pine weevil feeding on Norway spruce bark has a stronger impact on needle
969 VOC emissions than enhanced ultraviolet-B radiation, *Environ. Pollut.*, 157, 174-180, [10.1016/j.envpol.2008.07.007](https://doi.org/10.1016/j.envpol.2008.07.007), 2009.

970

971 Boy, M., Kulmala, M., Ruuskanen, T. M., Pihlatie, M., Reissell, A., Aalto, P. P., Keronen, P., Dal Maso, M., Hellen, H.,
972 Hakola, H., Jansson, R., Hanke, M., and Arnold, F.: Sulphuric acid closure and contribution to nucleation mode particle growth,
973 *Atmos. Chem. Phys.*, 5, 863–878, <https://doi.org/10.5194/acp-5-863-2005>, 2005.

974

975 Boyd, I. L., Freer-Smith, P. H., Gilligan, C. A., and Godfray, H. C. J.: The consequence of tree pests and diseases for ecosystem
976 services, *Science*, 342, 1235773, doi: 10.1126/science.1235773, 2013.

977

978 Brillì, F., Ciccìoli, P., Frattoni, M., Prestinìnzì, M., Spanedda, A. F., and Loreto, F.: Constitutive and herbivore-induced
979 monoterpenes emitted by *Populus × euroamericana* leaves are key volatiles that orient *Chrysomela populi* beetles, *Plant Cell*
980 *Environ.*, 32, 542-552, 10.1111/j.1365-3040.2009.01948.x, 2009.

981

982 Bylund, H.: Long-term interactions between the autumnal moth and mountain birch: The roles of resources, competitors,
983 natural enemies, and weather (PhD Thesis). Swedish University Agricultural Sciences, 1995.

984

985 Cannon, R. J. C.: The implications of predicted climate change for insect pests in the UK, with emphasis on non-indigenous
986 species, *Glob. Chang. Biol.*, 4, 785-796, 10.1046/j.1365-2486.1998.00190.x, 1998.

987

988 Calvert, J., Atkinson, R., Kerr, J. A., Madronich, S., Moortgat, G. K., Wallington, T. J., and Yarwood, G.: The Mechanisms
989 of Atmospheric Oxidation of the Alkenes, Oxford University Press, Oxford, UK, 2000.

990

991 Coleman, T. W., Haavik, L. J., Foelker, C., and Liebhold, A. M.: Forest Insect & Disease Leaflet 162 April 2020, US Forest
992 Service.

993

994 Copolovici, L., Väärtnõu, F., Portillo Estrada, M., and Niinemets, Ü.: Oak powdery mildew (*Erysiphe alphitoides*)-induced
995 volatile emissions scale with the degree of infection in *Quercus robur*, *Tree Physiol.*, 34, 1399-1410,
996 <https://doi.org/10.1093/treephys/tpu091>, 2014.

997

998 Copolovici, L., Pag, A., Kännaste, A., Bodescu, A., Tomescu, D., Copolovici, D., Soran, M.-L., and Niinemets, Ü.:
999 Disproportionate photosynthetic decline and inverse relationship between constitutive and induced volatile emissions upon
1000 feeding of *Quercus robur* leaves by large larvae of gypsy moth (*Lymantria dispar*), *Environ. Exp. Bot.* 138 184-192,
1001 <https://doi.org/10.1016/j.envexpbot.2017.03.014>, 2017.

1002

1003 Covarelli, L., Beccari, G., Tosi, L., Fabre, B., and Frey, P.: Three-year investigations on leaf rust of poplar cultivated for
1004 biomass production in Umbria, Central Italy, *Biomass Bioenerg.*, 49, 315-322,
1005 <https://doi.org/10.1016/j.biombioe.2012.12.032>, 2013.

1006

1007 Dahlberg, U., Berge, T. W., Petersson, H., and Vencatasawmy, C. P.: Modelling biomass and leaf area index in a sub-arctic
1008 Scandinavian mountain area, *Scand. J. Forest Res.*, 19, 60-71, <https://doi.org/10.1080/02827580310019266>, 2004.

1009

1010 Dal Maso, M., Sogacheva, L., Aalto, P. P., Riipinen, I., Komppula, M., Tunved, P., Korhonen, L., Suur-Uski, V., Hirsikko,
1011 A., Kurtén, T., Kerminen, V.-M., Lihavainen, H., Viisanen, Y., Hansson, H.-C., and Kulmala, M.: Aerosol size distribution
1012 measurements at four Nordic field stations: identification, analysis and trajectory analysis of new particle formation bursts,
1013 *Tellus B*, 59, 350-361, doi: 10.1111/j.1600-0889.2007.00267.x, 2007.

1014

1015 Dal Maso, M., Hyvärinen, A., Komppula, M., Tunved, P., Kerminen, V.-M., Lihavainen, H., Viisanen, Y., Hansson, H.-C.,
1016 and Kulmala, M.: Annual and interannual variation in boreal forest aerosol particle number and volume concentration and their
1017 connection to particle formation, *Tellus* 60B, 495-508, <https://doi.org/10.1111/j.1600-0889.2008.00366.x>, 2008.

1018

1019 Desprez-Loustau, M. L., Feau, N., Mougou-Hamdane, A., and Dutech, C.: Interspecific and intraspecific diversity in oak
1020 powdery mildews in Europe: coevolution history and adaptation to their hosts, *Mycoscience*, 52, 165-173,
1021 <https://doi.org/10.1007/s10267-010-0100-5>, 2011.

1022

1023 Di Carlo, P., Brune, W. H., Martinez, M., Harder, H., Leshner, R., Ren, X., Thornberry, T., Carroll, M. A., Young, V., Shepson,
1024 P. B., Riemer, D., Apel, E., and Campbell, C.: Missing OH reactivity in a forest: Evidence for unknown reactive biogenic
1025 VOCs, *Science*, 304, 722–725, doi: 10.1126/science.1094392, 2004.

1026

1027 Donahue, N. M., Ortega, I. K., Chuang, W., Riipinen, I., Riccobono, F., Schobesberger, S., Dommen, J., Baltensperger, U.,
1028 Kulmala, M., Worsnop, D. R., Vehkamäki, H.: How do organic vapors contribute to new-particle formation?, *Faraday Discuss.*,
1029 165, 91-104, 10.1039/C3FD00046J, 2013.

1030

1031 Douma, J. C., Ganzeveld, L. N., Unsicker, S. B., Boeckler, A., and Dicke, M.: What makes a volatile organic compound a
1032 reliable indicator of insect herbivory?, *Plant Cell Environ.*, 42, 3308-3325, <https://doi.org/10.1111/pce.13624>, 2019.

1033

1034 Dunne, E. M., Gordon, H., Kürten, A., Almeida, J., Duplissy, J., Williamson, C., Ortega, I. K., Pringle, K. J., Adamov, A.,
1035 Baltensperger, U., Barmet, P., Benduhn, F., Bianchi, F., Breitenlechner, M., Clarke, A., Curtius, J., Dommen, J., Donahue, N.
1036 M., Ehrhart, S., Flagan, R. C., Franchin, A., Guida, R., Hakala, J., Hansel, A., Heinritzi, M., Jokinen, T., Kangasluoma, J.,
1037 Kirkby, J., Kulmala, M., Kupic, A., Lawler, M. J., Lehtipalo, K., Makhmutov, V., Mann, G., Mathot, S., Merikanto, J.,
1038 Miettinen, P., Nenes, A., Onnela, A., Rap, A., Reddington, C. L. S., Riccobono, F., Richards, N. A. D., Rissanen, M. P., Rondo,
1039 L., Sarnela, N., Schobesberger, S., Sengupta, K., Simon, M., Sipilä, M., Smith, J. N., Stozkhov, Y., Tomé, A., Tröstl, J.,
1040 Wagner, P. E., Wimmer, D., Winkler, P. M., Worsnop, D. R., and Carslaw, K. S.: Global atmospheric particle formation from
1041 CERN CLOUD measurements, *Science*, 354, 1119-1124, DOI: 10.1126/science.aaf2649, 2016.

1042

1043 Ehn, M., Kleist, E., Junninen, H., Petäjä, T., Lönn, G., Schobesberger, S., Dal Maso, M., Trimborn, A., Kulmala, M., Worsnop,
1044 D. R., Wahner, A., Wildt, J., and Mentel, Th. F.: Gas phase formation of extremely oxidized pinene reaction products in
1045 chamber and ambient air, *Atmos. Chem. Phys.*, 12, 5113–5127, <https://doi.org/10.5194/acp-12-5113-2012>, 2012.

1046

1047 Ehn, M., Thornton, J. A., Kleist, E., Sipilä, M., Junninen, H., Pullinen, I., Springer, M., Rubach, F., Tillmann, R., Lee, B.,
1048 Lopez-Hilfiker, F., Andres, S., Acir, I-H., Rissanen, M., Jokinen, T., Schobesberger, S., Kangasluoma, J., Kontkanen, J.,
1049 Nieminen, T., Kurtén, T., Nielsen, L. B., Jørgensen, S., Kjaergaard, H. G., Canagaratna, M., Maso, M. D., Berndt, T., Petäjä,
1050 T., Wahner, A., Kerminen, V.-M., Kulmala, M., Worsnop, D. R., Wildt, J., and Mentel, T. F.: A large source of low-volatility
1051 secondary organic aerosol, *Nature* 506, 476-479, <https://doi.org/10.1038/nature13032>, 2014.

1052

1053 El-Ghany, T. M. A., Eman, M. E., and El-Sheikh, H. H.: Efficacy of fungal rust disease on willow plant in Egypt, *Aust. J.*
1054 *Basic Appl. Sci.*, 3, 1527-1539, 2009.

1055

1056 Faiola, C. and Taipale, D.: Impact of insect herbivory on plant stress volatile emissions from trees: A synthesis of quantitative
1057 measurements and recommendations for future research, *Atmos. Environ.* X, 5, 100060,
1058 <https://doi.org/10.1016/j.aeaoa.2019.100060>, 2020.

1059

1060 Faiola, C. L., Buchholz, A., Kari, E., Yli-Pirilä, P., Holopainen, J. K., Kivimäenpää, M., Miettinen, P., Worsnop, D. R.,
1061 Lehtinen, K. E. J., Guenther, A. B., and Virtanen, A.: Terpene composition complexity controls secondary organic aerosol
1062 yields from Scots pine volatile emissions, *Sci. Rep.*, 8, 3053, 10.1038/s41598-018-21045-1, 2018.

1063

1064 Faiola, C. L., Pullinen, I., Buchholz, A., Khalaj, F., Ylisirniö, A., Kari, E., Miettinen, P., Holopainen, J. K., Kivimäenpää, M.,
1065 Schobesberger, S., Yli-Juuti, T., and Virtanen, A.: Secondary Organic aerosol formation from healthy and aphid-stressed Scots
1066 pine emissions, *ACS Earth Space Chem.*, 3, 1756-1772, <https://doi.org/10.1021/acsearthspacechem.9b00118>, 2019.

1067

1068 Fiedler, V., Dal Maso, M., Boy, M., Aufmhoff, H., Hoffmann, J., Schuck, T., Birmili, W., Hanke, M., Uecker, J., Arnold, F.,
1069 and Kulmala, M.: The contribution of sulphuric acid to atmospheric particle formation and growth: a comparison between
1070 boundary layers in Northern and Central Europe, *Atmos. Chem. Phys.*, 5, 1773–1785, [https://doi.org/10.5194/acp-5-1773-](https://doi.org/10.5194/acp-5-1773-2005)
1071 2005, 2005.

1072

1073 Gérard, P. R., Husson, C., Pinon, J., and Frey, P.: Comparison of genetic and virulence diversity of *Melampsora larici-populina*
1074 populations on wild and cultivated poplar and influence of the alternate host, *Phytopathology*, 96, 1027-1036, doi:
1075 10.1094/PHYTO-96-1027, 2006.

1076

1077 Ghimire, R. P., Kivimäenpää, M., Kasurinen, A., Häikiö, E., Holopainen, T., and Holopainen, J. K.: Herbivore-induced BVOC
1078 emissions of Scots pine under warming, elevated ozone and increased nitrogen availability in an open-field exposure, *Agric.*
1079 *For. Meteorol.*, 242, 21-32, 10.1016/j.agrformet.2017.04.008, 2017.

1080

1081 Ghirardo, A., Koch, K., Taipale, R., Zimmer, I., Schnitzler, J.-P., and Rinne, J.: Determination of de novo and pool emissions
1082 of terpenes from four common boreal/alpine trees by ¹³CO₂ labelling and PTR-MS analysis, *Plant Cell Environ.*, 33, 781-792,
1083 <https://doi.org/10.1111/j.1365-3040.2009.02104.x>, 2010.

1084

1085 Gill, A. L., Gallinat, A. S., Sanders-DeMott, R., Rigden, A. J., Short Gianotti, D. J., Mantooth, J. A., and Templer, P. H.:
1086 Changes in autumn senescence in northern hemisphere deciduous trees: a meta-analysis of autumn phenology studies. *Ann.*
1087 *Bot.* 116, 875-888, doi: 10.1093/aob/mcv055, 2015.

1088

1089 Glawe, D. A.: The powdery mildews: a review of the world's most familiar (yet poorly known) plant pathogens, *Annu. Rev.*
1090 *Phytopathol.*, 46, 27-51, doi: 10.1146/annurev.phyto.46.081407.104740, 2008.

1091

1092 Goldstein, A., Goulden, M., Munger, J. W., Wofsy, S., and Geron, C.: Seasonal course of isoprene emissions from a midlatitude
1093 forest, *J. Geophys. Res.*, 103, 31 045–31 056, <https://doi.org/10.1029/98JD02708>, 1998.

1094

1095 Größ, J., Hamed, A., Sonntag, A., Spindler, G., Manninen, H. E., Nieminen, T., Kulmala, M., Hörrak, U., Plass-Dülmer, C.,
1096 Wiedensohler, A., and Birmili, W.: Atmospheric new particle formation at the research station Melpitz, Germany: connection
1097 with gaseous precursors and meteorological parameters, *Atmos. Chem. Phys.*, 18, 1835–1861, [https://doi.org/10.5194/acp-18-](https://doi.org/10.5194/acp-18-1835-2018)
1098 1835-2018, 2018.

1099

1100 Grote, R., Monson, R. K., Niinemets, Ü.: Leaf-level models of constitutive and stress-driven volatile organic compound
1101 emissions, *Biology, Controls and Models of Tree Volatile Organic Compound Emissions*, *Tree Physiology*, Springer,
1102 Dordrecht, 315-355, 10.1007/978-94-007-6606-8_12, 2013.

1103

1104 Grote, R., Sharma, M., Ghirardo, A., Schnitzler, J.-P.: A new modeling approach for estimating abiotic and biotic stress-
1105 induced de novo emissions of biogenic volatile organic compounds from plants, *Front. For. Glob. Change*, 2, 26, doi:
1106 10.3389/ffgc.2019.00026, 2019.

1107

1108 Gryspeerdt, E., Stier, P., and Partridge, D. G.: Satellite observations of cloud regime development: the role of aerosol processes,
1109 *Atmos. Chem. Phys.*, 14, 1141–1158, <https://doi.org/10.5194/acp-14-1141-2014>, 2014.

1110

1111 Guenther, A.: Seasonal and spatial variations in natural volatile organic compound emissions, *Ecol. Appl.*, 7, 34-45,
1112 [https://doi.org/10.1890/1051-0761\(1997\)007\[0034:SASVIN\]2.0.CO;2](https://doi.org/10.1890/1051-0761(1997)007[0034:SASVIN]2.0.CO;2), 1997.

1113

1114 Guenther, A. B., Monson, R. K., and Fall, R.: Isoprene and monoterpene emission rate variability: Observations with
1115 eucalyptus and emission rate algorithm development, *J. Geophys. Res.*, 96, 10799-10808, <https://doi.org/10.1029/91JD00960>,
1116 1991.

1117

1118 Guenther, A., Zimmerman, P., and Wildermuth, M.: Natural volatile organic compound emission rate estimates for U.S.
1119 woodland landscapes, *Atmos. Environ.*, 28, 1197-1210, [https://doi.org/10.1016/1352-2310\(94\)90297-6](https://doi.org/10.1016/1352-2310(94)90297-6), 1994.

1120

1121 Guenther, A., Karl, T., Harley, P., Wiedinmyer, C., Palmer, P. I., and Geron, C.: Estimates of global terrestrial isoprene
1122 emissions using MEGAN (Model of Emissions of Gases and Aerosols from Nature), *Atmos. Chem. Phys.*, 6, 3181–3210,
1123 <https://doi.org/10.5194/acp-6-3181-2006>, 2006.

1124

1125 Guenther, A. B., Jiang, X., Heald, C. L., Sakulyanontvittaya, T., Duhl, T., Emmons, L. K., and Wang, X.: The Model of
1126 Emissions of Gases and Aerosols from Nature version 2.1 (MEGAN2.1): an extended and updated framework for modeling
1127 biogenic emissions, *Geosci. Model Dev.*, 5, 1471–1492, <https://doi.org/10.5194/gmd-5-1471-2012>, 2012.

1128

1129 Hajji, M., Dreyer, M., and Marçais, B.: Impact of *Erysiphe alphitoides* on transpiration and photosynthesis in *Quercus robur*
1130 leaves, *Eur. J. Plant. Pathol.*, 125, 63-72, <https://doi.org/10.1007/s10658-009-9458-7>, 2009.

1131

1132 Häkkinen, S. A. K., Manninen, H. E., Yli-Juuti, T., Merikanto, J., Kajos, M. K., Nieminen, T., D'Andrea, S. D., Asmi, A.,
1133 Pierce, J. R., Kulmala, M., and Riipinen, I.: Semi-empirical parameterization of size-dependent atmospheric nanoparticle
1134 growth in continental environments, *Atmos. Chem. Phys.*, 13, 7665–7682, <https://doi.org/10.5194/acp-13-7665-2013>, 2013.

1135

1136 Hakola, H., Arey, J., Aschmann, S. M., and Atkinson, R.: Product formation from the gas phase reactions of OH radicals and
1137 O₃ with a series of monoterpenes, *J. Atmos. Chem.*, 18, 75-102, <https://doi.org/10.1007/BF00694375>, 1994.

1138

1139 Hari, P., Kulmala, M., Pohja, T., Lahti, T., Siivola, R., Palva, L., Aalto, P., Hämeri, K., Vesala, T., Luoma, S., and Pulliainen,
1140 E.: Air pollution in eastern Lapland: challenge for an environmental measurement station, *Silva Fenn.*, 28, 29-39,
1141 <https://doi.org/10.14214/sf.a9160>, 1994.

1142

1143 Harrington, R., Clark, S. J., Welham, S. J., Verrier, P. J., Denholm, C. H., Hullé, M., Maurice, D., Rounsevell, M. D., and
1144 Cocu, N.: Environmental change and the phenology of European aphids, *Glob. Chang. Biol.*, 13, 1550-1564, 10.1111/j.1365-
1145 2486.2007.01394.x, 2007.

1146

1147 Haukioja, E., Neuvonen, S., Hanhimäki, S., and Niemelä, P.: The autumnal moth in Fennoscandia. In: Dynamics of forest
1148 insect populations, Springer, pp. 163-178, 1988.

1149

1150 Heinritzi, M., Dada, L., Simon, M., Stolzenburg, D., Wagner, A. C., Fischer, L., Ahonen, L. R., Amanatidis, S., Baalbaki, R.,
1151 Baccarini, A., Bauer, P. S., Baumgartner, B., Bianchi, F., Brilke, S., Chen, D., Chiu, R., Dias, A., Dommen, J., Duplissy, J.,
1152 Finkenzeller, H., Frege, C., Fuchs, C., Garmash, O., Gordon, H., Granzin, M., El Haddad, I., He, X., Helm, J., Hofbauer, V.,
1153 Hoyle, C. R., Kangasluoma, J., Keber, T., Kim, C., Kürten, A., Lamkaddam, H., Laurila, T. M., Lampilahti, J., Lee, C. P.,
1154 Lehtipalo, K., Leiminger, M., Mai, H., Makhmutov, V., Manninen, H. E., Marten, R., Mathot, S., Mauldin, R. L., Mentler, B.,
1155 Molteni, U., Müller, T., Nie, W., Nieminen, T., Onnela, A., Partoll, E., Passananti, M., Petäjä, T., Pfeifer, J., Pospisilova, V.,
1156 Quéléver, L. L. J., Rissanen, M. P., Rose, C., Schobesberger, S., Scholz, W., Scholze, K., Sipilä, M., Steiner, G., Stozhkov,
1157 Y., Tauber, C., Tham, Y. J., Vazquez-Pufleau, M., Virtanen, A., Vogel, A. L., Volkamer, R., Wagner, R., Wang, M., Weitz,
1158 L., Wimmer, D., Xiao, M., Yan, C., Ye, P., Zha, Q., Zhou, X., Amorim, A., Baltensperger, U., Hansel, A., Kulmala, M., Tomé,
1159 A., Winkler, P. M., Worsnop, D. R., Donahue, N. M., Kirkby, J., and Curtius, J.: Molecular understanding of the suppression
1160 of new-particle formation by isoprene, *Atmos. Chem. Phys.*, 20, 11809–11821, <https://doi.org/10.5194/acp-20-11809-2020>,
1161 2020.

1162

1163 Heiskanen, J.: Estimating aboveground tree biomass and leaf area index in a mountain birch forest using ASTER satellite data,
1164 *Int. J. Remote Sens.*, 6, 1135-1158, <https://doi.org/10.1080/01431160500353858>, 2006.

1165

1166 Hirsikko, A., Laakso, L., Hörrak, U., Aalto, P. P., Kerminen, V.-M., and Kulmala, M.: Annual and size dependent variation of
1167 growth rates and ion concentrations in boreal forest, *Boreal Environ. Res.*, 10, 357-369, 2005.

1168

1169 Holopainen, J. K. and Gershenson, J.: Multiple stress factors and the emission of plant VOCs, *Trends Plant Sci. Special Issue:*
1170 *Induc. Biog. Volatile Org. Compd. Plant*, 15, 176-184, 10.1016/j.tplants.2010.01.006, 2010.

1171

1172 Hunter, M. D., Kozlov, M. V., Itämies, J., Pulliainen, E., Bäck, J., Kyrö, E. M., and Niemelä, P.: Current temporal trends in
1173 moth abundance are counter to predicted effects of climate change in an assemblage of subarctic forest moths, *Glob. Change*
1174 *Biol.*, 20, 1723-1737, doi: 10.1111/gcb.12529, 2014.

1175

1176 Hyvönen, S., Junninen, H., Laakso, L., Dal Maso, M., Grönholm, T., Bonn, B., Keronen, P., Aalto, P., Hiltunen, V., Pohja, T.,
1177 Launiainen, S., Hari, P., Mannila, H., and Kulmala, M.: A look at aerosol formation using data mining techniques, *Atmos.*
1178 *Chem. Phys.*, 5, 3345–3356, <https://doi.org/10.5194/acp-5-3345-2005>, 2005.

1179

1180 ICP Forests - Forest Condition in Europe: The 2020 Assessment, ICP Forests Technical Report under the UNECE Convention
1181 on Long-range Transboundary Air Pollution (Air Convention), https://www.icp-forests.org/pdf/ICPForests_TR2020.pdf

1182

1183 IPCC (2013). “Climate Change 2013: the physical science basis,” in Contribution of Working Group I to the Fifth Assessment
1184 Report of the Intergovernmental Panel on Climate Change, eds F. T. Stocker et al. (Cambridge: Cambridge University Press),
1185 1535.

1186

1187 Jenkin, M. E. and Clemitshaw, K. C.: Ozone and other secondary photochemical pollutants: chemical processes governing
1188 their formation in the planetary boundary layer, *Atmos. Environ.*, 34, 2499-2527, 2000.

1189

1190 Jenkin, M. E., Young, J. C., and Rickard, A. R.: The MCM v3.3.1 degradation scheme for isoprene, *Atmos. Chem. Phys.*, 15,
1191 11433–11459, <https://doi.org/10.5194/acp-15-11433-2015>, 2015.

1192

1193 Jiang, Y., Ye, J., Veromann, L.-L., and Niinemets, Ü.: Scaling of photosynthesis and constitutive and induced volatile
1194 emissions with severity of leaf infection by rust fungus (*Melampsora larici-populina*) in *Populus balsamifera* var. *suaveolens*,
1195 *Tree Physiol.*, 36, 856-872, doi: 10.1093/treephys/tpw035, 2016.

1196

1197 Jimenez, J. L., Canagaratna, M. R., Donahue, N. M., Prevot, A. S., Zhang, Q., Kroll, J. H., DeCarlo, P. F., Allan, J. D., Coe,
1198 H., Ng, N. L., Aiken, A. C., Docherty, K. S., Ulbrich, I. M., Grieshop, A. P., Robinson, A. L., Duplissy, J., Smith, J. D., Wilson,
1199 K. R., Lanz, V. A., Hueglin, C., Sun, Y. L., Tian, J., Laaksonen, A., Raatikainen, T., Rautiainen, J., Vaattovaara, P., Ehn, M.,
1200 Kulmala, M., Tomlinson, J. M., Collins, D. R., Cubison, M. J., Dunlea, E. J., Huffman, J. A., Onasch, T. B., Alfarra, M. R.,
1201 Williams, P. I., Bower, K., Kondo, Y., Schneider, J., Drewnick, F., Borrmann, S., Weimer, S., Demerjian, K., Salcedo, D.,
1202 Cottrell, L., Griffin, R., Takami, A., Miyoshi, T., Hatakeyama, S., Shimono, A., Sun, J. Y., Zhang, Y. M., Dzepina, K., Kimmel,
1203 J. R., Sueper, D., Jayne, J. T., Herndon, S. C., Trimborn, A. M., Williams, L. R., Wood, E. C., Middlebrook, A. M., Kolb, C.
1204 E., Baltensperger, U., Worsnop, D. R.: Evolution of organic aerosols in the atmosphere, *Science*, 326, 1525-1529, doi:
1205 10.1126/science.1180353, 2009.

1206

1207 Johnson, D. M., Liebhold, A. M., and Bjørnstad, O. N.: Geographical variation in the periodicity of gypsy moth outbreaks,
1208 *Ecogeg.*, 29, 367-374, doi: 10.1111/j.2006.0906-7590.04448.x,2006.

1209

1210 Johansson, L. K.-H. and Alström, S.: Field resistance to willow leaf rust *Melampsora epitea* in inter- and intraspecific hybrids
1211 of *Salix viminalis* and *S. dasyclados*, *Eur. J. Plant Pathol.*, 106, 763-769, <https://doi.org/10.1023/A:1026573219481>, 2000.

1212

1213 Jokinen, T., Berndt, T., Makkonen, R., Kerminen, V.-M., Junninen, H., Paasonen, P., Stratmann, F., Herrmann, H., Guenther,
1214 A. B., Worsnop, D. R., Kulmala, M., Ehn, M., and Sipilä, M.: Production of extremely low volatile organic compounds from
1215 biogenic emissions: Measured yields and atmospheric implications, *Proc. Natl. Acad. Sci. U. S. A.*, 112, 7123-7128,
1216 <https://doi.org/10.1073/pnas.1423977112>, 2015.

1217

1218 Joutsensaari, J., Yli-Pirilä, P., Korhonen, H., Arola, A., Blande, J. D., Heijari, J., Kivimäenpää, M., Mikkonen, S., Hao, L.,
1219 Miettinen, P., Lyytikäinen-Saarenmaa, P., Faiola, C. L., Laaksonen, A., and Holopainen, J. K.: Biotic stress accelerates
1220 formation of climate-relevant aerosols in boreal forests, *Atmos. Chem. Phys.*, 15, 12139–12157, [https://doi.org/10.5194/acp-](https://doi.org/10.5194/acp-15-12139-2015)
1221 [15-12139-2015](https://doi.org/10.5194/acp-15-12139-2015), 2015.

1222

1223 Kaitaniemi, P., Ruohomäki, K., and Haukioja, E.: Consequences of defoliation on phenological interaction between *Epirrita*
1224 *autumnata* and its host plant, mountain birch, *Funct. Ecol.*, 11, 199-208, <https://doi.org/10.1046/j.1365-2435.1997.00063.x>,
1225 1997.

1226

1227 Kaitaniemi, P., Ruohomäki, K., Ossipov, V., Haukioja, E., and Pihlaja, K.: Delayed induced changes in the biochemical
1228 composition of host plant leaves during an insect outbreak, *Oecologia*, 116, 182-190, <https://doi.org/10.1007/s004420050578>,
1229 1998.

1230

1231 Kaitaniemi, P. and Ruohomäki, K.: Effects of autumn temperature and oviposition date on timing of larval development and
1232 risk of parasitism in a spring folivore, *Oikos*, 84, 435-442, doi: 10.2307/3546422, 1999.

1233

1234 Kanakidou, M., Seinfeld, J. H., Pandis, S. N., Barnes, I., Dentener, F. J., Facchini, M. C., Van Dingenen, R., Ervens, B., Nenes,
1235 A., Nielsen, C. J., Swietlicki, E., Putaud, J. P., Balkanski, Y., Fuzzi, S., Horth, J., Moortgat, G. K., Winterhalter, R., Myhre,
1236 C. E. L., Tsigaridis, K., Vignati, E., Stephanou, E. G., and Wilson, J.: Organic aerosol and global climate modelling: a review,
1237 *Atmos. Chem. Phys.*, 5, 1053–1123, <https://doi.org/10.5194/acp-5-1053-2005>, 2005.
1238

1239 Kanawade, V. P., Jobson, B. T., Guenther, A. B., Erupe, M. E., Pressley, S. N., Tripathi, S. N., and Lee, S.-H.: Isoprene
1240 suppression of new particle formation in a mixed deciduous forest, *Atmos. Chem. Phys.*, 11, 6013–6027,
1241 <https://doi.org/10.5194/acp-11-6013-2011>, 2011.
1242

1243 Karel, T. H. and Man, G.: Major Forest Insect and Disease Conditions in the United States: 2015 (No. FS-1093), U. S.
1244 Department of Agriculture, 2017.
1245

1246 Kari, E., Faiola, C. L., Isokääntä, S., Miettinen, P., Yli-Pirilä, P., Buchholz, A., Kivimäenpää, M., Mikkonen, S., Holopainen,
1247 J. K., and Virtanen, A.: Time-resolved characterization of biotic stress emissions from Scots pines being fed upon by pine
1248 weevil by means of PTR-ToF-MS, *Boreal Environ. Res.*, 24, 25-49, 2019.
1249

1250 Kerminen, V.-M. and Kulmala, M.: Analytical formulae connecting the “real” and the “apparent” nucleation rate and the nuclei
1251 number concentration for atmospheric nucleation events, *J. Aerosol Sci.*, 33, 609-622, doi: 10.1016/S0021-8502(01)00194-X,
1252 2002.
1253

1254 Kerminen, V.-M., Lihavainen, H., Komppula, M., Viisanen, Y., and Kulmala, M.: Direct observational evidence linking
1255 atmospheric aerosol formation and cloud droplet activation, *Geophys. Res. Lett.*, 32, 10.1029/2005GL023130, 2005.
1256

1257 Kerminen, V.-M., Paramonov, M., Anttila, T., Riipinen, I., Fountoukis, C., Korhonen, H., Asmi, E., Laakso, L., Lihavainen,
1258 H., Swietlicki, E., Svenningsson, B., Asmi, A., Pandis, S. N., Kulmala, M., and Petäjä, T.: Cloud condensation nuclei
1259 production associated with atmospheric nucleation: a synthesis based on existing literature and new results, *Atmos. Chem.*
1260 *Phys.*, 12, 12037– 12059, <https://doi.org/10.5194/acp-12-12037-2012>, 2012.
1261

1262 Kiendler-Scharr, A., Wildt, J., Dal Maso, M., Hohaus, T., Kleist, E., Mentel, T. F., Tillmann, R., Uerlings, R., Schurr, U., and
1263 Wahner, A.: New particle formation in forests inhibited by isoprene emissions, *Nature*, 461, 381-384, DOI:
1264 10.1038/nature08292, 2009.
1265

1266 Kiendler-Scharr, A., Andres, S., Bachner, M., Behnke, K., Broch, S., Hofzumahaus, A., Holland, F., Kleist, E., Mentel, T. F.,
1267 Rubach, F., Springer, M., Steitz, B., Tillmann, R., Wahner, A., Schnitzler, J.-P., and Wildt, J.: Isoprene in poplar emissions:
1268 effects on new particle formation and OH concentrations, *Atmos. Chem. Phys.*, 12, 1021–1030, [https://doi.org/10.5194/acp-](https://doi.org/10.5194/acp-12-1021-2012)
1269 [12-1021-2012](https://doi.org/10.5194/acp-12-1021-2012), 2012.
1270

1271 Kirkby, J., Duplissy, J., Sengupta, K., Frege, C., Gordon, H., Williamson, C., Heinritzi, M., Simon, M., Yan, C., Almeida, J.,
1272 Tröstl, J., Nieminen, T., Ortega, I. K., Wagner, R., Adamov, A., Amorim, A., Bernhammer, A.-K., Bianchi, F., Breitenlechner,
1273 M., Brilke, S., Chen, X., Craven, J., Dias, A., Ehrhart, S., Flagan, R. C., Franchin, A., Fuchs, C., Guida, R., Hakal, J., Hoyle,
1274 C. R., Jokinen, T., Junninen, H., Kangasluoma, J., Him, J., Krapf, M., Kürten, A., Laaksonen, A., Lehtipalo, K., Makhmutov,
1275 V., Mathot, S., Molteni, U., Onnela, A., Peräkylä, O., Piel, F., Petäjä, T., Praplan, A. P., Pringle, K., Rap, A., Richards, N. A.
1276 D., Riipinen, I., Rissanen, M. P., Rondo, L., Sarnela, N., Schobesberger, S., Scott, C. E., Seinfeld, J. H., Sipilä, M., Steiner,
1277 G., Stozhkov, Y., Stratmann, F., Tomé, A., Virtanen, A., Vogel, A. L., Wagner, A. C., Wagner, P. E., Weingartner, E.,

1278 Wimmer, D., Winkler, P. M., Ye, P., Zhang, X., Hansel, A., Dommen, J., Donahue, N. M., Worsnop, D. R., Baltensperger, U.,
1279 Kulmala, M., Carslaw, K. S., and Curtius, J.: Ion-induced nucleation of pure biogenic particles, *Nature*, 533, 521–526,
1280 <https://doi.org/10.1038/nature17953>, 2016.

1281

1282 Kivimäenpää, M., Ghimire, R. P., Sutinen, S., Häikiö, E., Kasurinen, A., Holopainen, T., and Holopainen, J. K.: Increases in
1283 volatile organic compound emissions of Scots pine in response to elevated ozone and warming are modified by herbivory and
1284 soil nitrogen availability, *Eur. J. For. Res.*, 135, 343-360, [10.1007/s10342-016-0939-x](https://doi.org/10.1007/s10342-016-0939-x), 2016.

1285

1286 Klemola, T., Ruohomäki, K., Andersson, T., and Neuvonen, S.: Reduction in size and fecundity of the autumnal moth, *Epirrita*
1287 *autumnata*, in the increase phase of a population cycle, *Oecologia*, 141, 47-56, <https://doi.org/10.1007/s00442-004-1642-z>,
1288 2004.

1289

1290 Komppula, M., Sihto, S.-L., Korhonen, H., Lihavainen, H., Kerminen, V.-M., Kulmala, M., and Viisanen, Y.: New particle
1291 formation in air mass transported between two measurement sites in Northern Finland, *Atmos. Chem. Phys.*, 6, 2811–2824,
1292 <https://doi.org/10.5194/acp-6-2811-2006>, 2006.

1293

1294 Kula, E., Pešlová, A., Martinek, P., and Mazal, P.: The development of caterpillars of gypsy moth (*Lymantria dispar* L.) feeding
1295 on food affected by nitrogen, *Sumar. List*, 137, 51-60, 2013.

1296

1297 Kulmala, M., Petäjä, T., Nieminen, T., Sipilä, M., Manninen, H. E., Lehtipalo, K., Dal Maso, M., Aalto, P. P., Junninen, H.,
1298 Paasonen, P., Riipinen, I., Lehtinen, K. E. J., Laaksonen, A., and Kerminen, V.-M.: Measurement of the nucleation of
1299 atmospheric aerosol particles, *Nat. Protoc.*, 7, 1651–1667, <https://doi.org/10.1038/nprot.2012.091>, 2012.

1300

1301 Kulmala, M., Kontkanen, J., Junninen, H., Lehtipalo, K., Manninen, H. E., Nieminen, T., Petäjä, T., Sipilä, M., Schobesberger,
1302 S., Rantala, P., Franchin, A., Jokinen, T., Järvinen, E., Äijälä, M., Kangasluoma, J., Hakala, J., Aalto, P. P., Paasonen, P.,
1303 Mikkilä, J., Vanhanen, J., Aalto, J., Hakola, H., Makkonen, U., Ruuskanen, T., Mauldin, R. L. III, Duplissy, J., Vehkamäki,
1304 H., Bäck, J., Kortelainen, A., Riipinen, I., Kurtén, T., Johnston, M. V., Smith, J. N., Ehn, M., Mentel, T. F., Lehtinen, K. E. J.,
1305 Laaksonen, A., Kerminen, V.-M., and Worsnop, D. R.: Direct observations of atmospheric aerosol nucleation, *Science*, 339,
1306 943-946, DOI: [10.1126/science.1227385](https://doi.org/10.1126/science.1227385), 2013.

1307

1308 Kulmala, M., Petäjä, T., Ehn, M., Thornton, J., Sipilä, M., Worsnop, D. R., Kerminen, V.-M.: Chemistry of atmospheric
1309 nucleation: on the recent advances on precursor characterization and atmospheric cluster composition in connection with
1310 atmospheric new particle formation, *Annu. Rev. Phys. Chem.*, 65, 21-37, <https://doi.org/10.1146/annurev-physchem-040412-110014>, 2014.

1311

1312

1313 Kyrö, E.-M., Väänänen, R., Kerminen, V.-M., Virkkula, A., Petäjä, T., Asmi, A., Dal Maso, M., Nieminen, T., Juhola, S.,
1314 Shcherbinin, A., Riipinen, I., Lehtipalo, K., Keronen, P., Aalto, P. P., Hari, P., and Kulmala, M.: Trends in new particle
1315 formation in eastern Lapland, Finland: effect of decreasing sulfur emissions from Kola Peninsula, *Atmos. Chem. Phys.*, 14,
1316 4383–4396, <https://doi.org/10.5194/acp-14-4383-2014>, 2014.

1317

1318 Lee, S.-H., Uin, J., Guenther, A. B., de Gouw, J. A., Yu, F., Nadykto, A. B., Herb, J., Ng, N. L., Koss, A., Brune, W. B.,
1319 Baumann, K., Kanawade, V. P., Keutsch, F. N., Nenes, A., Olsen, K., Goldstein, A., and Ouyang, Q.: Isoprene suppression of
1320 new particle formation: Potential mechanisms and implications, *J. Geophys. Res.*, 121, 14621-14635,
1321 <https://doi.org/10.1002/2016JD024844>, 2016.

1322

1323 Lehtinen, K. E. J., Dal Maso, M., Kulmala, M., and Kerminen, V. M.: Estimating nucleation rates from apparent particle
1324 formation rates and vice versa: Revised formulation of the Kerminen-Kulmala equation, *J. Aerosol Sci.*, 38, 988-994,
1325 <https://doi.org/10.1016/j.jaerosci.2007.06.009>, 2007.

1326

1327 Lelieveld, J., Butler, T. M., Crowley, J. N., Dillon, T. J., Fischer, H., Ganzeveld, L., Harder, H., Lawrence, M. G., Martinez,
1328 M., Taraborrelli, D., and Williams, J.: Atmospheric oxidation capacity sustained by a tropical forest, *Nature*, 452, 737–740,
1329 <https://doi.org/10.1038/nature06870>, 2008.

1330

1331 Lempa, K., Agrawal, A. A., Salminen, J.P., Turunen, T., Ossipov, V., Ossipova, S., Haukioja, E., and Pihlaja, K.: Rapid
1332 herbivore-induced changes in mountain birch phenolics and nutritive compounds and their effects on performance of the major
1333 defoliator, *Epirrita autumnata*, *J. Chem. Ecol.*, 30, 303-321, <https://doi.org/10.1023/B:JOEC.0000017979.94420.78>, 2004.

1334

1335 Li, T., Holst, T., Michelsen, A., and Rinnan, R.: Amplification of plant volatile defence against insect herbivory in a warming
1336 Arctic tundra, *Nat. Plants*, 5, 568-574, doi:10.1038/s41477-019-0439-3, 2019.

1337

1338 Lin, Y. H., Zhang, H., Pye, H. O. T., Zhang, Z., Marth, W. J., Park, S., Arashiro, M., Cui, T., Budisulistiorini, S. H., Sexton,
1339 K. G., Vizuete, W., Xie, Y., Luecken, D. J., Piletic, I. R., Edney, E. O., Bartolotti, L. J., Gold, A., and Surratt, J. D.: Epoxide
1340 as a precursor to secondary organic aerosol formation from isoprene photooxidation in the presence of nitrogen oxides, *Proc.*
1341 *Natl. Acad. Sci. U.S.A.*, 110, 6718–6723, <https://doi.org/10.1073/pnas.1221150110>, 2013.

1342

1343 Major, I. T., Nicole, M.-C., Duplessis, S., and Seguin, A.: Photosynthetic and respiratory changes in leaves of poplar elicited
1344 by rust infection, *Photosynth. Res.*, 104, 41-48, doi: 10.1007/s11120-009-9507-2, 2010.

1345

1346 Makkonen, R., Asmi, A., Korhonen, H., Kokkola, H., Järvenoja, S., Räisänen, P., Lehtinen, K. E. J., Laaksonen, A., Kerminen,
1347 V.-M., Järvinen, H., Lohmann, U., Bennartz, R., Feichter, J., Kulmala, M.: Sensitivity of aerosol concentrations and cloud
1348 properties to nucleation and secondary organic distribution in ECHAM5-HAM global circulation model, *Atmos. Chem. Phys.*,
1349 9, 1747-1766, 10.5194/acp-9-1747-2009, 2009.

1350

1351 Marçais, B. and Desprez-Loustau, M.-L.: European oak powdery mildew: impact on trees, effects of environmental factors,
1352 and potential effects of climate change, *Ann. For. Sci.*, 71, 633-642, <https://doi.org/10.1007/s13595-012-0252-x>, 2014.

1353

1354 Marçais, B., Kavkova, M., and Desprez-Loustau, M.-L.: Phenotypic variation in the phenology of ascospore production
1355 between European populations of oak powdery mildew, *Ann. For. Sci.*, 66, 814-822, <https://doi.org/10.1051/forest/2009077>,
1356 2009.

1357

1358 McFiggans, G., Mentel, T. F., Wildt, J., Pullinen, I., Kang, S., Kleist, E., Schmitt, S., Springer, M., Tillmann, R., Wu, C., Zhao,
1359 D., Hallquist, M., Faxon, C., Le Breton, M., Hallquist, Å. M., Simpson, D., Bergström, R., Jenkin, M. E., Ehn, M., Thornton,
1360 J. A., Alfarra, M. R., Bannan, T. J., Percival, C. J., Priestley, M., Topping, D., and Kiendler-Scharr, A.: Secondary organic
1361 aerosol reduced by mixture of atmospheric vapours, *Nature*, 565, 587-593, 10.1038/s41586-018-0871- y, 2019.

1362

1363 McManus, M., Schneeberger, N., Reardon, R., and Mason, G.: Forest insect and disease (No 162): Gypsy Moth, Washington,
1364 D.C.: United States Department of Agriculture Forest Service, 1989.

1365

1366 Mentel, Th. F., Kleist, E., Andres, S., Dal Maso, M., Hohaus, T., Kiendler-Scharr, A., Rudich, Y., Springer, M., Tillmann, R.,
1367 Uerlings, R., Wahner, A., and Wildt, J.: Secondary aerosol formation from stress-induced biogenic emissions and possible
1368 climate feedbacks, *Atmos. Chem. Phys.*, 13, 8755-8770, <https://doi.org/10.5194/acp-13-8755-2013>, 2013.

1369

1370 Merikanto, J., Spracklen, D. V., Mann, G. W., Pickering, S. J., and Carslaw, K. S.: Impact of nucleation on global CCN,
1371 *Atmos. Chem. Phys.*, 9, 8601-8616, [10.5194/acp-9-8601-2009](https://doi.org/10.5194/acp-9-8601-2009), 2009.

1372

1373 Miller, J. C., Hanson, P. E., and Kimberling, D. N.: Development of the gypsy moth (Lepidoptera: Lymantriidae) on garry oak
1374 and red alder in Western North America, *Environ. Entomol.*, 20, 1097-1101, <https://doi.org/10.1093/ee/20.4.1097>, 1991.

1375

1376 Mogensen, D., Smolander, S., Sogachev, A., Zhou, L., Sinha, V., Guenther, A., Williams, J., Nieminen, T., Kajos, M. K.,
1377 Rinne, J., Kulmala, M., and Boy, M.: Modelling atmospheric OH-reactivity in a boreal forest ecosystem, *Atmos. Chem. Phys.*,
1378 11, 9709–9719, <https://doi.org/10.5194/acp-11-9709-2011>, 2011.

1379

1380 Mogensen, D., Gierens, R., Crowley, J. N., Keronen, P., Smolander, S., Sogachev, A., Nölscher, A. C., Zhou, L., Kulmala,
1381 M., Tang, M. J., Williams, J., and Boy, M.: Simulations of atmospheric OH, O₃ and NO₃ reactivities within and above the
1382 boreal forest, *Atmos. Chem. Phys.*, 15, 3909–3932, <https://doi.org/10.5194/acp-15-3909-2015>, 2015.

1383

1384 Monson, R. K., Harley, P. C., Litvak, M. E., Wildermuth, M., Guenther, A. B., Zimmerman, P. R., and Fall, R.: Environmental
1385 and developmental controls over the seasonal pattern of isoprene emission from aspen leaves, *Oecologia*, 99, 260–270,
1386 <https://doi.org/10.1007/BF00627738>, 1994.

1387

1388 Mutzel, A., Poulain, L., Berndt, T., Iinuma, Y., Rodigast, M., Böge, O., Richters, S., Spindler, G., Sipilä, M., Jokinen, T.,
1389 Kulmala, M., and Herrmann, H.: Highly oxidized multifunctional organic compounds observed in tropospheric particles: a
1390 field and laboratory study, *Environ. Sci. Technol.*, 49, 7754-7761, <https://doi.org/10.1021/acs.est.5b00885>, 2015.

1391

1392 Naja, M., Akimoto, H., and Staehelin, J.: Ozone in background and photochemically aged air over central Europe: analysis of
1393 long-term ozonesonde data from Hohenpeissenberg and Payerne, *J. Geophys. Res.*, 108, 4063, doi:10.1029/2002JD002477
1394 2003.

1395

1396 Nieminen, T., Lehtinen, K. E. J., and Kulmala, M.: Sub-10 nm particle growth by vapor condensation – effects of vapor
1397 molecule size and particle thermal speed, *Atmos. Chem. Phys.*, 10, 9773–9779, <https://doi.org/10.5194/acp-10-9773-2010>,
1398 2010.

1399

1400 Nieminen, T., Asmi, A., Dal Maso, M., Aalto, P. P., Keronen, P., Petäjä, T., Kulmala, M., and Kerminen, V.-M.: Trends in
1401 atmospheric new-particle formation: 16 years of observations in a boreal-forest environment, *Boreal Environ. Res.*, 19, suppl.
1402 B, 191–214, 2014.

1403

1404 Nieminen, T., Yli-Juuti, T., Manninen, H., Petäjä, T., Kerminen, V.-M., and Kulmala, M.: Technical note: New particle
1405 formation event forecasts during PEGASOS–Zeppelin Northern mission 2013 in Hyytiälä, Finland, *Atmos. Chem. Phys.*, 15,
1406 12385–12396, doi:10.5194/acp-15-12385-2015, 2015.

1407

1408 Niinemets, Ü.: Mild versus severe stress and BVOCs: thresholds, priming and consequences, *Trends Plant Sci.*, 15, 145-153,
1409 <https://doi.org/10.1016/j.tplants.2009.11.008>, 2010.

1410

1411 Niinemets, Ü., Reichstein, M., Staudt, M., Seufert, G., and Tenhunen, J. D.: Stomatal constraints may affect emission of
1412 oxygenated monoterpenoids from the foliage of *Pinus pinea*, *Plant Physiol.*, 130, 1371-1385,
1413 <https://doi.org/10.1104/pp.009670>, 2002.

1414

1415 Niinemets Ü., Kännaste, A., and Copolovici, L.: Quantitative patterns between plant volatile emissions induced by biotic
1416 stresses and the degree of damage, *Front. Plant Sci.*, 4, 262, <https://doi.org/10.3389/fpls.2013.00262>, 2013.

1417

1418 Nikula, A.: *Animals as Forest Pests in Finnish Lapland*, 22-29, 1993.

1419

1420 Nölscher, A. C., Williams, J., Sinha, V., Custer, T., Song, W., Johnson, A. M., Axinte, R., Bozem, H., Fischer, H., Pouvesle,
1421 N., Phillips, G., Crowley, J. N., Rantala, P., Rinne, J., Kulmala, M., Gonzales, D., Valverde-Canossa, J., Vogel, A., Hoffmann,
1422 T., Ouwersloot, H. G., Vilà-Guerau de Arellano, J., and Lelieveld, J.: Summertime total OH reactivity measurements from
1423 boreal forest during HUMPPA-COPEC 2010, *Atmos. Chem. Phys.*, 12, 8257–8270, [https://doi.org/10.5194/acp-12-8257-](https://doi.org/10.5194/acp-12-8257-2012)
1424 2012, 2012.

1425

1426 Nölscher, A. C., Yañez-Serrano, A. M., Wolff, S., Carioca de Araujo, A., Lavrič, J. V., Kesselmeier, J., and Williams, J.:
1427 Unexpected seasonality in quantity and composition of Amazon rainforest air reactivity, *Nat. Commun.*, 7, 10383,
1428 <https://doi.org/10.1038/ncomms10383>, 2016.

1429

1430 Oláh, V., Szöllösi, E., Lakatos, Á., Kanalas, P., Nyitrai, B., and Mészáros, I.: Springtime leaf development of mature sessile
1431 oak trees as based on multi-seasonal monitoring data, *Acta Silv. Lign. Hung.*, 8, 21-30, [https://doi.org/10.2478/v10303-012-](https://doi.org/10.2478/v10303-012-0002-7)
1432 0002-7, 2012.

1433

1434 Paasonen, P., Nieminen, T., Asmi, E., Manninen, H. E., Petäjä, T., Plass-Dülmer, C., Flentje, H., Birmili, W., Wiedensohler,
1435 A., Hörrak, U., Metzger, A., Hamed, A., Laaksonen, A., Facchini, M. C., Kerminen, V.-M., and Kulmala, M.: On the roles of
1436 sulphuric acid and low-volatility organic vapours in the initial steps of atmospheric new particle formation, *Atmos. Chem.*
1437 *Phys.*, 10, 11223–11242, <https://doi.org/10.5194/acp-10-11223-2010>, 2010.

1438

1439 Paasonen, P., Asmi, A., Petäjä, T., Kajos, M. K., Äijälä, M., Junninen, H., Holst, T., Abbatt, J. P. D., Arneth, A., Birmili, W.,
1440 van der Gon, H. D., Hamed, A., Hoffer, A., Laakso, L., Laaksonen, A., Leaitch, W. R., Plass-Dülmer, C., Pryor, S. C.,
1441 Räisänen, P., Swietlicki, E., Wiedensohler, A., Worsnop, D. R., Kerminen, V.-M., and Kulmala, M.: Warming-induced
1442 increase in aerosol number concentration likely to moderate climate change, *Nat. Geosci.*, 6, 438-442,
1443 <https://doi.org/10.1038/ngeo1800>, 2013.

1444

1445 Pacifico, F., Folberth, G. A., Sitch, S., Haywood, J. M., Rizzo, L. V., Malavelle, F. F., and Artaxo, P.: Biomass burning related
1446 ozone damage on vegetation over the Amazon forest: a model sensitivity study, *Atmos. Chem. Phys.*, 15, 2791–2804,
1447 <https://doi.org/10.5194/acp-15-2791-2015>, 2015.

1448

1449 Pautasso, M., Döring, T. F., Garbelotto, M., Pellis, L., and Jeger, M. J.: Impacts of climate change on plant diseases - opinions
1450 and trends, *Eur. J. Plant Pathol.*, 133, 295-313, <https://doi.org/10.1007/s10658-012-9936-1>, 2012.

1451

1452 Perez-Rial, D., Penuelas, J., Lopez-Mahia, P., and Llusia, J.: Terpene emissions from *Quercus robur*. A case study of Galicia
1453 (NW Spain), *J. Environ. Monitor.*, 11, 1268-1275, doi: 10.1039/b819960d, 2009.

1454

1455 Petäjä, T., Mauldin, III, R. L., Kosciuch, E., McGrath, J., Nieminen, T., Paasonen, P., Boy, M., Adamov, A., Kotiaho, T., and
1456 Kulmala, M.: Sulfuric acid and OH concentrations in a boreal forest site, *Atmos. Chem. Phys.*, 9, 7435–7448,
1457 <https://doi.org/10.5194/acp-9-7435-2009>, 2009.

1458

1459 Petron, G., Harley, P., Greenberg, J., and Guenther, A.: Seasonal temperature variations influence isoprene emission, *Geophys.*
1460 *Res. Lett.*, 28 (9), 1707–1710, <https://doi.org/10.1029/2000GL011583>, 2001.

1461

1462 Pinon, J., Frey, P., and Husson, C.: Wettability of poplar leaves influences dew formation and infection by *Melampsora*
1463 *laricipopulina*, *Plant Dis.*, 90, 177-184, doi: 10.1094/PD-90-0177, 2006.

1464

1465 Pöhlker, C., Wiedemann, K. T., Sinha, B., Shiraiwa, M., Gunthe, S. S., Smith, M., Su, H., Artaxo, P., Chen, Q., Cheng, Y.,
1466 Elbert, W., Gilles, M. K., Kilcoyne, A. L. D., Moffet, R. C., Weigand, M., Martin, S. T., Pöschl, U., and Andreae, M. O.:
1467 Biogenic potassium salt particles as seeds for secondary organic aerosol in the Amazon, *Science*, 337, 1075-1078, DOI:
1468 10.1126/science.1223264, 2012.

1469

1470 Pöschl, U., Martin, S. T., Sinha, B., Chen, Q., Gunthe, S. S., Huffman, J. A., Borrmann, S., Farmer, D. K., Garland, R. M.,
1471 Helas, G., Jimenez, J. L., King, S. M., Manzi, A., Mikhailov, E., Pauliquevis, T., Petters, M. D., Prenni, A. J., Roldin, P., Rose,
1472 D., Schneider, J., Su, H., Zorn, S. R., Artaxo, P., and O., A. M.: Rainforest aerosols as biogenic nuclei of clouds and
1473 precipitation in the Amazon, *Science*, 329, 1513–1516, DOI: 10.1126/science.1191056, 2010.

1474

1475 Praplan, A. P., Tykkä, T., Chen, D., Boy, M., Taipale, D., Vakkari, V., Zhou, P., Petäjä, T., and Hellén, H.: Long-term total
1476 OH reactivity measurements in a boreal forest, *Atmos. Chem. Phys.*, 19, 14431–14453, [https://doi.org/10.5194/acp-19-14431-](https://doi.org/10.5194/acp-19-14431-2019)
1477 2019, 2019.

1478

1479 Pullinen, I., Schmitt, S., Kang, S., Sarrafzadeh, M., Schlag, P., Andres, S., Kleist, E., Mentel, T. F., Rohrer, F., Springer, M.,
1480 Tillmann, R., Wildt, J., Wu, C., Zhao, D., Wahner, A., and Kiendler-Scharr, A.: Impact of NO_x on secondary organic aerosol
1481 (SOA) formation from α -pinene and β -pinene photooxidation: the role of highly oxygenated organic nitrates, *Atmos. Chem.*
1482 *Phys.*, 20, 10125–10147, <https://doi.org/10.5194/acp-20-10125-2020>, 2020.

1483

1484 Quéléver, L. L. J., Kristensen, K., Normann Jensen, L., Rosati, B., Teiwes, R., Daellenbach, K. R., Peräkylä, O., Roldin, P.,
1485 Bossi, R., Pedersen, H. B., Glasius, M., Bilde, M., and Ehn, M.: Effect of temperature on the formation of highly oxygenated
1486 organic molecules (HOMs) from alpha-pinene ozonolysis, *Atmos. Chem. Phys.*, 19, 7609–7625, [https://doi.org/10.5194/acp-](https://doi.org/10.5194/acp-19-7609-2019)
1487 19-7609-2019, 2019.

1488

1489 Riccobono, F., Schobesberger, S., Scott, C. E., Dommen, J., Ortega, I. K., Rondo, L., Almeida, J., Amorim, A., Bianchi, F.,
1490 Breitenlechner, M., David, A., Downard, A., Dunne, E. M., Duplissy, J., Ehrhart, S., Flagan, R. C., Franchin, A., Hansel, A.,
1491 Junninen, H., Kajos, M., Keskinen, H., Kupc, A., Kürten, A., Kvashin, A. N., Laaksonen, A., Lehtipalo, K., Makhmutov, V.,
1492 Mathot, S., Nieminen, T., Onnela, A., Petäjä, T., Praplan, A. P., Santos, F. D., Schallhart, S., Seinfeld, J. H., Sipilä, M.,
1493 Spracklen, D. V., Stozhkov, Y., Stratmann, F., Tomé, A., Tsagkogeorgas, G., Vaattovaara, P., Viisanen, Y., Vrtala, A., Wagner,
1494 P. E., Weingartner, E., Wex, H., Wimmer, D., Carslaw, K. S., Curtius, J., Donahue, N. M., Kirkby, J., Kulmala, M., Worsnop,
1495 D. R., and Baltensperger, U.: Oxidation products of biogenic emissions contribute to nucleation of atmospheric particles,
1496 *Science*, 344, 717-721, DOI: 10.1126/science.1243527, 2014.

1497

1498 Rieksta, J., Li, T., Junker, R. R., Jepsen, J. U., Ryde, I., and Rinnan, R.: Insect herbivory strongly modifies mountain birch
1499 volatile emissions, *Front. Plant Sci.*, 11: 558979, <https://doi.org/10.3389/fpls.2020.558979>, 2020.

1500

1501 Riipi, M., Lempa, K., Haukioja, E., Ossipov, V., and Pihlaja, K.: Effects of simulated winter browsing on mountain birch foliar
1502 chemistry and on the performance of insect herbivores, *Oikos*, 111, 221-234, [https://doi.org/10.1111/j.0030-](https://doi.org/10.1111/j.0030-1299.2005.13781.x)
1503 [1299.2005.13781.x](https://doi.org/10.1111/j.0030-1299.2005.13781.x), 2005.

1504

1505 Riipinen, I., Yli-Juuti, T., Pierce, J. R., Petäjä, T., Worsnop, D. R., Kulmala, M., and Donahue, N. M.: The contribution of
1506 organics to atmospheric nanoparticle growth, *Nat. Geosci.*, 5, 453-458, <https://doi.org/10.1038/ngeo1499>, 2012.

1507

1508 Rohrer, F. and Berresheim, H.: Strong correlation between levels of tropospheric hydroxyl radicals and solar ultraviolet
1509 radiation, *Nature*, 442, 184-187, <https://doi.org/10.1038/nature04924>, 2006.

1510

1511 Rosenfeld, D., Andreae, M. O., Asmi, A., Chin, M., de Leeuw, G., Donovan, D. P., Kahn, R., Kinne, S., Kivekäs, N., Kulmala,
1512 M., Lau, W., Schmidt, S., Suni, T., Wagner, T., Wildt, M., and Quass, J.: Global observations of aerosol-cloud-precipitation-
1513 climate interactions, *Rev. Geophys.*, 52, 750–808, <https://doi.org/10.1002/2013RG000441>, 2014.

1514

1515 Ruohomäki, K., Tanhuanpää, M., Ayres, M. P., Kaitaniemi, P., Tammaru, T., and Haukioja, E.: Causes of cyclicality of *Epirrita*
1516 *autumnata* (Lepidoptera, Geometridae): grandiose theory and tedious practice, *Popul. Ecol.*, 42, 211-223,
1517 <https://doi.org/10.1007/PL00012000>, 2000.

1518

1519 Ruuhola, T., Salminen, J.-P., Haviola, S., Yang, S., and Rantala, M. J.: Immunological memory of mountain birches: effects
1520 of phenolics on performance of the autumnal moth depend on herbivory history of trees, *J. Chem. Ecol.*, 33, 1160-1176, doi:
1521 [10.1007/s10886-007-9308-z](https://doi.org/10.1007/s10886-007-9308-z), 2007.

1522

1523 Ruuskanen, T. M., Reissell, A., Keronen, P., Aalto, P. P., Laakso, L., Grönholm, T., Hari, P., and Kulmala, M.: Atmospheric
1524 trace gas and aerosol particle concentration measurements in Eastern Lapland, Finland 1992-2001, *Boreal Environ. Res.*, 8,
1525 335-349, 2003.

1526

1527 Schaub, A., Blande, J. D., Graus, M., Oksanen, E., Holopainen, J. K., and Hansel, A.: Real-time monitoring of herbivore
1528 induced volatile emissions in the field, *Physiol. Plant.*, 138, 123-133, [10.1111/j.1399-3054.2009.01322.x](https://doi.org/10.1111/j.1399-3054.2009.01322.x), 2010.

1529

1530 Schnitzler, J.-P., Lehning, A., and Steinbrecher, R.: Seasonal pattern of isoprene synthase activity in *Quercus robur* leaves and
1531 its significance for modeling isoprene emission rates, *Bot. Acta*, 110, 240–243, [https://doi.org/10.1111/j.1438-](https://doi.org/10.1111/j.1438-8677.1997.tb00635.x)
1532 [8677.1997.tb00635.x](https://doi.org/10.1111/j.1438-8677.1997.tb00635.x), 1997.

1533

1534 Schobesberger, S., Junninen, H., Bianchi, F., Lönn, G., Ehn, M., Lehtipalo, K., Dommen, J., Ehrhart, S., Ortega, I. K., Franchin,
1535 A., Nieminen, T., Riccobono, F., Hutterli, M., Duplissy, J., Almeida, J., Amorim, A., Breitenlechner, M., Downard, A. J.,
1536 Dunne, E. M., Flagan, R. C., Kajos, M., Keskinen, H., Kirkby, J., Kupc, A., Kürten, A., Kurtén, T., Laaksonen, A., Mathot,
1537 S., Onnela, A., Praplan, A. P., Rondo, L., Santos, F. D., Schallhart, S., Schnitzhofer, R., Sipilä, M., Tomé, A., Tsagkogeorgas,
1538 G., Vehkamäki, H., Wimmer, D., Baltensperger, U., Carslaw, K. S., Curtius, J., Hansel, A., Petäjä, T., Kulmala, M., Donahue,
1539 N. M., and Worsnop, D. R.: Molecular understanding of atmospheric particle formation from sulfuric acid and large oxidized
1540 organic molecules, *PNAS* 110, 17223-17228, <https://doi.org/10.1073/pnas.1306973110>, 2013.

1541

1542 Seidel, D. J., Zhang, Y., Beljaars, A., Golaz, J.-C., Jacobson, A. R., and Medeiros, B.: Climatology of the planetary boundary
1543 layer over the continental United States and Europe, *J. Geophys. Res. A*, 117, D17106, doi:10.1029/2012JD018143, 2012.

1544

1545 Shifflett, S. D., Hazel, D. W., and Guthrie Nichols, E.: Sub-soiling and genotype selection improves *Populus* productivity
1546 grown on a North Carolina sandy soil, *Forests*, 7, 74–84, doi: 10.3390/f7040074, 2016.

1547

1548 Simon, M., Dada, L., Heinritzi, M., Scholz, W., Stolzenburg, D., Fischer, L., Wagner, A. C., Kürten, A., Rörup, B., He, X.-C.,
1549 Almeida, J., Baalbaki, R., Baccharini, A., Bauer, P. S., Beck, L., Bergen, A., Bianchi, F., Bräkling, S., Brilke, S., Caudillo, L.,
1550 Chen, D., Chu, B., Dias, A., Draper, D. C., Duplissy, J., El-Haddad, I., Finkenzeller, H., Frege, C., Gonzalez-Carracedo, L.,
1551 Gordon, H., Granzin, M., Hakala, J., Hofbauer, V., Hoyle, C. R., Kim, C., Kong, W., Lamkaddam, H., Lee, C. P., Lehtipalo,
1552 K., Leiminger, M., Mai, H., Manninen, H. E., Marie, G., Marten, R., Mentler, B., Molteni, U., Nichman, L., Nie, W., Ojdanic,
1553 A., Onnela, A., Partoll, E., Petäjä, T., Pfeifer, J., Philippov, M., Quéléver, L. L. J., Ranjithkumar, A., Rissanen, M. P.,
1554 Schallhart, S., Schobesberger, S., Schuchmann, S., Shen, J., Sipilä, M., Steiner, G., Stozhkov, Y., Tauber, C., Tham, Y. J.,
1555 Tomé, A. R., Vazquez-Pufleau, M., Vogel, A. L., Wagner, R., Wang, M., Wang, D. S., Wang, Y., Weber, S. K., Wu, Y., Xiao,
1556 M., Yan, C., Ye, P., Ye, Q., Zauner-Wieczorek, M., Zhou, X., Baltensperger, U., Dommen, J., Flagan, R. C., Hansel, A.,
1557 Kulmala, M., Volkamer, R., Winkler, P. M., Worsnop, D. R., Donahue, N. M., Kirkby, J., and Curtius, J.: Molecular
1558 understanding of new-particle formation from α -pinene between -50 and $+25$ °C, *Atmos. Chem. Phys.*, 20, 9183–9207,
1559 <https://doi.org/10.5194/acp-20-9183-2020>, 2020.

1560

1561 Simpson, D. Winiwarter, W., Börjesson, G., Cinderby, S., Ferreira, A., Guenther, A., Hewitt, C. N., Janson, R., Aslam K.
1562 Khalil, M., Owen, S., Pierce, T. E., Puxbaum, H., Shearer, M., Skiba, U., Steinbrecher, R., Tarrasón, L., and Öquist, M. G.:
1563 Inventorying emissions from Nature in Europe, *J. Geophys. Res. A*, 104, 8113–8152, <https://doi.org/10.1029/98JD02747>,
1564 1999.

1565

1566 Simpson, D., Benedictow, A., Berge, H., Bergström, R., Emberson, L. D., Fagerli, H., Flechard, C. R., Hayman, G. D., Gauss,
1567 M., Jonson, J. E., Jenkin, M. E., Nyíri, A., Richter, C., Semeena, V. S., Tsyro, S., Tuovinen, J.-P., Valdebenito, Á., and Wind,
1568 P.: The EMEP MSC-W chemical transport model – technical description, *Atmos. Chem. Phys.*, 12, 7825–7865,
1569 <https://doi.org/10.5194/acp-12-7825-2012>, 2012.

1570

1571 Sinha, V., Williams, J., Lelieveld, J., Ruuskanen, T. M., Kajos, M. K., Patokoski, J., Hellén, H., Hakola, H., Mogensen, D.,
1572 Boy, M., Rinne, J., and Kulmala, M.: OH reactivity measurements within a boreal forest: evidence for unknown reactive
1573 emissions, *Environ. Sci. Technol.*, 44, 6614–6620, 2010.

1574

1575 Smiatek, G. and Steinbrecher, R.: Temporal and spatial variation of forest VOC emissions in Germany in the decade 1994–
1576 2003, *Atmos. Environ.*, 40, S166, 166–177, <https://doi.org/10.1016/j.atmosenv.2005.11.071>, 2006.

1577

1578 Spear, R. J. *The Great Gypsy Moth War: A history of the first campaign in Massachusetts to eradicate the gypsy moth, 1890–*
1579 *1901*, University of Massachusetts Press, 2005.

1580

1581 Spracklen, D. V., Carslaw, K. S., Kulmala, M., Kerminen, V.-M., Sihto, S.-L., Riipinen, I., Merikanto, J., Mann, G. W.,
1582 Chipperfield, M. P., Wiedensohler, A., Birmili, W., and Lihavainen, H.: Contribution of particle formation to global cloud
1583 condensation nuclei concentrations, *Geophys. Res. Lett.*, 35, doi: 10.1029/2007GL033038, 2008.

1584

1585 Stolzenburg, D., Fischer, L., Vogel, A. L., Heinritzi, M., Schervish, M., Simon, M., Wagner, A. C., Dada, L., Ahonen, L. R.,
1586 Amorim, A., Baccarini, A., Bauer, P. S., Baumgartner, B., Bergen, A., Bianchi, F., Breitenlechner, M., Brilke, S., Mazon, S.
1587 B., Chen, D., Dias, A., Draper, D. C., Duplissy, J., El Haddad, I., Finkenzeller, H., Frege, C., Fuchs, C., Garmash, O., Gordon,
1588 H., He, X., Helm, J., Hofbauer, V., Hoyle, C. R., Kim, C., Kirkby, J., Kontkanen, J., Kürten, A., Lampilahti, J., Lawler, M.,
1589 Lehtipalo, K., Leiminger, M., Mai, H., Mathot, S., Mentler, B., Molteni, U., Nie, W., Nieminen, T., Nowak, J. B., Ojdanic, A.,
1590 Onnela, A., Passananti, M., Petäjä, T., Quéléver, L. L. J., Rissanen, M. P., Sarnela, N., Schallhart, S., Tauber, C., Tomé, A.,
1591 Wagner, R., Wang, M., Weitz, L., Wimmer, D., Xiao, M., Yan, C., Ye, P., Zha, Q., Baltensperger, U., Curtius, J., Dommen,
1592 J., Flagan, R. C., Kulmala, M., Smith, J. N., Worsnop, D. R., Hansel, A., Donahue, N. M., and Winkler, P. M.: Rapid growth
1593 of organic aerosol nanoparticles over a wide tropospheric temperature range, *P. Natl. Acad. Sci. USA*, 115, 9122-9127,
1594 <https://doi.org/10.1073/pnas.1807604115>, 2018.

1595

1596 Stoyenoff, J. L., Witter, J. A., and Montgomery, M. E.: Nutritional indices in the gypsy moth (*Lymantria dispar* (L.)) under
1597 field conditions and host switching situations, *Oecologia*, 97, 158-170, <https://doi.org/10.1007/BF00323145>, 1994.

1598

1599 Sun, Z., Copolovici, L., and Niinemets, Ü.: Can the capacity for isoprene emission acclimate to environmental modifications
1600 during autumn senescence in temperate deciduous tree species *Populus tremula*?, *J. Plant Res.*, 125, 263–274,
1601 <https://doi.org/10.1007/s10265-011-0429-7>, 2012.

1602

1603 Surratt, J. D., Chan, A. W. H., Eddingsaas, N. C., Chan, M., Loza, C. L., Kwan, A. J., Hersey, S. P., Flagan, R. C., Wennberg,
1604 P. O., and Seinfeld, J. H.: Reactive intermediates revealed in secondary organic aerosol formation from isoprene, *Proc. Natl.*
1605 *Acad. Sci. U. S. A.*, 107, 6640-6645, <https://doi.org/10.1073/pnas.0911114107>, 2010.

1606

1607 Tammaru, T., Kaitaniemi, P., and Ruohomäki, K.: Realized fecundity in *Epirrita autumnata* (Lepidoptera: Geometridae):
1608 relation to body size and consequences to population dynamics, *Oikos*, 77, 407-16, doi: 10.2307/3545931, 1996.

1609

1610 Taipale, D., Aalto, J., Schiestl-Aalto, P., Kulmala, M., and Bäck, J.: The importance of accounting for enhanced emissions of
1611 monoterpenes from new Scots pine foliage in models - A Finnish case study, *Atmos. Environ. X.*, 8, 100097,
1612 <https://doi.org/10.1016/j.aeaoa.2020.100097>, 2020.

1613

1614 Taraborrelli, D., Lawrence, M., G., Crowley, J. N., Dillon, T. J., Gromov, S., Groß, C. B. M., Vereecken, L., and Lelieveld,
1615 J.: Hydroxyl radical buffered by isoprene oxidation over tropical forests, *Nat. Geosci.*, 5, 190-193,
1616 <https://doi.org/10.1038/ngeo1405>, 2012.

1617

1618 Tenow, O.: Topographical dependence of an outbreak of *oporia autumnata* Bkh. (lep., geometridae) in a mountain birch
1619 forest in northern Sweden, *Zoon*, 3, 85-110, 1975.

1620

1621 Tripathi, A. M., Fischer, M., Orság, M., Marek, M. V., Žalud, Z., and Trnka, M.: Evaluation of indirect measurement method
1622 of seasonal patterns of leaf area index in a high-density short rotation coppice culture of poplar, *Acta Univ. Agric. Silvic.*
1623 *Mendelianae Brun.*, 64, 549-556, <https://doi.org/10.11118/actaun201664020549>, 2016.

1624

1625 Tröstl, J., Chuang, W. K., Gordon, H., Heinritzi, M., Yan, C., Molteni, U., Ahlm, L., Frege, C., Bianchi, F., Wagner, R., Simon,
1626 M., Lehtipalo, K., Williamson, C., Craven, J. S., Duplissy, J., Adamov, A., Almeida, J., Bernhammer, A.-K., Breitenlechner,
1627 M., Brilke, S., Dias, A., Ehrhart, S., Flagan, R. C., Franchin, A., Fuchs, C., Guida, R., Gysel, M., Hansel, A., Hoyle, C. R.,
1628 Jokinen, T., Junninen, H., Kangasluoma, J., Keskinen, H., Kim, J., Krapf, M., Kürten, A., Laaksonen, A., Lawler, M.,

1629 Leiminger, M., Mathot, S., Möhler, O., Nieminen, T., Onnela, A., Petäjä, T., Piel, F. M., Miettinen, P., Rissanen, M. P., Rondo,
1630 L., Sarnela, N., Schobesberger, S., Sengupta, K., Sipilä, M., Smith, J. N., Steiner, G., Tomè, A., Virtanen, A., Wagner, A. C.,
1631 Weingartner, E., Wimmer, D., Winkler, P. M., Ye, P., Carslaw, K. S., Curtius, J., Dommen, J., Kirkby, J., Kulmala, M.,
1632 Riipinen, I., Worsnop, D. R., Donahue, N. M., and Baltensperger, U.: The role of low-volatility organic compounds in initial
1633 particle growth in the atmosphere, *Nature*, 533, 527–531, <https://doi.org/10.1038/nature18271>, 2016.

1634

1635 Twomey, S.: The influence of pollution on the shortwave albedo of clouds, *J., Atmos. Sci.*, 34, 1149–1152,
1636 [https://doi.org/10.1175/1520-0469\(1977\)034<1149:TIOPOT>2.0.CO;2](https://doi.org/10.1175/1520-0469(1977)034<1149:TIOPOT>2.0.CO;2), 1977.

1637

1638 Vana, M., Komsaare, K., Hörrak, U., Mirme, S., Nieminen, T., Kontkanen, J., Manninen, H. E., Petäjä, T., Noe, S. M., and
1639 Kulmala, M.: Characteristics of new-particle formation at three SMEAR stations, *Boreal Environ. Res.*, 21, 345–362, 2016.

1640

1641 van Meeningen, Y., Schurgers, G., Rinnan, R., and Holst, T.: BVOC emissions from English oak (*Quercus robur*) and European
1642 beech (*Fagus sylvatica*) along a latitudinal gradient, *Biogeosciences*, 13, 6067–6080, [https://doi.org/10.5194/bg-13-6067-](https://doi.org/10.5194/bg-13-6067-2016)
1643 2016, 2016.

1644

1645 Vapaavuori, E., Holopainen, J. K., Holopainen, T., Julkunen-Tiitto, R., Kaakinen, S., Kasurinen, A., Kontunen-Soppela, S.,
1646 Kostianen, K., Oksanen, E., Peltonen, P., Riikonen, J., and Tulva, I.: Rising atmospheric CO₂ concentration partially masks
1647 the negative effects of elevated O₃ in silver birch (*Betula pendula* roth), *Ambio*, 38, 418–424, [10.1579/0044-7447-38.8.418](https://doi.org/10.1579/0044-7447-38.8.418),
1648 2009.

1649

1650 Verlinden, M. S., Broeckx, L. S., Van den Bulcke, J., Van Acker, J., and Ceulemans, R.: Comparative study of biomass
1651 determinants of 12 poplar (*Populus*) genotypes in a high-density short-rotation culture, *Forest Ecol. Manag.*, 307, 101–111,
1652 <https://doi.org/10.1016/j.foreco.2013.06.062>, 2013.

1653

1654 Vialle, A., Frey, P., Hambleton, S., Bernier, L., and Hamelin, R. C.: Poplar rust systematics and refinement of *Melampsora*
1655 species delineation, *Fungal Divers.*, 50, 227–248, <https://doi.org/10.1007/s13225-011-0129-6>, 2011.

1656

1657 Voegelé, R. T. and Mendgen, K.: Rust haustoria: nutrient uptake and beyond, *New Phytol.*, 159, 93–100,
1658 <https://doi.org/10.1046/j.1469-8137.2003.00761.x>, 2003.

1659

1660 Waring, P. and Townsend, M.: *Field Guide to the Moths of Great Britain and Ireland*, British Wildlife Publishing, 2009.

1661

1662 Wells, K. C., Millet, D. B., Payne, V. H., Deventer, M. J., Bates, K. H., de Gouw, J., Graus, M., Warneke, C., Wisthaler, A.,
1663 and Fuentes, J. D.: Satellite isoprene retrievals constrain emissions and atmospheric oxidation, *Nature*, 585, 225–233,
1664 <https://doi.org/10.1038/s41586-020-2664-3>, 2020.

1665

1666 Williamson, C. J., Kupc, A., Axisa, D., Bilsback, K. R., Bui, T., Campuzano-Jost, P., Dollner, M., Froyd, K. D., Hodshire, A.
1667 L., Jimenez, J. L., Kodros, J. K., Luo, G., Murphy, D. M., Nault, B. A., Ray, E. A., Weinzierl, B., Wilson, J. C., Yu, F., Yu,
1668 P., Pierce, J. R., and Brock, C. A.: A large source of cloud condensation nuclei from new particle formation in the tropics,
1669 *Nature*, 574, 399–403, <https://doi.org/10.1038/s41586-019-1638-9>, 2019.

1670

1671 Winterhalter, R., Herrmann, F., Kanawati, B., Nguyen, T. L., Peeters, J., Vereecken, L., and Moortgat, G. K.: The gas-phase
1672 ozonolysis of β -caryophyllene (C₁₅H₂₄), Part I: an experimental study, *Phys. Chem. Chem. Phys.*, 11, 4152-4172,
1673 <https://doi.org/10.1039/B817824K>, 2009.

1674

1675 Yan, C., Nie, W., Vogel, A. L., Dada, L., Lehtipalo, K., Stolzenburg, D., Wagner, R., Rissanen, M. P., Xiao, M., Ahonen, L.,
1676 Fischer, L., Rose, C., Bianchi, F., Gordon, H., Simon, M., Heinritzi, M., Garmash, O., Roldin, P., Dias, A., Ye, P., Hofbauer,
1677 V., Amorim, A., Bauer, P. S., Bergen, A., Bernhammer, A.-K., Breitenlechner, M., Brilke, S., Buchholz, A., Buenrostro
1678 Mazon, S., Canagaratna, M. R., Chen, X., Ding, A., Dommen, J., Draper, D. C., Duplissy, J., Frege, C., Heyn, C., Guida, R.,
1679 Hakala, J., Heikkinen, L., Hoyle, C. R., Jokinen, T., Kangasluoma, J., Kirkby, J., Kontkanen, J., Kürten, A., Lawler, M. J.,
1680 Mai, H., Mathot, S., Maulding III, R. L., Molteni, U., Nichman, L., Nieminen, T., Nowak, J., Ojdanic, A., Onnela, A., Pajunoja,
1681 A., Petäjä, T., Piel, F., Quéléver, L. L. J., Sarnela, N., Schallhart, S., Sengupta, K., Sipilä, M., Tomé, A., Tröstl, J., Väisänen,
1682 O., Wagner, A. C., Ylisirniö, A., Zha, Q., Baltensperger, U., Carslaw, K. S., Curtius, J., Flagan, R. C., Hansel, A., Riipinen,
1683 I., Smith, J. N., Virtanen, A., Winkler, P. M., Donahue, N. M., Kerminen, V.-M., Kulmala, M., Ehn, M., and Worsnop, D. R.:
1684 Size-dependent influence of NO_x on the growth rates of organic aerosol particles, *Sci. Adv.*, 6, eaay4945, doi:
1685 10.1126/sciadv.aay4945, 2020.

1686

1687 Ye, J., Jiang, Y., Veromann-Jürgenson, L.-L., Niinemets, Ü.: Petiole gall aphid (*Pemphigus spyrothecae*) infestation of *Populus*
1688 \times *petrovskiana* leaves alters foliage photosynthetic characteristics and leads to enhanced emissions of both constitutive and
1689 stress-induced volatiles, *Trees*, 33, 37–51, [10.1007/s00468-018-1756-2](https://doi.org/10.1007/s00468-018-1756-2), 2019.

1690

1691 Yli-Juuti, T., Riipinen, I., Aalto, P. P., Nieminen, T., Maenhaut, W., Janssens, I. A., Claeys, M., Salma, I., Ocskay, R., Hoffer,
1692 A., Imre, K., and Kulmala, M.: Characteristics of new particle formation events and cluster ions at K-pusztá, Hungary, *Boreal*
1693 *Environ. Res.*, 14, 683-698, 2009.

1694

1695 Yli-Juuti, T., Nieminen, T., Hirsikko, A., Aalto, P. P., Asmi, E., Hörrak, U., Manninen, H. E., Patokoski, J., Dal Maso, M.,
1696 Petäjä, T., Rinne, J., Kulmala, M., and Riipinen, I.: Growth rates of nucleation mode particles in Hyytiälä during 2003–2009:
1697 variation with particle size, season, data analysis method and ambient conditions, *Atmos. Chem. Phys.*, 11, 12865–12886,
1698 <https://doi.org/10.5194/acp-11-12865-2011>, 2011.

1699

1700 Yli-Pirilä, P., Copolovici, L., Kännaste, A., Noe, S., Blande, J. D., Mikkonen, S., Klemola, T., Pulkkinen, J., Virtanen, A.,
1701 Laaksonen, A., Joutsensaari, J., Niinemets, Ü., Holopainen, J. K.: Herbivory by an outbreaking moth increases emissions of
1702 biogenic volatiles and leads to enhanced secondary organic aerosol formation capacity, *Environ. Sci. Technol.*, 50, 11501-
1703 11510, doi: [10.1021/acs.est.6b02800](https://doi.org/10.1021/acs.est.6b02800), 2016.

1704

1705 Ylisirniö, A., Buchholz, A., Mohr, C., Li, Z., Barreira, L., Lambe, A., Faiola, C., Kari, E., Yli-Juuti, T., Nizkorodov, S. A.,
1706 Worsnop, D. R., Virtanen, A., and Schobesberger, S.: Composition and volatility of secondary organic aerosol (SOA) formed
1707 from oxidation of real tree emissions compared to simplified volatile organic compound (VOC) systems, *Atmos. Chem. Phys.*,
1708 20, 5629–5644, <https://doi.org/10.5194/acp-20-5629-2020>, 2020.

1709

1710 Ylivinkka, I., Itämies, J., Klemola, T., Ruohomäki, K., Kulmala, M., and Taipale, D.: Investigating evidence of enhanced
1711 aerosol formation and growth due to autumnal moth larvae feeding on mountain birch at SMEAR I in northern Finland, *Boreal*
1712 *Environ. Res.*, 25, 121-143, 2020.

1713

1714 Yu, H., Ortega, J., Smith, J. N., Guenther, A. B., Kanawade, V. P., You, Yi., Liu, Y., Hosman, K., Karl, T., Seco, R., Geron,
 1715 C., Pallardy, S. G., Gu, L., Mikkilä, J., and Lee, S.-H.: New particle formation and growth in an isoprene-dominated Ozark
 1716 forest: from sub-5 nm to CCN-active sizes, *Aerosol Sci. Technol.*, 48, 1285-1298, DOI: 10.1080/02786826.2014.984801,
 1717 2014.

1718

1719 Zannoni, N., Gros, V., Lanza, M., Sarda, R., Bonsang, B., Kalogridis, C., Preunkert, S., Legrand, M., Jambert, C., Boissard,
 1720 C., and Lathiere, J.: OH reactivity and concentrations of biogenic volatile organic compounds in a Mediterranean forest of
 1721 downy oak trees, *Atmos. Chem. Phys.*, 16, 1619–1636, <https://doi.org/10.5194/acp-16-1619-2016>, 2016.

1722

1723 Zhao, D., Pullinen, I., Fuchs, H., Schrade, S., Wu, R., Acir, I.-H., Tillmann, R., Rohrer, F., Wildt, J., Guo, Y., Kiendler-Scharr,
 1724 A., Wahner, A., Kang, S., Vereecken, L., and Mentel, T. F.: Highly oxygenated organic molecules (HOM) formation in the
 1725 isoprene oxidation by NO₃ radical, *Atmos. Chem. Phys. Discuss.*, <https://doi.org/10.5194/acp-2020-1178>, in review, 2020.

1726

1727 Zúbrik, M., Novotný, J., and Kozánek, M.: The effect of gamma radiation on the host preferences of the gypsy moth larvae
 1728 (*Lymantria dispar* L., Lep.: Lymantriidae), *Lesn. Čas. For. J.*, 53, 15-23, 2007.

1729

1730 Appendix A: Emission factors at a few different degrees of stress

1731 The emission factors utilised in our simulations depend on the degree of stress. The equations to calculate the emission factors,
 1732 as a function of the degree of stress, are presented in Table 1 in the main paper. In this appendix, the emission factors at a few
 1733 different degrees of stress are shown (Table A1). 25 °C and 1000 μmol m⁻² s⁻¹ are here considered standard conditions (see
 1734 Sec. 2.4).

1735

1736 **Table A1.** Emission factors ($\varepsilon_{i,\mathcal{A}}$, in unit nmol m⁻² one-sided LAI s⁻¹) at a few different degrees of stress (\mathcal{A}). ISO = isoprene,
 1737 MT = monoterpenes, MeSa = methyl salicylate, LOX = lipoxygenase pathway volatile compounds, DMNT = 4,8-dimethyl-
 1738 1,3,7-nonatriene, MeOH = methanol, SQT = sesquiterpenes, α -Eud = α -Eudesmol.

Infestation of pedunculate oak (<i>Quercus robur</i>) by European gypsy moth (<i>Lymantria dispar</i>) based on Copolovici et al. (2017).					
\mathcal{A} (%)	0	10	30	60	80
ε_{iso} (nmol m ⁻² s ⁻¹)	30.3	19.6	8.21	0.161	0.0804
ε_{MT} (nmol m ⁻² s ⁻¹)	0.0400	2.16	4.40	5.96	6.54
$\varepsilon_{\text{MeSa}}$ (nmol m ⁻² s ⁻¹)	0.0	0.0347	0.104	0.208	0.277
ε_{LOX} (nmol m ⁻² s ⁻¹)	0.0	0.577	2.37	6.63	10.5
$\varepsilon_{\text{DNMT}}$ (nmol m ⁻² s ⁻¹)	0.0	0.0138	0.0475	0.113	0.167
Infection of pedunculate oak (<i>Quercus robur</i>) by oak powdery mildew (<i>Erysiphe alphitoides</i>) based on Copolovici et al. (2014)					
\mathcal{A} (%)	0	10	30	60	80

ε_{iso} (nmol m ⁻² s ⁻¹)	10.6	8.50	6.04	4.79	4.17
ε_{MT} (nmol m ⁻² s ⁻¹)	0.0400	0.120	0.247	0.386	0.471
$\varepsilon_{\text{MeSa}}$ (nmol m ⁻² s ⁻¹)	0.0	0.136	0.279	0.437	0.533
ε_{LOX} (nmol m ⁻² s ⁻¹)	0.00213	0.0645	0.189	0.377	0.501
Infection of balsam poplar (<i>Populus balsamifera</i> var. <i>suaveolens</i>) by poplar rust (<i>Melampsora larici-populina</i>) based on Jiang et al. (2016)					
\mathcal{A} (%)	0	10	30	60	80
ε_{iso} (nmol m ⁻² s ⁻¹)	86.0	36.8	22.8	17.9	16.6
ε_{MT} (nmol m ⁻² s ⁻¹)	0.0625	0.145	0.302	0.762	1.22
$\varepsilon_{\text{MeSa}}$ (nmol m ⁻² s ⁻¹)	0.0	0.0552	0.128	0.194	0.249
ε_{LOX} (nmol m ⁻² s ⁻¹)	0.481	1.96	3.96	11.8	19.8
$\varepsilon_{\text{DNMT}}$ (nmol m ⁻² s ⁻¹)	0.0	0.0199	0.0460	0.0698	0.0898
$\varepsilon_{\text{MeOH}}$ (nmol m ⁻² s ⁻¹)	16.9	14.9	19.0	45.6	76.9
ε_{SQT} (nmol m ⁻² s ⁻¹)	0.0	0.133	0.308	0.468	0.602
$\varepsilon_{\alpha\text{-Eud}}$ (nmol m ⁻² s ⁻¹)	0.0	0.0219	0.0507	0.0768	0.0989
Infestation of mountain birch (<i>Betula pubescens</i> var. <i>pumila</i>) by autumnal moth (<i>Epirrita autumnata</i>) based on Yli-Pirilä et al. (2016)					
\mathcal{A} (%)	0	10	30	60	80
ε_{MT} (nmol m ⁻² s ⁻¹)	0.131	0.278	0.423	0.475	0.485
ε_{LOX} (nmol m ⁻² s ⁻¹)	0.0868	0.200	0.425	0.764	0.989
$\varepsilon_{\text{DNMT}}$ (nmol m ⁻² s ⁻¹)	0.00122	0.00662	0.0125	0.0148	0.0153
ε_{SQT} (nmol m ⁻² s ⁻¹)	0.0437	0.0926	0.141	0.158	0.161

1739

1740 **Appendix B: Leaf age effect**1741 **Simulations of pedunculate oak infested with European gypsy moth larvae**

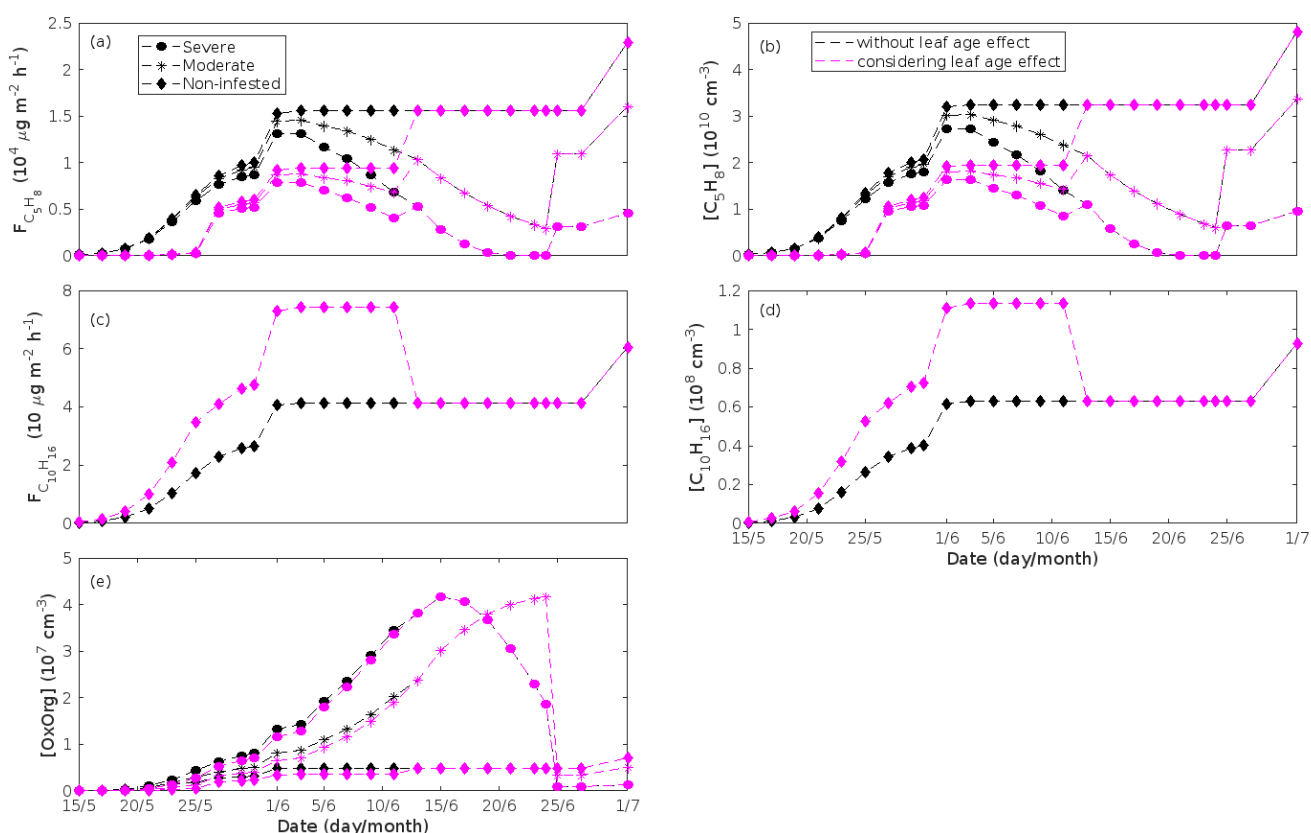
1742 It seems likely that Copolovici et al. (2017) conducted their measurements on leaves that emit isoprene at peak rate, since their
1743 reported emission rate of isoprene from non-infested leaves is comparable to the rates reported from mature leaves in previous
1744 studies (e.g. Smiatek and Steinbrecher, 2006; Perez-Rial et al., 2009; van Meeningen et al., 2016). The impact of leaf age was
1745 tested during the period with stress utilising the moderations shown in Table B1. The first period covers the number of days
1746 between budbreak and the induction of isoprene emission, while the second period ends when initiation of peak isoprene

1747 emission rates has been reached. The duration of these two periods were calculated using Eq. 18a and Eq. 19 in Guenther et
 1748 al. (2006) and our assumptions about the ambient temperature conditions (Fig. 4b). Since isoprene does not show an induced
 1749 response in emission upon gypsy moth herbivory, the emission rate of isoprene was reduced in simulations of both non-infested
 1750 and infested oak forest. The applied factors used for reductions are from Guenther et al. (2012). The emission rate of
 1751 monoterpenes was increased in the beginning of the growing season for simulations of a non-infested oak stand utilising the
 1752 coefficients from Guenther et al. (2012). Stress-induced emissions were not altered, since we do not know the effect of leaf
 1753 age on these types of emissions and Guenther et al. (2012) e.g. also assumed the same. The results are shown in Fig. B1-2.
 1754

1755 **Table B1.** Moderations made in order to consider the effect of leaf age. $\epsilon_{isoprene}$ and $\epsilon_{monoterpenes}$ are the emission factors
 1756 of isoprene and monoterpenes, respectively, used in the simulations when the leaf age effect has been considered, while
 1757 $\epsilon_{iso,mature}$ and $\epsilon_{mono,mature}$ are the emission factors of isoprene and monoterpenes, respectively, used in the default
 1758 simulations (i.e. resulting in Fig. 5-6). The moderations have been applied to the simulations of either only non-infested oak
 1759 or also stressed oak as indicated under “simulations”.

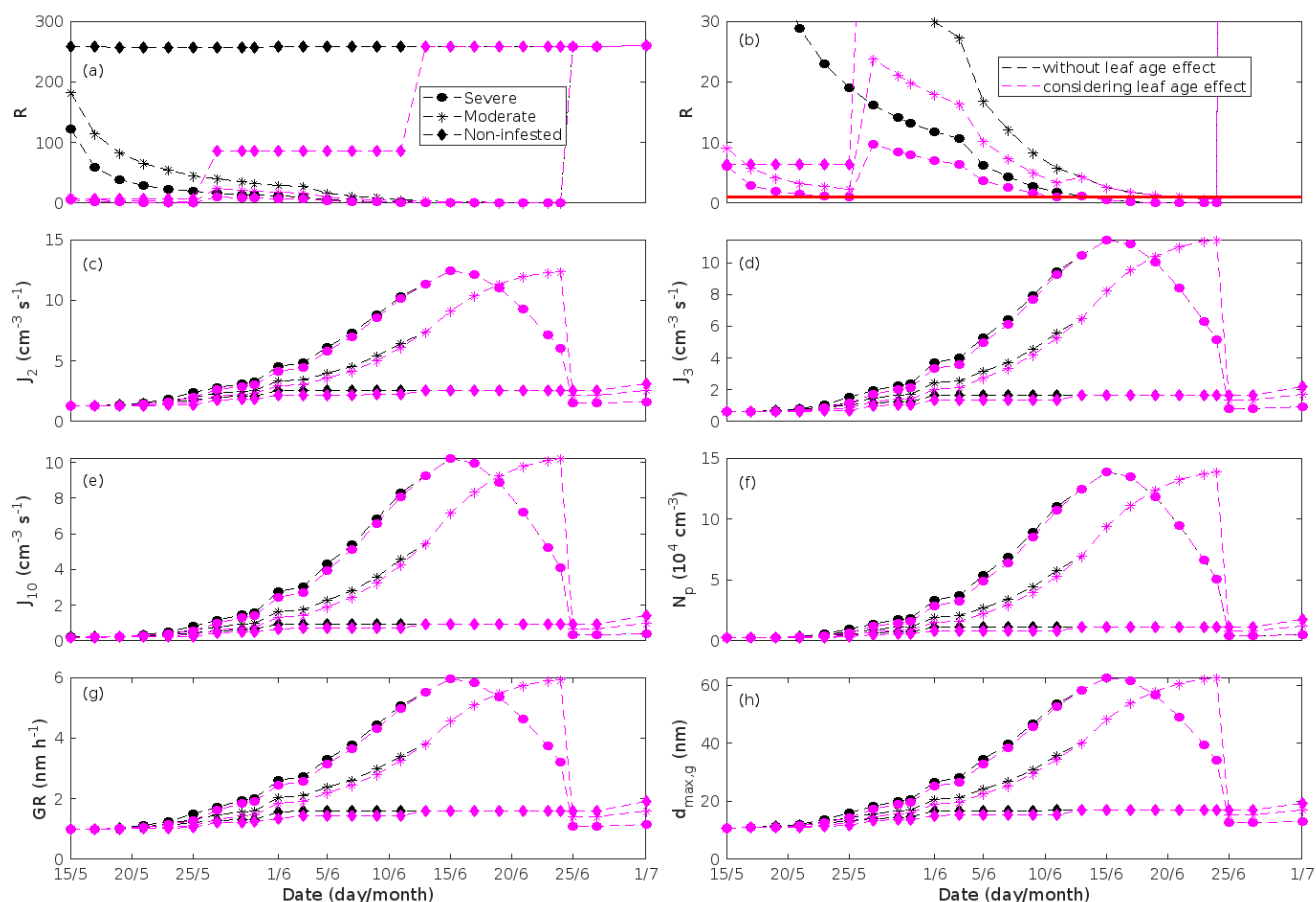
Period (day/month)	$\epsilon_{isoprene}$	Simulations	$\epsilon_{monoterpenes}$	Simulations
15-26/5	$0.05 \times \epsilon_{iso,mature}$	Non-infested, moderate stress, severe stress	$2 \times \epsilon_{mono,mature}$	Non-infested
27/5-11/6	$0.6 \times \epsilon_{iso,mature}$	Non-infested, moderate stress, severe stress	$1.8 \times \epsilon_{mono,mature}$	Non-infested
12/6-	$\epsilon_{iso,mature}$	Non-infested, moderate stress, severe stress	$\epsilon_{mono,mature}$	Non-infested, moderate stress, severe stress

1760



1761
 1762 **Figure B1.** An oak stand infested with European gypsy moth larvae in comparison to a non-infested oak stand simulated with
 1763 and without considering the impact of leaf age on the rates of emissions. Canopy emissions of (a) isoprene and (c)
 1764 monoterpenes, atmospheric concentrations of (b) isoprene, (d) monoterpenes and (e) OxOrg. “Moderately” and “severely”

1765 refer to 30 % and 80 %, respectively, of the leaf area that has been consumed by the end of the feeding period. Black markers
 1766 are for simulations where the effect of leaf age was not considered, while magenta markers are for simulations where the effect
 1767 of leaf age was considered. Simulation results (independently of whether the effect of leaf age was considered or not) for
 1768 “severe” is always indicated by circles, for “moderate” by asterisks, and for “non-infested” by diamonds.
 1769



1770
 1771 **Figure B2.** An oak stand infested with European gypsy moth larvae in comparison to a non-infested oak stand simulated with
 1772 and without considering the impact of leaf age on the rates of emissions. (a) the ratios of isoprene-to-monoterpene carbon
 1773 concentrations provided as a zoom in (b), where the red line indicates $R = 1$. Formation rates of (c) 2, (d) 3 and (e) 10 nm
 1774 particles. (f) number concentrations of formed particles, (g) growth rates of newly formed particles, and (h) the daily maxima
 1775 diameter of the growing particle mode. Symbols mean the same as in Fig. B1.
 1776

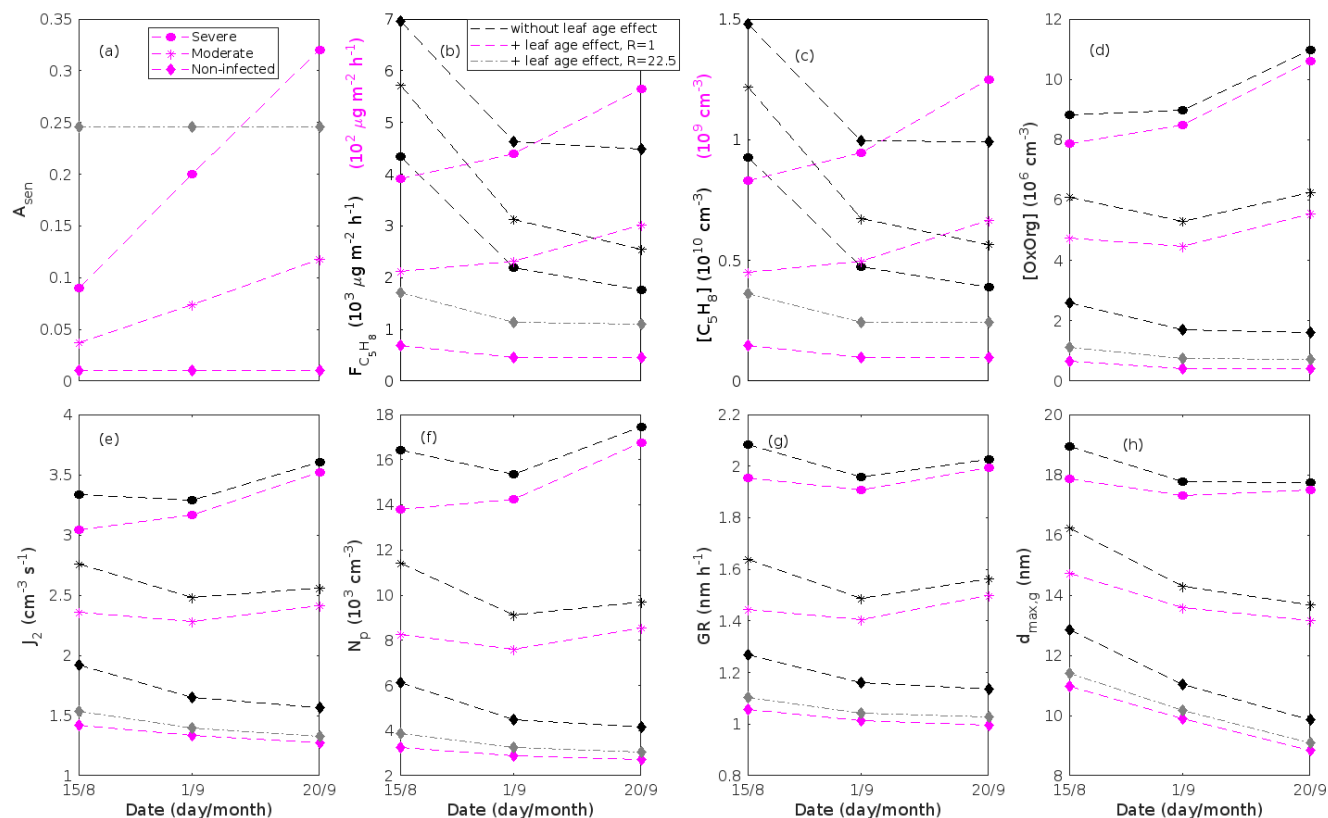
1777 **Simulations of pedunculate oak infected by oak powdery mildew and balsam poplar infected by rust fungi**

1778 The emission rates used for simulations of oak and poplar, with and without pathogenic infection, were measured in the middle
 1779 and beginning of September, respectively, in Estonia (Copolovici et al., 2014; Jiang et al. 2016). Representative photographs
 1780 of control leaves indicate that the measured leaves were mature and without any visible signs of senescence (Copolovici et al.,
 1781 2014; Jiang et al. 2016).

1782 When leaves grow old, they eventually lose their ability to photosynthesise and produce isoprene (Monson et al.,
 1783 1994; Schnitzler et al., 1997; Sun et al., 2012) and Guenther et al. (2012) e.g. assumed a reduction of 10 % in the emissions of
 1784 isoprene from senescing leaves (compared to that of mature leaves). However, a reduction on such a scale (i.e. 10 %) is not
 1785 sufficient to decrease the ratio of isoprene to monoterpene carbon concentration to less than one in our simulations of oak and
 1786 poplar infected by fungi. The impact of leaf age was therefore tested during the period with stress by decreasing the emissio n
 1787 rate of isoprene to such a degree that R was either just under 22.5 or just under 1. Since isoprene does not show an induced

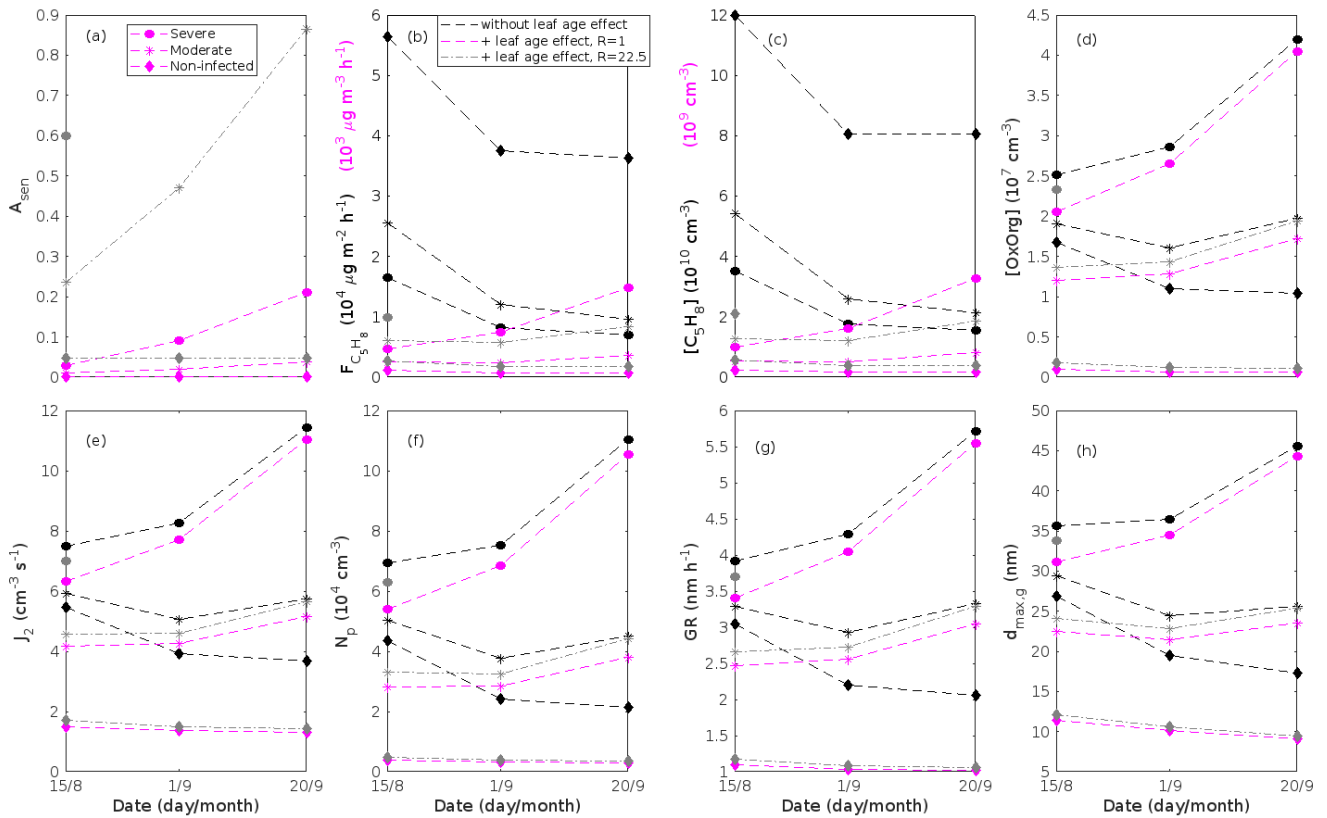
1788
1789
1790

response in emission upon oak powdery mildew or rust infection, the emission rate of isoprene was reduced in simulations of both non-infected and stressed oak and poplar forest. The results are shown in Fig. B3-4.



1791
1792
1793
1794
1795
1796
1797
1798
1799
1800
1801
1802
1803
1804
1805
1806
1807
1808

Figure B3. An oak stand infected by oak powdery mildew in comparison to a non-infected oak stand simulated with and without considering the impact of leaf age on the rates of isoprene emissions. **(a)** the fraction of isoprene emitted in comparison to simulations where the leaf age effect was not considered. For example, in order to reach $R = 1$ in simulations of a non-infected stand (magenta diamonds), the leaves are assumed to only emit 1 % of isoprene compared to our default simulations of a non-infected stand (black diamonds in Fig. 7a). The syntax is equivalent to that of Guenther et al. (2012, p. 1476). **(b)** canopy emissions of isoprene and atmospheric concentrations of **(c)** isoprene and **(d)** OxOrg. The units provided in black in **(b-c)** are connected to black and grey data points, while the units in magenta in **(b-c)** are connected to magenta data points. **(e)** formation rate of 2 nm particles, **(f)** number concentrations of formed particles, **(g)** growth rates of newly formed particles, and **(h)** the daily maxima diameter of the growing particle mode. The values of other parameters during these simulations are the same as in Fig. 7. “Moderately” and “severely” refer to 30 % and 80 %, respectively, of the leaf area being infected by fungi by the 20th of September. Black makers are for simulations where the effect of leaf age was not considered (see Fig. 7 for what R is then), while magenta markers are for simulations where the emission of isoprene was reduced sufficiently for R to be just under 1. Grey diamonds are used to illustrate simulation results of a non-infected oak stand, where the emission of isoprene has been reduced sufficiently for R to be just under 22.5. Simulation results (independently of whether the effect of leaf age was considered or not) for “severe” are always indicated by circles, for “moderate” by asterisks, and for “non-infected” by diamonds.



1809

1810

1811

1812

1813

1814

1815

1816

1817

1818

Figure B4. A poplar stand infected by rust in comparison to a non-infected poplar stand simulated with and without considering the impact of leaf age on the rates of isoprene emissions. (a) the fraction of isoprene emitted in comparison to simulations where the leaf age effect was not considered. (b) canopy emissions of isoprene and atmospheric concentrations of (c) isoprene and (d) OxOrg. The units provided in black in (b-c) are connected to black and grey data points, while the units in magenta in (b-c) are connected to magenta data points. (e) formation rate of 2 nm particles, (f) number concentrations of formed particles, (g) growth rates of newly formed particles, and (h) the daily maxima diameter of the growing particle mode. The values of other parameters during these simulations are the same as in Fig. 8. Grey markers are for simulations where the emission of isoprene was reduced sufficiently for R to be just under 22.5. Symbols are the same as in Fig. B3.

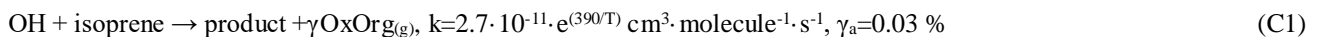
1819

Appendix C: Chemical reactions in the model

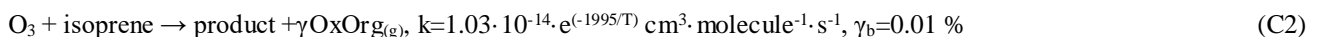
1820

We considered the following chemical reactions in our model:

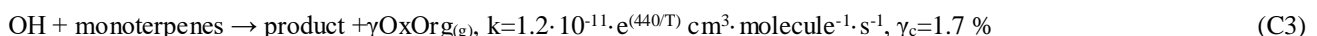
1821



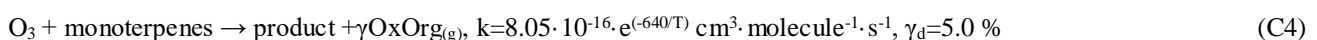
1822



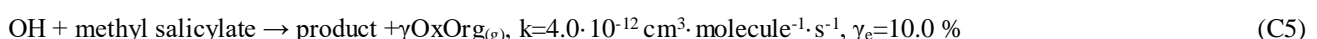
1823



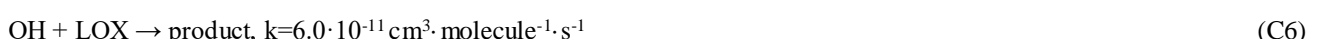
1824



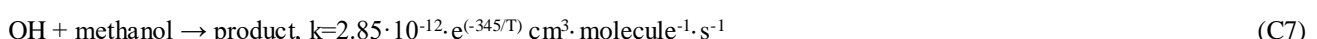
1825



1826



1827



1828



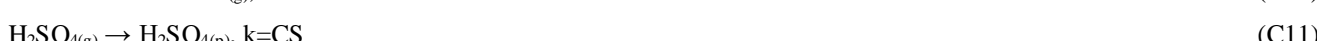
1829



1830



1831



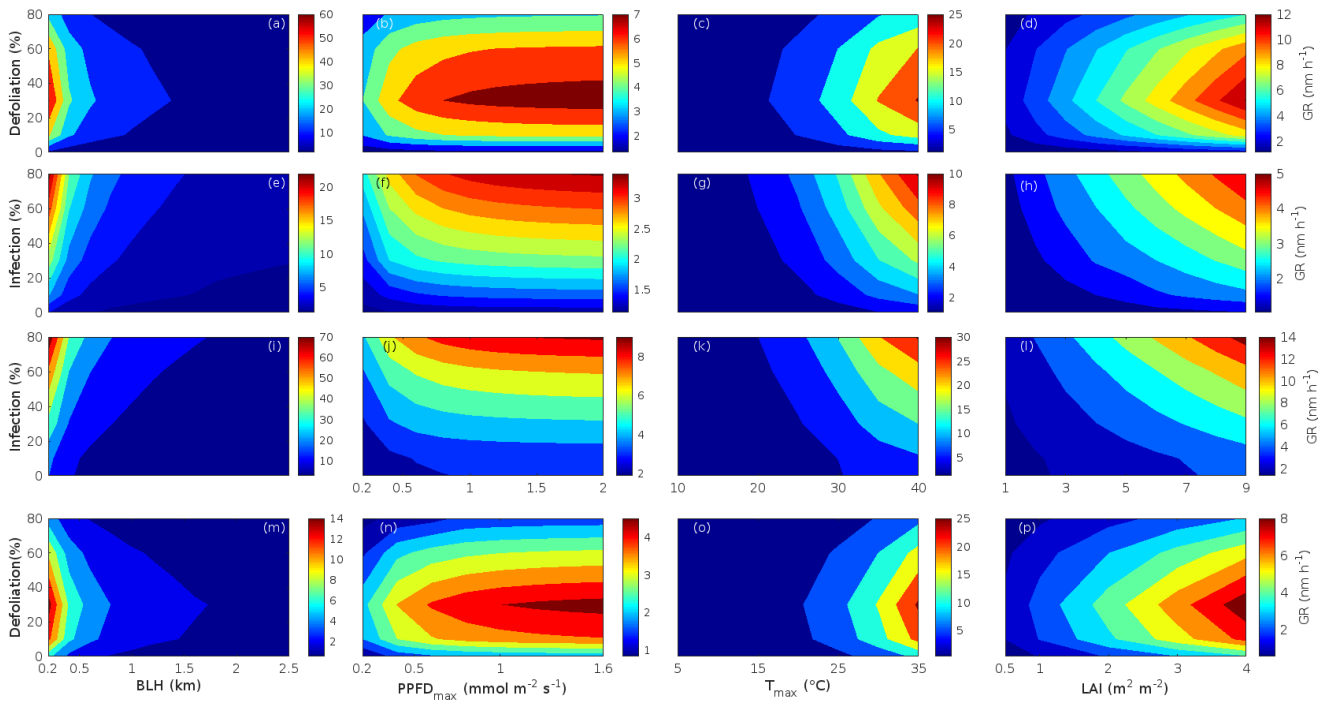
1832 T is temperature (K), p indicates “particle phase”, CS is the condensation sink, while γ_i are the fractions of organic products
 1833 which can partition to the particle phase (OxOrg). In practice, γ_i are either reported HOM yields, as defined in Ehn et al. (2014),
 1834 or reported SOA yields / 2.2. SOA yields are decreased by a factor of 2.2 in order to account for the fact that SOA yields
 1835 represent mass yields, and not molar yields as it is the case of HOM yields. We utilised HOM yields based on Jokinen et al.
 1836 (2015) ($\gamma_a, \gamma_b, \gamma_c, \gamma_d$), Berndt et al. (2016) (γ_c), and Ehn et al. (2014) (γ_d). We used SOA yields from Mentel et al. (2013) (γ_e
 1837 , γ_f).

1838 Appendix D: Sensitivity tests

1839 **Table D1.** Constrained parameters for sensitivity tests and their range of values. Nine different sensitivity tests (ST1-9) were
 1840 conducted for all plant species and infections, where only one parameter was changed at a time. BHL is the planetary boundary
 1841 layer height, PPF_{D_{max}} is the daily maximum photosynthetic photon flux density, T_{max} is the maximum daily temperature, LAI
 1842 is the leaf area index of non-infested leaves, CS is the condensation sink, and γ_{OxOrg} is the yield of OxOrg. “HPB” and “SMEAR
 1843 I” refer to simulations conducted in Hohenpeissenberg (i.e. oak and poplar) and SMEAR I (i.e. birch) conditions, respectively.

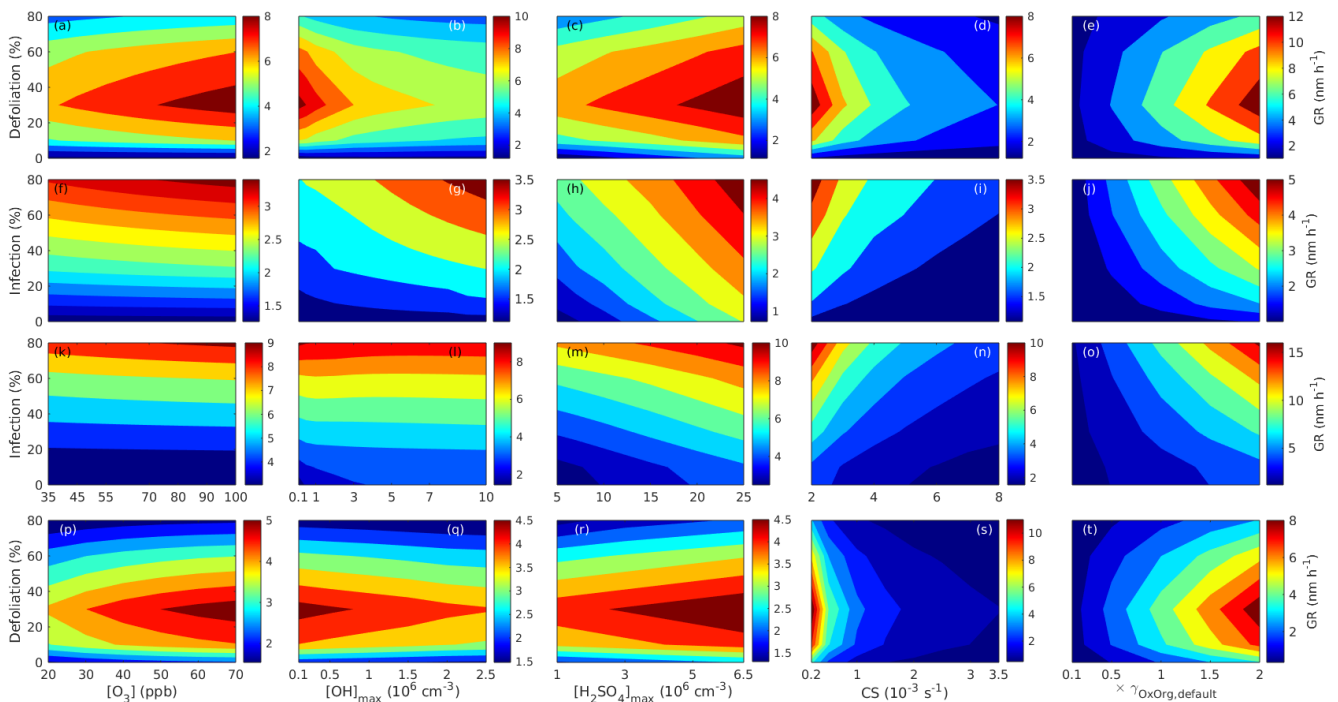
Sensitivity test no.	Parameter that changes	HPB	SMEAR I	Notes and references
ST1	BLH (m)	200 - 2500		Classical textbook example.
ST2	PPFD _{max} ($\mu\text{mol m}^{-2} \text{s}^{-1}$)	200 – 2000	200 - 1600	The lower limit is based on observations at the SMEAR I station, the upper on the theoretical clear sky maxima.
ST3	T _{max} (°C)	10 - 40	5 - 35	Based on observations and the IPCC 2014 predictions of the regional temperature increase.
ST4	LAI ($\text{m}^2 \text{m}^{-2}$)	1 - 9	0.5 – 4	The upper limit is based on Tripathi et al. (2016).
ST5	[O ₃] (ppb)	35 - 100	20 - 70	Naja et al. (2003), Ruuskanen et al. (2003). The upper end for HPB simulations is similar to the highest values which are observed in the Amazon where concentrations of isoprene can be very high (e.g. Pacifico et al., 2015)
ST6	[OH] _{max} (molec cm^{-3})	0.1-10·10 ⁶	1-25·10 ⁵	Petäjä et al. (2009), Berresheim et al. (2000), Rohrer and Berresheim (2006). The lower limit has not been observed in HPB, but is included in order to test the impact of potential OH depletion on our results.
ST7	[H ₂ SO ₄] _{max} (molec cm^{-3})	5-25·10 ⁶	1-6.5·10 ⁶	Birmili et al. (2003), Kyrö et al. (2014).
ST8	CS (s^{-1})	2-8·10 ⁻³	0.2-3.5·10 ⁻³	Birmili et al. (2003), Vana et al. (2016), Kyrö et al. (2014).
ST9	γ_{OxOrg}	0.1 - 2· $\gamma_{\text{OxOrg,default}}$		Ehn et al. (2014), Jokinen et al. (2015), Bianchi et al. (2019), McFiggans et al. (2019).

1844



1845
1846
1847
1848
1849

Figure D1. Impact of changed boundary conditions on the growth rate of small particles in non-infected and biotically stressed forest stands. The subplots correspond to those in Fig. 10, except the subplots here display growth rate, and not number of particles. Thus we refer to Fig. 10 for further explanations.



1850
1851
1852
1853

Figure D2. Impact of changed boundary conditions on the growth rate of small particles in non-infected and biotically stressed forest stands. The subplots correspond to those in Fig. 11, except the subplots here display growth rate, and not number of particles. Thus we refer to Fig. 11 for further explanations.